Università degli Studi di Messina

Dipartimento di Scienze Matematiche e Informatiche,
Scienze Fisiche e Scienze della Terra

ACOUSTIC LEVITATION SAMPLE-ENVIRONMENT DEVICE FOR BIOPHYSICAL APPLICATIONS

Relator:
Prof. Salvatore Magazù

Dr. Antonio Cannuli

ABSTRACT

The thesis work is mainly focused on issues concerning an acoustic levitation sample-environment device for biophysical applications and the employment of a portable neutron source for biophysical and electronic applications.

Sample preparation and sample-container interaction are critical components for many research investigations. In fact, on the one hand, the reactions between the sample and its container can limit accessibility conditions; on the other hand, heterogeneous container nucleation limits the capacities of "supercooled" liquids or to make over-saturated solutions. In this context, acoustic levitation can be employed for sample preparation as in the case of high concentrated mixtures, starting from solutions.

The aim is to characterize and clarify the physical-chemical mechanisms involved in the formulation processes, the vectorization processes, the stability of the formulations against the stress factors, the associated effects in the presence of bio-protector matrices, characterized by different values of kinematic and thermodynamic fragility, without neglecting the theoretical processes that underlie the acoustic levitation. In this regard, a physical-mathematical model was implemented to study the drying process of a single droplet of solution placed inside a levitator. The aim was to investigate the physical phenomena involved in this process and thus contribute to the general understanding of the drying process in an ultrasonic levitator.

The second thesis section deals with the employ of a portable neutron source, for neutrons activation and detection, is mainly addressed to biophysical and electronic applications. More in detail, the MP320 neutron generator of Thermo Scientific was employed in conjunction with a PINS-GMX

Ortec solid-state photon detector, made with high purity n-type germanium, which allows the entire external contact from implanted ions, for INAA (Instrumental Neutron Activation Analysis) investigations. Various simulations have been made with MCNP (Montecarlo N-Particles software) and a special shield has been designed to perform indoor measurements. Main applications of the source, in addition to the aforementioned, are closely related to the other research topics covered such as the field of biomedical, biology, anthropology, nutritional sciences, environmental, history and archaeology, ecology, environmental sciences, materials sciences and as a reference for materials.

TABLE OF CONTENTS

ACOUSTIC LEVITATION SAMPLE-ENVIRONMENT DEVICE FOR BIOPHYSICAL APPLICATIONS

The thesis work is mainly focused on issues concerning an acoustic levitation sample-environment device for biophysical applications and the employment of a portable neutron source for biophysical and electronic applications.

i) ACOUSTIC LEVITATOR

The main purpose of this section is to gather a framework of conceptual knowledge on the biophysical processes underlying the formulation processes to develop new protocols for the samples preparation, in particular the structural, dynamic and functional properties were studied, as well as the aggregation, stabilization and protection mechanisms to rationalize the formulation process and to extend their use to a large number of applications in the pharmaceutical, cosmetic, nutritional, cultural heritage and for the study of extremophile organisms.

Sample preparation and sample-container interaction are critical components for many research investigations. In fact, on the one hand, the reactions between the sample and its container can limit accessibility conditions; on the other hand, heterogeneous container nucleation limits the capacities of "supercooled" liquids or to make over-saturated solutions. In this context, acoustic levitation can be employed for sample preparation as in the case of high concentrated mixtures, starting from solutions. Single-axis Acoustic Levitator is shown in Figure 1. The aim is to characterize and clarify the physical-chemical mechanisms involved in the formulation processes, the vectorization processes, the stability of the formulations against the stress factors, the associated effects in the presence of bio-protector matrices, characterized by different values of kinematic and thermodynamic fragility, without neglecting the theoretical processes that underlie the acoustic levitation. In this regard, a physical-mathematical model was implemented to study the drying process of a single droplet of solution placed inside a levitator. The aim was to investigate the physical phenomena involved in this process and thus contribute to the general understanding of the drying process in an ultrasonic levitator. The acoustic levitation technique was implemented to study polymers and disaccharides

aqueous solutions, specifically mixtures of water and EthyleneGlycol (EG) and PolyEthyleneGlycol (PEG) with a nominal weight of 200 and 600 Dalton, trehalose, sucrose and maltose; this study also included measurements of surface tension, wettability and density. Such integration approach, in which liquid samples are suspended in the air, by means of an ultrasound field and then analysed by thermodynamic techniques, allowed to follow the drying process as a function of time and to modify the original mixture in a gel-like compound, where extensive chemical cross-linking processes occur. Nowadays, acoustic levitation technique, for the characterization of the structural and dynamical properties of the investigated samples, has been employed in peculiar thermodynamic conditions and in perturbations of a different nature, as in the presence of an electromagnetic field. Furthermore, a study on the development of a prototype that would allow joint, acoustic and electromagnetic levitation is in progress.

Frame and levitator system dimensions	30 x 45 x 60 cm
Controller dimensions	60 x 45 x 20 cm
Total weight	30 Kg
Electrical specifications	100/120V 60 Hz, 15A 230 V 50/60 Hz, 15A
Nominal resonant frequency	22 kHz
Sound pressure levels	< 160 dB
Transducers distance	150 mm

Figure 1: Single-axis Acoustic Levitator together with the main characteristics.

ii) PORTABLE NEUTRON SOURCE

The diffusion of electronic devices now reached the most varied fields of application, some of them involve particular operating conditions that require an adequate study of the devices response to external stresses. The electronic components used in the presence of ionizing radiation fields, such as devices used in space applications or in the nuclear field, fall within this field. These last examples are connected by the specificity of the operating conditions, since the devices are subjected to very intense radiation fields. To these application fields, others can be added. For example, can be

considered, the power electronics, increasingly widespread in energy applications, which, due to the particular operating conditions, makes the devices used in this field sensitive to the effect of the radiation fields to which they are subject, such as the field of atmospheric radiation. Other examples can be the devices applied in medical applications that involve the use of radiation fields that can significantly compromise the functioning of the associated electronics, such as in nuclear medicine and radiotherapy. In all the cited areas, the gamma and neutron radiations are very important since, being not equipped with charge, they can interact at atomic and nuclear level with the atoms of the crystalline lattice of the materials constituting the devices, with effects that can go from deterioration of the functioning characteristics of the device to the destruction of the same. In this context, at a European and global level, the compact portable systems of neutrons production are of increasing interest. Investigation techniques that employ neutrons as "probe", able to provide information on the structure of matter, were developed over the years and are constantly increasing. Consequently, the applications of these techniques have also expanded and, today, neutron investigation techniques involve various sectors of research, technological and industrial development. In this second thesis section, the use of a portable neutron source, for neutrons activation and detection, is mainly addressed to biophysical and electronic applications. More in detail, the MP320 neutron generator of Thermo Scientific was employed in conjunction with a PINS-GMX Ortec solid-state photon detector (Figure 2), made with high purity n-type germanium, which allows the entire external contact from implanted ions, for INAA (Instrumental Neutron Activation Analysis) investigations. Various simulations have been made with MCNP (Montecarlo N-Particles software) and a special shield has been designed to perform indoor measurements. Main applications of the source, in addition to the aforementioned, are closely related to the other research topics covered such as the field of biomedical, biology, anthropology, nutritional sciences, environmental, history and archaeology, ecology, environmental sciences, materials sciences and as a reference for materials.

Figure 2: MP320 neutron generator of Thermo Scientific in conjunction with a PINS-GMX Ortec solid-state photon detector.

INTRODUCTION

In the last years, contactless methods are increasingly employed for the liquid mixtures preparation and experimental investigations; in particular, levitation techniques solve the problems related to container interactions and contamination, furnish a method to study the sample with a very high degree of control.

In general, at high temperatures, reactions with crucibles limit the accessed conditions; while, at lower temperatures, heterogeneous nucleation by containers limits the ability to supercool liquids below their equilibrium melting point or to make supersaturated solutions. The functional behavior and characteristics of cosmetics and pharmaceuticals products depend on their structure. Containerless techniques provide a means of access to supercooled liquids regularly and supersaturated solutions under well-controlled conditions. Using containerless methods enable the synthesis of non-equilibrium forms of materials, often with novel structures.

The word “levitation” derives from the Latin “levitas”, that means lightness and it is the process by which an object is suspended by a physical force against gravity. In particular, acoustic levitation is a phenomenon that allows to move solid objects or liquids in the air, without a contact occurs, taking advantage of the pressure generated by the sound waves and that can be obtained through some physical principles that counteract gravity. More in detail, levitation is a process in which an upward force counteracts downward gravitational force of an object so that there is no physical contact between levitated object and ground.

While at the beginning levitation was claimed by many ancient scholars, such as Isaac Newton, that investigated the possibility of levitation as an opposite force to gravitation, today again some physics investigate several ways of levitation.

Contactless techniques allow to create an opposing force to the gravity to hold the analyzed solution in suspension. Different levitation methods have been studied by, such as optical [2-3], electro-magnetic [4-7], electrostatic [8-11], gas-film [12-14], aerodynamic [15-29] and acoustic levitation [30-51].

Optical levitation is generated by an optical trap that is formed by a focused laser beam with an objective lens of high numerical aperture. A dielectric particle will experience a force due to the transfer of momentum from the incident photons.

Electro-magnetic levitation, mostly suitable for electrically conductive materials [1], is generated by a radio-frequency field (≈ 150 kHz), produced by a coil, which induces Foucault currents in the sample. Foucault currents interact with the magnetic field of the coil causing a force that counteracts gravity. This force is proportional to the absorbed power by the sample, as a function of the square of the magnetic field strength and the electrical conductivity of the sample material.

Electro-static levitation is applicable for electrically charged samples which are levitated in an electrostatic field generated between two electrodes. One disadvantage is connected with the experimental setup complexity which hinder its use in combination with many other techniques. It permits to work under vacuum, so to prevent contamination and it also enables to study poor electrical materials with a low melting point.

Gas-film levitation enables the levitation of an object against gravitational force by floating on a thin gas film through a porous membrane. The sample-membrane closeness hampers the use in association with many techniques. It enables to levitate a large amount of material of few grams, that can be also heated thought a furnace.

Aerodynamic levitation, has proved to be a powerful and versatile technique for studying highly reactive liquids. The basic idea is to circulate levitation gas through a nozzle onto the sample from below in order to counteract gravity and lift it above the nozzle. It has the outstanding advantage of supporting any type of material ranging from insulators through semiconductors to metals. The sample can be heated to the desired temperature by means of lasers. Furthermore, the gas flow is regulated and monitored by a mass flow controller enabling to maintain the sample stable for long counting times.

Among these techniques, acoustic levitation has the advantage of not requiring any specific physical properties of the sample, for example a specific electrical charge, a certain refractive index or transparency.

Table 1 reports some distinctive features of levitation techniques as the sample size and weight, the possible processable materials, the required atmosphere and the typical temperature range.

Levitation techniques	sample size	sample weight	processable materials	required atmophere	temperature range
Optical	≈ µm	≈ µg	solids and liquids, conductors and non conductors	not required	not applicable
Electromagnetic	1 – 8 mm	up to Kg	solids and liquids, conductors and non conductors only as function of frequency	as needed (also vacuum if request)	limited by material properties
Electrostatic	1 – 3 mm	up to g	solids and liquids, conductors and non conductors	as needed (also vacuum if request)	high, but only for short experiments
Gas film	5 – 50 mm	g	solids and liquids, conductors and non conductors	as needed	limited by material properties
Aerodynamic	0,5 – 3,5 mm	g	solids, conductors and non conductors	required	up to melting point
Acoustic	0,5 – 3 mm	g	solids and liquids, conductors and non conductors	required	limited by material properties

Table 1: Distinctive features of levitation techniques: sample size, sample weight, processable materials, required atmosphere and temperature range.

The first use of acoustic levitation dates back to 1933, when Bucks and Muller noticed acoustic fields throughout alcohol mists and droplets [52]. Subsequently, in 1985 Barmatz and Collas developed techniques that used resonant cavities to create regions that can trap small samples [53]. All the described levitation techniques are reported in Figure 1.

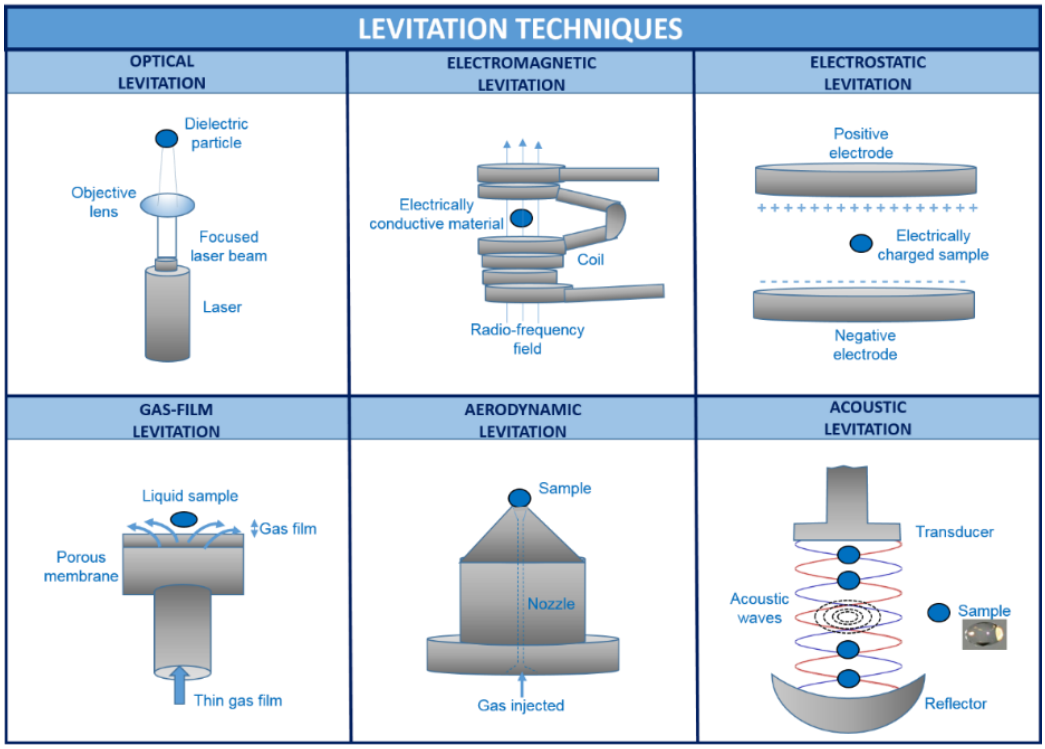

Figure 1: Overview on different levitation techniques: i.e. optical, electromagnetic, electrostatic, gas-film, aerodynamic and acoustic levitations.

CHAPTER 1

Chapter 1 reports an overview on levitation techniques with a particular reference to acoustic levitation, furthermore drying processes in an ultrasonic levitator are introduced. Finally a specific application for historic cultural heritage conservation.

Recent developments in acoustic levitation and microgravity enable containerless analyses on supercooled liquids and are suitable for investigation of non-equilibrium processes. The current available technology does not allow long experiments with samples larger than a few hundred milligrams, but only to process small samples for very short periods, while acoustic levitation can allow this, because the positioning forces are small and buoyancy-driven convection is eliminated.
Acoustic levitation has the advantage of not requiring any specific physical properties of the sample, such as a specific electrical charge, a certain refractive index or transparency.
In acoustic levitation, a standing wave is generated by a piezoelectric crystal, which gives rise to a stationary acoustic radiation force [1] when the distance between a transducer and a reflector is an integral multiple of the half wavelength. Is also possible to use two opposed transducers that control the position of the sample by electronically adjusting the acoustic phase. The distance between the two transducers is about 10 wavelengths. Liquid and solid drops, of about 0.5 and 3.5 mm diameter, can be levitated in the vicinity of the pressure nodes; these nodes and anti-nodes appear at fixed points separated by a distance of $\lambda/2$.
Figure 1.1 shows, in a schematic way, the container-medium-sample interaction mechanisms. The sample can be contaminated by the sample holder, especially at high temperatures (for example chemical reactions increase rapidly with the temperature). Containerless levitation allows the elimination of the extrinsic effects of the heterogeneous nucleation. After a certain time and with a specific power occur equilibrations between the investigated sample and the medium.

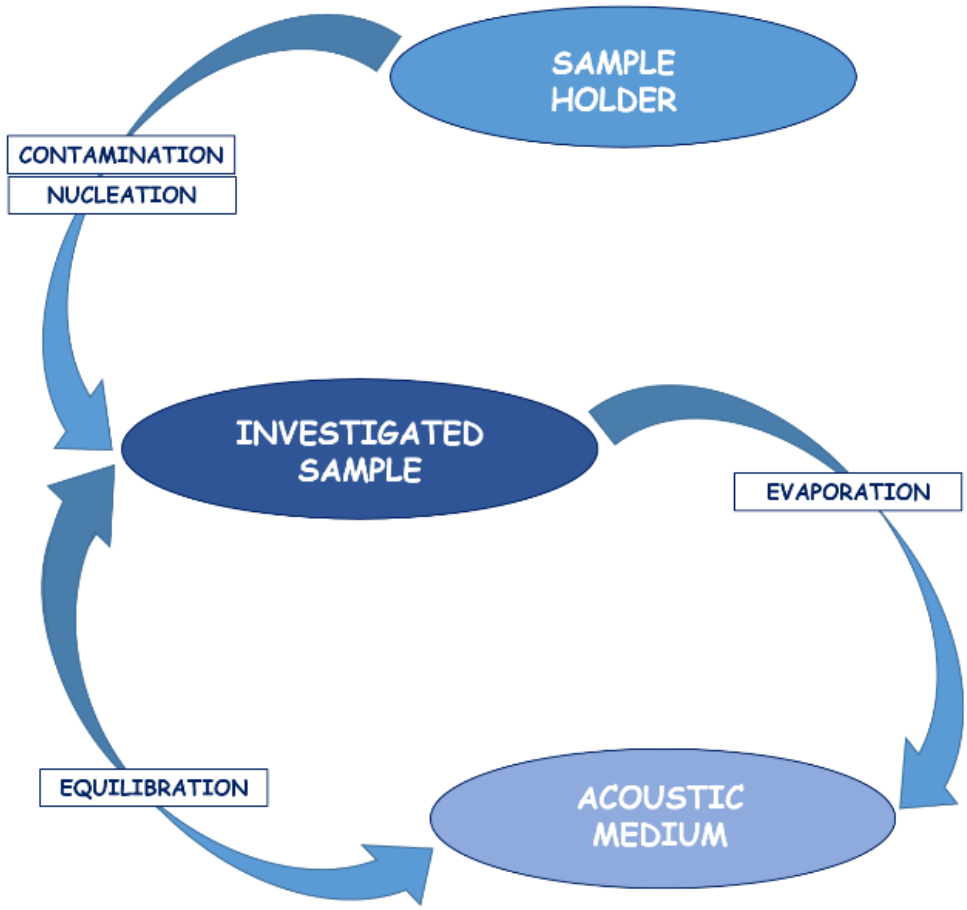

Figure 1.1: Potential interactions among the investigated sample, the sample holder and the acoustic medium. The sample holder causes contaminations and nucleations in the investigated sample; this latter can evaporate in the acoustic medium after a certain levitation time; at a given power equilibration between the sample and the acoustic medium may occur.

In Figure 1.2a the levitation forces that determine the droplet shape are reported: axial forces are mainly responsible for compensating the gravitational force, while radial forces hold the sample in the pressure node. Figure 1.2b shows a series of images of levitated mixtures drops obtained by varying the frequency of acoustic forces. The drop shape can be compressed by increasing the acoustic forces that can generate an atomization of the drop. Generally, the modulation of the acoustic forces causes oscillations of the drop and, when the stimulation frequency matches the drop resonant frequency, the amplitude of the oscillations becomes very large and this can cause the fall of the drop or its explosion. A further small increase in the acoustic power results in the drop suddenly fragmenting into a mist.

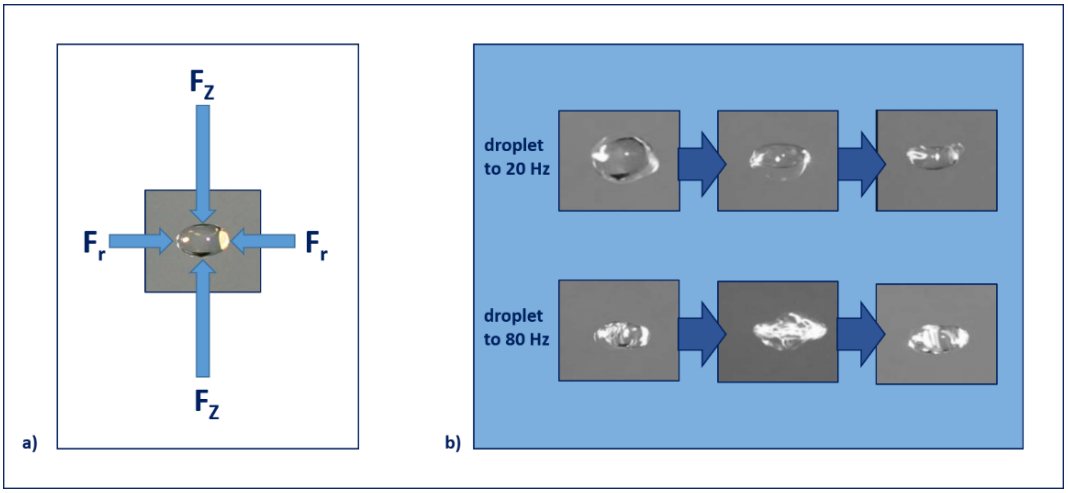

Figure 1.2. a) Radial and axial levitation forces. The axial forces (Fz) compensate the gravitational force, while the radial forces (Fr) hold the drop stable in the pressure node. b) Levitated mixtures drops excited by varying the acoustic forces using a sine wave function at different frequencies.

1.1 Drying Processes in an Ultrasonic Levitator

Nowadays, drying processes and evaporation kinetics of levitated droplets are considered complex mechanisms. Although many theoretical models on the drying behavior of suspended droplets have been formulated, only few experimental data are available. Previous investigations often provide only integral information while specific information about the individual physical processes taking place are missing.

In general, levitation [1-5] is a contactless technique that permits to remove sample-holder interplays and decreases contamination in order to study a solution with a high control degree. Among these techniques, acoustic levitation has the advantage of not requiring specific properties of the sample and can treated very small object. It allows obtaining very high concentrations of mixtures starting from solutions, impossible to achieve without the use of levitation. In particular, the importance of acoustic levitation resides in the access to supercooled liquids regularly and supersaturated solutions under well-controlled conditions. Furthermore, the latest updates in acoustic levitation allow container-less studies on supercooled liquids and are fit for analysis of non-equilibrium processes. The present technology assent only to process small samples for very short periods and not long-lasting experiments with samples of a few hundred milligrams; with the acoustic levitation, it is possible thanks to the smallness of the positioning forces and the elimination of the buoyancy-driven convection.

In this context, in acoustic levitation it is fundamental to implement an intuitive model of drying processes occurring when a single droplet is suspended in the air; furthermore, the observation of a single droplet upon drying often enables to track the physical and chemical changes and to get

information on the investigated systems. The acoustic levitator is an instrument suitable for the study of droplets kinetics.

Mechanisms of droplet drying are enough complex, in particular they involve a period in which the drying process is constant and it follows the well-known D^2-Law, followed by a period where the rate of drying falls.

In general, the evaporation rate of solutions is variable and it follows a non-linear dependence of the square diameter with time. In particular, on levitated droplets evaporation in levitators with strong acoustic fields it was shown that the acoustic streaming in the gas furnishes a convective mechanism bigger than the Stefan flow or natural convection. The acoustic streaming dominates the evaporation process in levitators and in the case of disaccharides aqueous droplets experimental data on D^2 (t) were correlated by a linear function reminiscent of the D^2-Law.

The D^2-Law predicts that the square of the droplet diameter decreases linearly with time.

Few important assumptions must be considered for a droplet in suspension, such as:

- heat and mass transfer between liquid and gas phase are diffusion controlled;
- a spherical symmetry is considered;
- no radiation effects take place;
- constant and uniform temperature occurs.

The mass flux of vapor leaving the droplet surface can be calculated as:

$$\dot{m}_v = \pi D \rho_{vapor} D_g Sh \left(\frac{Y_{vap,s} - Y_{vap,\infty}}{1 - Y_{vap,\infty}} \right) \quad (1)$$

where Y_{vap} is the mass fraction at the droplet surface which is supposed to be uniform. The outer boundary is noted with the subscript ∞ and represents the condition far away from the droplet.

The rate change of liquid droplet mass is expressed as follows:

$$\dot{m}_d = -\frac{dm_d}{dt} \quad (2)$$

$$\frac{dm_d}{dt} = -\rho_{droplet} \frac{dV}{dt} = -\rho_{droplet} \frac{\pi}{6} \frac{dD_S^3}{dt} = -\rho_{droplet} \frac{\pi D}{4} \frac{dD_S^2}{dt} \quad (3)$$

but $\dot{m}_v = -\dot{m}_d$, so, comparing eqn. (1) with the eqn. (3) the equation for the diameter becomes:

$$\pi D \rho_{vapor} D_g Sh \left(\frac{Y_{vap,s} - Y_{vap,\infty}}{1 - Y_{vap,\infty}} \right) = -\rho_{droplet} \frac{\pi D}{4} \frac{dD_S^2}{dt}$$

with $D_S^3 = D_S^2 \cdot D$.

D_S^3 can be divided in a constant diameter, that is D and in a variable diameter as function of time, D_S^2.

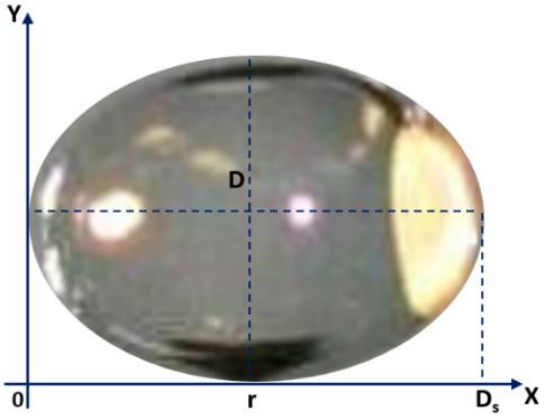

Figure 1: Droplet diameter, that can be divided in a constant diameter, that is D and in a variable diameter as function of time, D_S^2.

$$\frac{dD^2}{dt} = -4\frac{\rho_{gas}}{\rho_{droplet}} D_g Sh \left(\frac{Y_{vap,s} - Y_{vap,\infty}}{1 - Y_{vap,\infty}}\right) = -4\frac{\rho_{gas}}{\rho_{droplet}} D_g Sh \ln(1 + B_M) \tag{4}$$

For diffusion-controlled evaporation the film thickness goes into infinity, hence Sh_0=2.

The modified Sherwood number Sh takes the value 2 and after substituting the value of Sh_0 in eqn. (1), eqn. (4) becomes:

$$\frac{dD_S^2}{dt} = -8\frac{\rho_{gas}}{\rho_{droplet}} D_g \ln(1 + B_M) \tag{5}$$

$$\int \frac{dD_S^2}{dt} dt = \int -8\frac{\rho_{gas}}{\rho_{droplet}} D_g \ln(1 + B_M) dt$$

in which B_M is the Spalding mass transfer coefficient.

The integration of this equation for an initial condition D_0, i.e. at $t = 0$, gives the well-known D^2-Law that describes the temporal evolution of droplet surface of pure liquid:

$$\boldsymbol{D_s^2 = D_{0s}^2 - \beta t} \tag{6}$$

where β is the evaporation rate coefficient:

$$\beta = 8\frac{\rho_{gas}}{\rho_{droplet}} D_g \ln(1 + B_M) \tag{7}$$

The density of the liquid droplet is $\rho_{droplet}$, the density of the gas at the droplet surface is ρ_{gas}, the diffusion coefficient is $D_g$and the Spalding transfer number is B_M.

In addition to the evaporation rate, another important parameter in droplet evaporation is the lifetime of the droplet, also called evaporation time τ_{end}, which can be determined from eqn. (6) with $D|_{t=\tau_{end}} = 0$:

$$\tau_{end} = \frac{D_0^2}{\beta} \tag{8}$$

CHAPTER 2

In acoustic levitation a standing wave is generated by a piezoelectric crystal which gives rise to a stationary acoustic radiation force. In Physics Education, acoustic levitation furnishes an effective and straightforward method to localize the nodes of acoustic standing waves and to highlight some interesting physical phenomenologies. In Chapter 2 two mechanical models to study the damped oscillations of an acoustically levitated sphere are introduced and a method to determine surfece tension in complex systems. The work is addressed to graduate Physics, Engineering and Mathematics students.

One of the primary subjects of Physics is the concept of waves. Waves are perturbations originated from a source which, although of different nature, have in common the same characteristic equation. The property of the waves to be superimposed gives rise, among other things, to the phenomenon of non homogeneous distribution of their energy in space.

Transverse waves are those in which the oscillation occurs in a direction perpendicular to that in which the wave propagates.

In longitudinal waves the oscillation of the medium are parallel to the direction of propagation, as shown in Figure 2.1.

In gases, such as air, only longitudinal waves propagate, since cohesion effects able to recall the medium towards the equilibrium position are negligible. It should be noticed that, the particles that constitute the medium do not translate but oscillate around their equilibrium position. A wave, therefore, in a strict sense, does not involve the transfer of matter.

In the following the attention will be addressed only to the longitudinal waves and, in particular, to standing acoustic waves that propagate inside an acoustic levitator. It will be shown how particles

immersed in acoustic waves are influenced by forces that can be schematized by means of mechanical models constituted by a mass-spring system and by a stretched string.

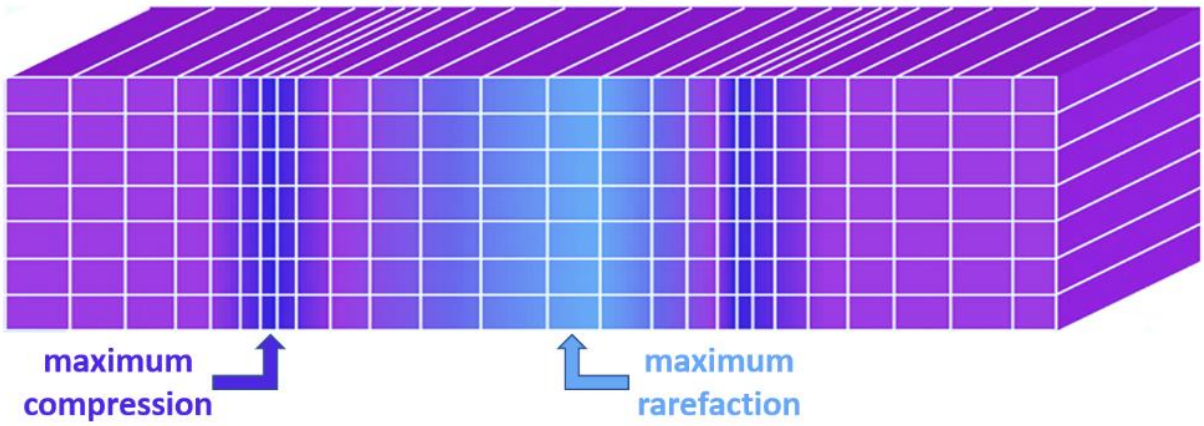

Figure 2.1. Longitudinal wave in which the oscillations of the medium consist of compressions and rarefactions that occur in the same direction in which the wave propagates.

It should be stressed that in most undergraduate and graduate Physics Education courses, students are usually introduced to the concept of standing waves by means of a discussion on the transverse standing waves on a string. In fact, static images of the standing waves on a fixed string are more easily understood because they show wave patterns corresponding to the transverse displacement of the string.

However, acoustic waves are longitudinal waves and the particle motion associated to a standing acoustic wave, for example in a pipe, is directed back and forth along the pipe axis. In this context, acoustic levitation furnishes an effective and straightforward method to visually show the nodes of acoustic standing waves whose positions are stationary.

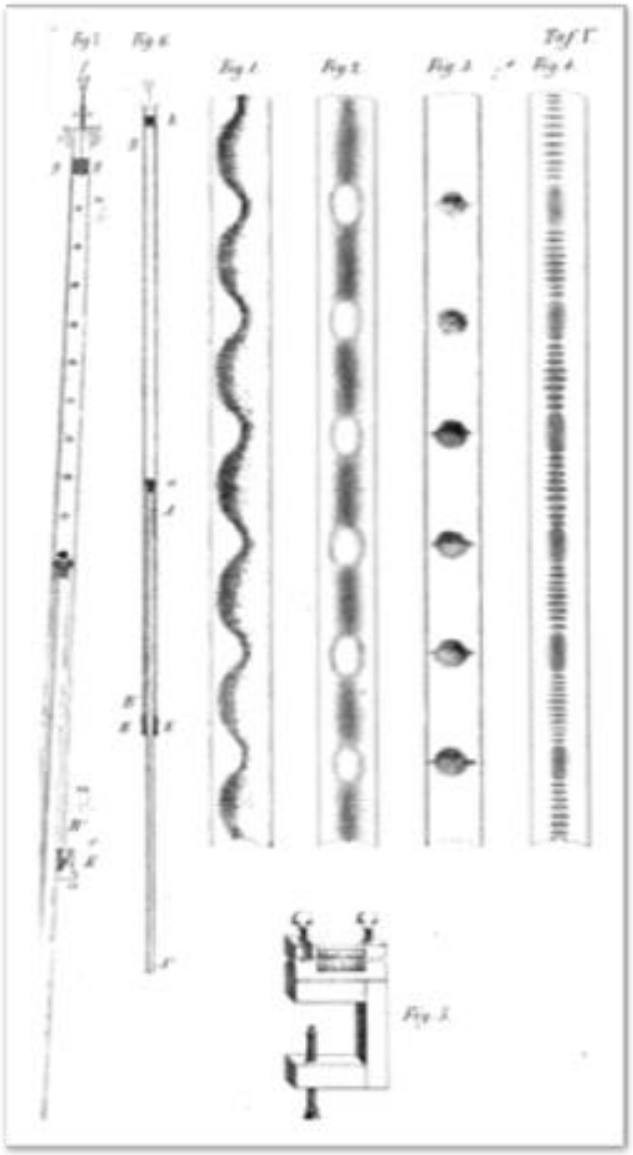

Figure 2.2. Drawing of the Kundt's tube apparatus (denoted inside Figure 2.2, as Figure 6 and Figure 7) and the powder patterns created by it (denoted inside Figure 2, as Figures 1, 2, 3 and 4).

Despite standing wave levitation phenomena were first observed in Kundt's tube experiment [1], the first use of acoustic levitation dates back to 1933 [2]. Subsequently, in 1985 Barmatz and Collas developed techniques that used resonant cavities to create regions that can trap small samples [3]. Figure 2.2 shows a drawing of the Kundt's tube (denoted inside Figure 2.2, as Figure 6 and Figure 7) and the powder patterns created by it (denoted inside Figure 2.2, Figures 1, 2, 3 and 4) [1]. This experimental apparatus allows the measurement of the sound speed in a gas or a solid rod and it was invented in 1866 by a German physicist August Kundt. It is used today only for demonstrating standing waves and acoustical forces.

In the last years, many levitation techniques [4] have been developed by scientists, for example optical [5-6], electro-magnetic [7-10], electrostatic [11-13], gas-film [14-15], aerodynamic [16-29] and acoustic levitation [30-55].

In many cases levitation is a contactless technique that permits to remove sample-holder interplays and to decrease contamination; furthermore, acoustic levitation is employed for obtaining high concentrations of mixtures starting from solutions. Electric levitation for example is achievable with conductive materials. For these reasons acoustic levitation is widely used in biophysics both for the investigation of aqueous solutions [56-59], disaccharides [60-85], proteins [86-93], polymers [94-138], polyols [139-145], nano-materials [146-148] and systems of biotechnological interest [149-150]. In particular acoustic levitation is more and more employed in the preparation of highly concentrated mixtures and in conjunction with spectroscopic techniques [151-156].

In this paper, an approach to explain standing waves by means of an acoustic levitator is presented. In particular, it is possible to visually show the nodes of the acoustic standing wave whose positions are stationary; furthermore, two mechanical models to study the damped oscillations of a suspended particle [157-162] are reported, showing as acoustic levitation allows to explain the physical principle of standing waves in an intuitive way.

2.1 Acoustic Standing Waves

Waves obey to the same differential equation and it is this property that allows to give a unified description. In general, considering a perturbation represented by a function $f = f(x,t)$, the wave equation is:

$$\frac{\partial^2 f}{\partial x^2} = \frac{1}{v^2}\frac{\partial^2 f}{\partial t^2} \tag{1}$$

where x is the position, v the velocity of the wave and t the time.

This is a differential equation to partial derivatives, linear of the second order. Solutions of eq. (1) can be written in the form:

$$f = f(x \pm vt) \tag{2}$$

It is relatively simple to prove that eq. (2) is solution of eq. (1), introducing the intermediate variable $s = x \pm vt$. It follows that:

$$\frac{\partial f}{\partial x} = \frac{df}{ds}\frac{\partial s}{\partial x} = \frac{\partial f}{\partial s}; \frac{\partial f}{\partial t} = \frac{df}{ds}\frac{\partial s}{\partial t} = \pm v\frac{df}{ds}. \tag{3}$$

Observing that the derivatives of the function f respect to x and t are obtained by multiplying the derivative respect to s, for 1 and for $\pm v$, it is possible to write:

$$\frac{\partial^2 f}{\partial x^2} = \frac{d^2 f}{ds^2}; \qquad \frac{\partial^2 f}{\partial t^2} = v^2 \frac{d^2 f}{ds^2}. \tag{4}$$

Substituting eq. (4) in eq. (1) it is possible to verify that eq. (1) is verified.

The two solutions, $f(x - vt)$ and $f(x \pm vt)$, describe respectively a wave that propagates in the direction of the x axis and in the opposite direction to that of x axis.

A particular case of relevant interest is that in which the source that generates the wave oscillates of harmonic motion, with a fixed pulsation ω. The argument of the wave function must therefore contain, in addition to x and t, also the pulsation ω; dimensional considerations suggest to express the function in the form:

$$f = Acos(kx \pm \omega t) \text{ or } f = Asin(kx \pm \omega t) \tag{5}$$

in which the argument of the trigonometric functions is called "phase." It is easy to verify that both these functions are solution of eq. (1), as long as exists the relationship:

$$k = \frac{\omega}{v} \tag{6}$$

The parameter k is called "wave number."

The following relationships are easily verifiable: $v = \frac{\lambda}{T} = \lambda v \frac{\omega}{k}$ and $\omega = \frac{2\pi}{T} = 2\pi v$.

The phenomenon called "standing waves" occurs when two waves of the same nature and of the same frequency propagate in the same medium in opposite directions and they overlap.
Sound is a longitudinal pressure wave, constituted by the alternation of compressed and rarefied air layers. Considering a long tube, full of air, closed at one end by a piston that can slide back and forth. As the piston advances, it compresses the volume of air adjacent to it; consequently, the air pressure contained in that volume increases and the air tends to expand from both sides, compressing the next volume of air and at the same time restoring the previous pressure from the piston side; in this way the impulse produced by the piston is transmitted along the tube (see Figure 3).
If the piston moves in the opposite direction a pressure vacuum is created.
Figure 4 shows what happens to a sphere volume at different times, as a rightward-traveling wave passes by. The darker regions indicate higher pressure and density zones, whereas the lighter regions indicate lower pressure and density zones.

In the 1st case, the sphere volume is located at its equilibrium position (indicated by the vertical blue line) moving towards the right side with maximum velocity; at this position the pressure and density take the maximum value too while the net force is zero. In the 2nd case, the sphere volume is decelerating due to the pressure which is higher on the right than on the left particle side. In the 3rd case, the sphere value is at its maximum displacement and acceleration, while its velocity is zero. In the 4rd case it is moving leftward while in the 5rd case, it crosses the equilibrium position with the maximum negative velocity.

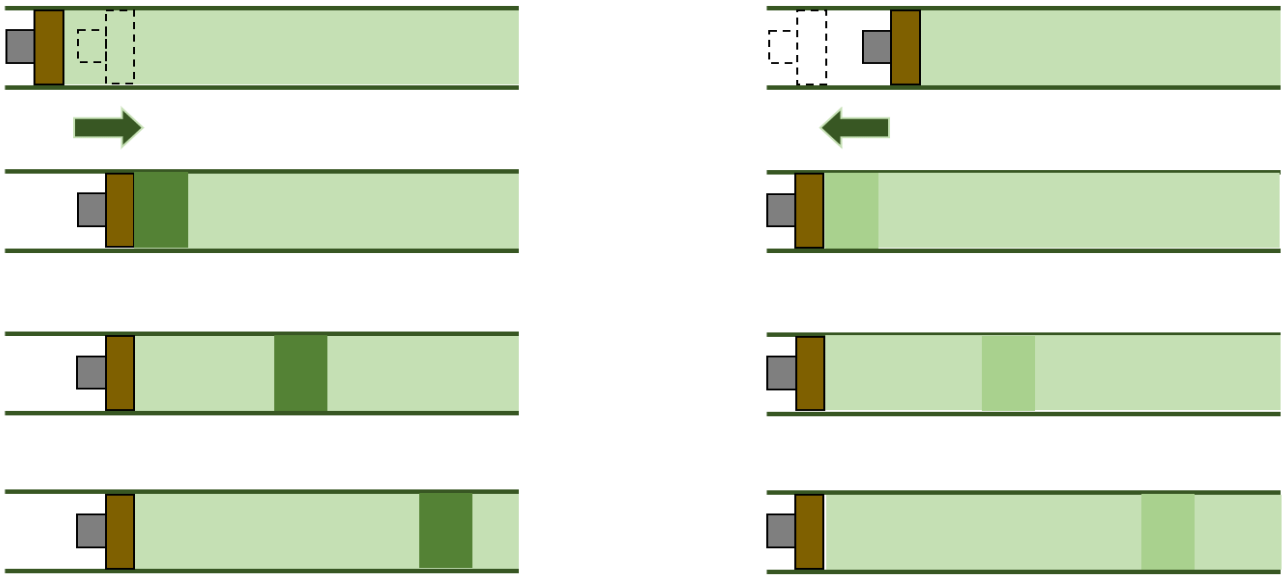

Figure 2.3. Longitudinal pressure wave, constituted by the alternation of compressed and rarefied air layers, represented by a long tube, full of air, closed at one end by a piston that can slide back and forth.

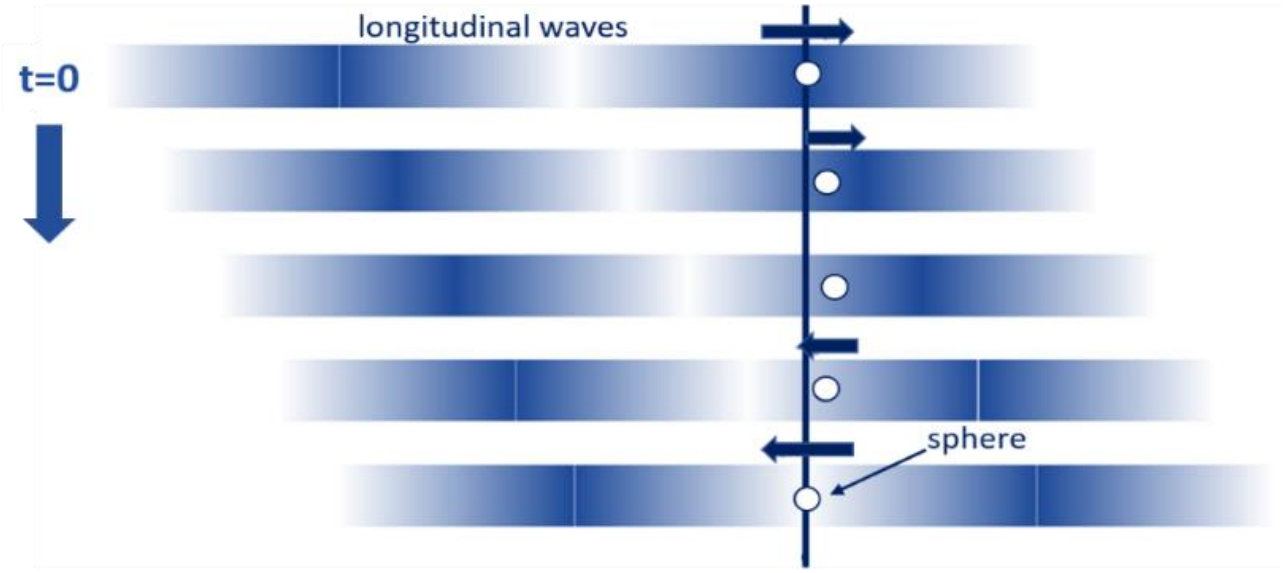

Figure 2.4. Half cycle of a sphere volume at a few different times, as a rightward-traveling wave passes by.

For an acoustic wave, intensity is defined as the energy carried by the wave per unit area and per unit of time.

The human ear can be considered as a sensitive receiver with the ability to perceive sounds whose intensity varies in a large interval. Ear response has a particular non-linear characteristic curve; it does not produce a double sound sensation when it doubles the objective intensity of the pressure wave, but has a logarithmic response. The ear response also depends on the sound frequency as shown in Figure 2.5. Each of the graph curves refers to sounds of different frequencies that generate the same sound sensation. The set of all isophonic curves defines the field of audibility.

Acoustic waves which can be perceived by the human ear have a frequency between 20 Hz and 20 KHz; below 20 Hz the waves are called "infrasonic" and above the 20 KHz "ultrasonic" (see Figure 5). The lower curve refers to the threshold of audibility, the highest one indicates the pain threshold (loudness level), at the frequency of 1000 Hz; they correspond respectively to 10^{-12} W/m^2 and 1 W/m^2.

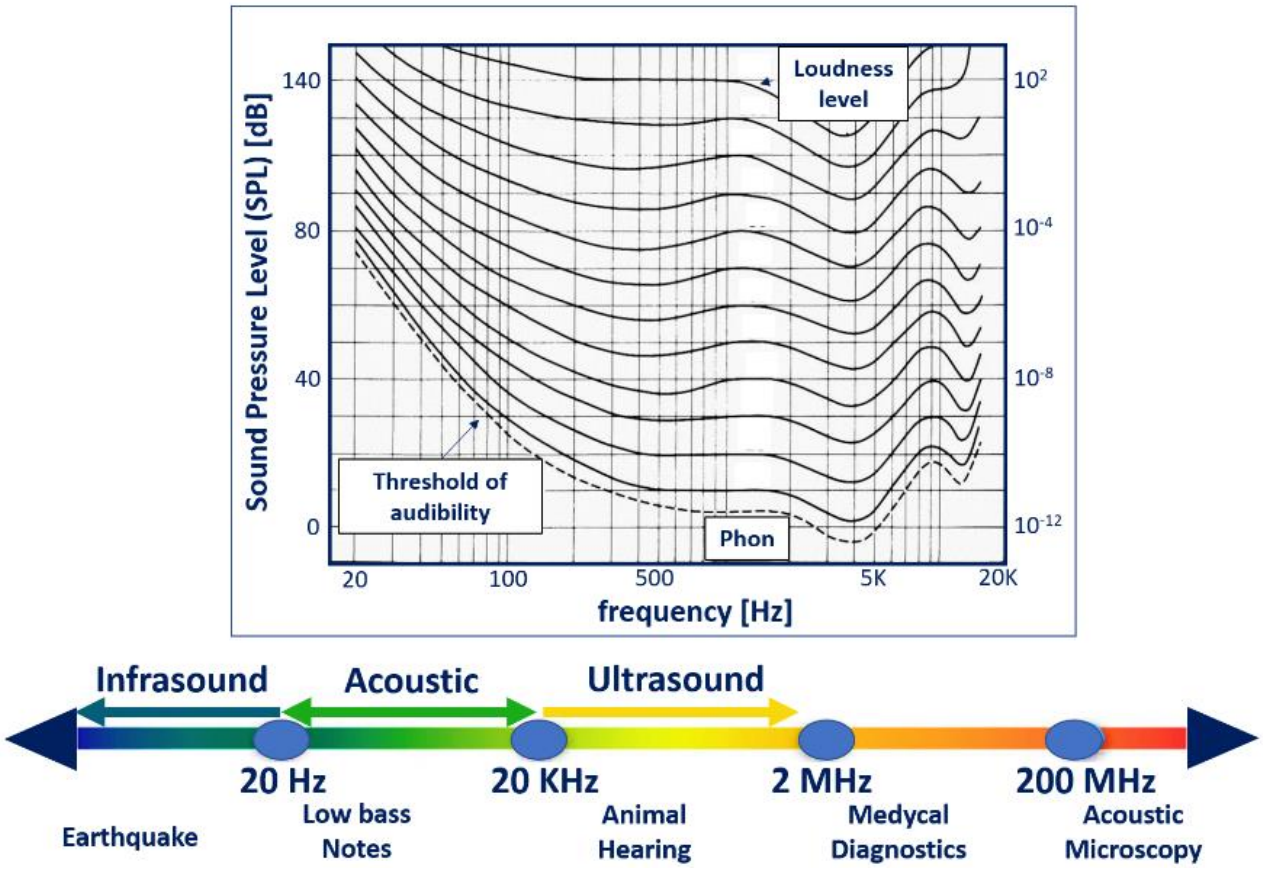

Figure 2.5. Field of audibility (upward). Sound range diagram (below), from infrasounds to ultrasounds. Acoustic waves perceived by human ear span, with a different weight, from 20 Hz to 20 KHz.

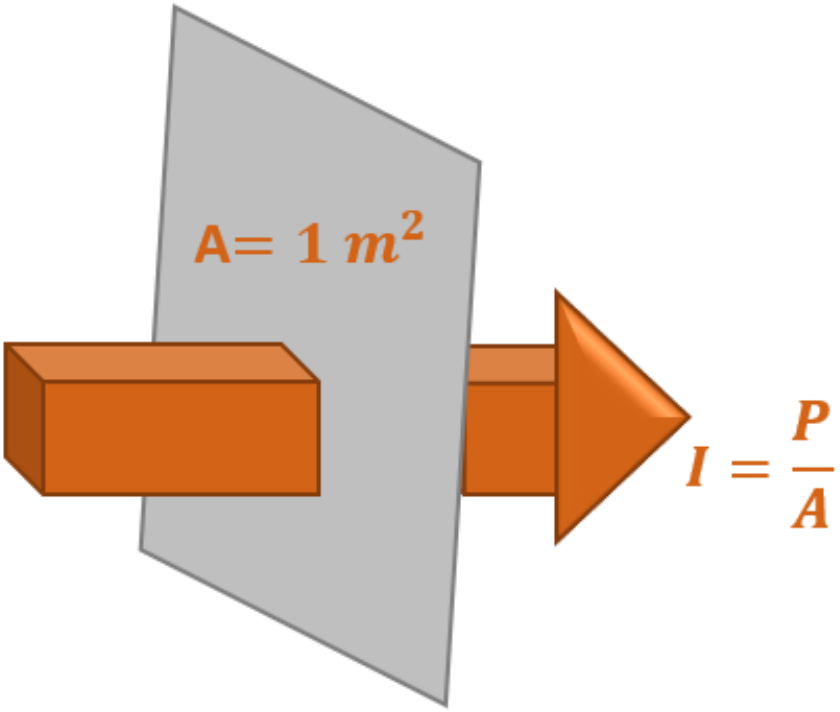

Figure 2.6. Intensity of a sound wave I that pass through a surface $A = 1\ m^2$.

The intensity of a sound wave I is the energy that it carries in the unity of time through a surface of 1 m^2 placed perpendicular to the direction of propagation of the wave (see Figure 2.6).

It is therefore a power per unit of surface and its measure unit is W/m^2:

$$I = \frac{E}{\Delta t \cdot A} = \frac{P}{A} \tag{7}$$

This definition adapts to any type of wave; from it derives an important property of the energy transmission through the waves. It is such as a small sound source that emits with the same intensity in all directions (isotropic source) and it considers the energy that flows inside a pyramid that has as vertex the source (see Figure 2.7).

From the definition of Ifollows: $I_1 = \frac{P}{A_1} = \frac{P}{l_1^2}$ and $I_2 = \frac{P}{A_2} = \frac{P}{l_2^2}$ from which it derives: $\frac{I_2}{I_1} = \frac{l_2^2}{l_1^2}$.

Figure 2.7 shows that the triangles of vertex O and basis l_1 and l_2 are similar, so derives that: $\frac{l_1}{l_2} = \frac{d_1}{d_2}$.

Substituting it in the previous equation it is possible to obtain: $\frac{I_2}{I_1} = \frac{d_1^2}{d_2^2}$ that is the inverse square law of distance.

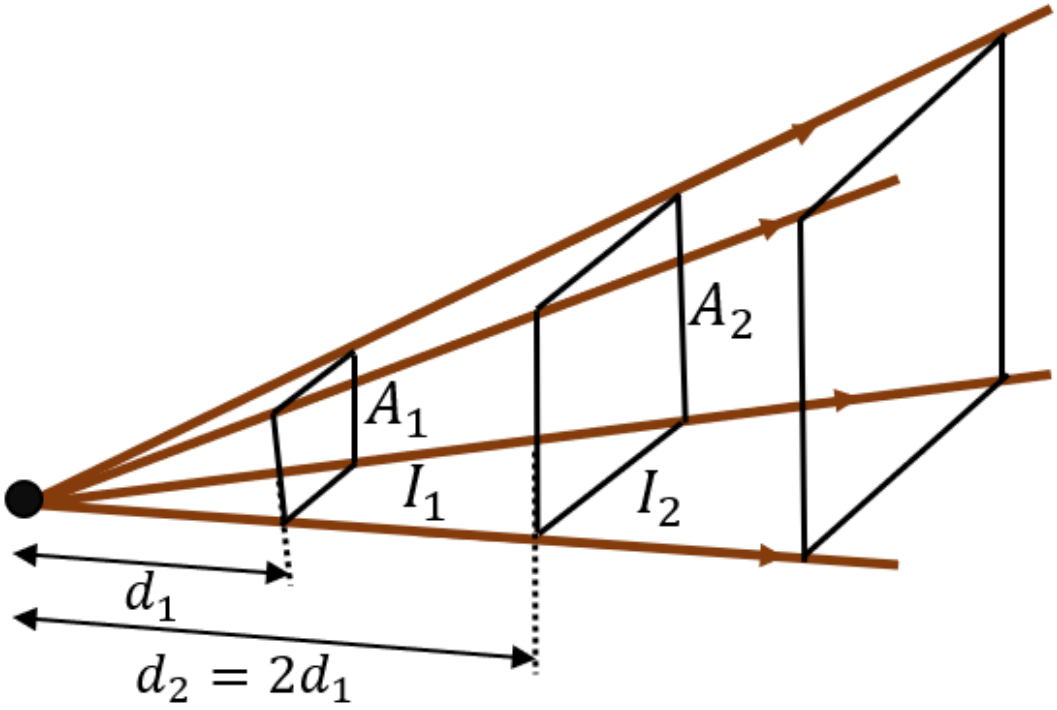

Figure 2.7. Wave propagation follows the inverse square law of distance.

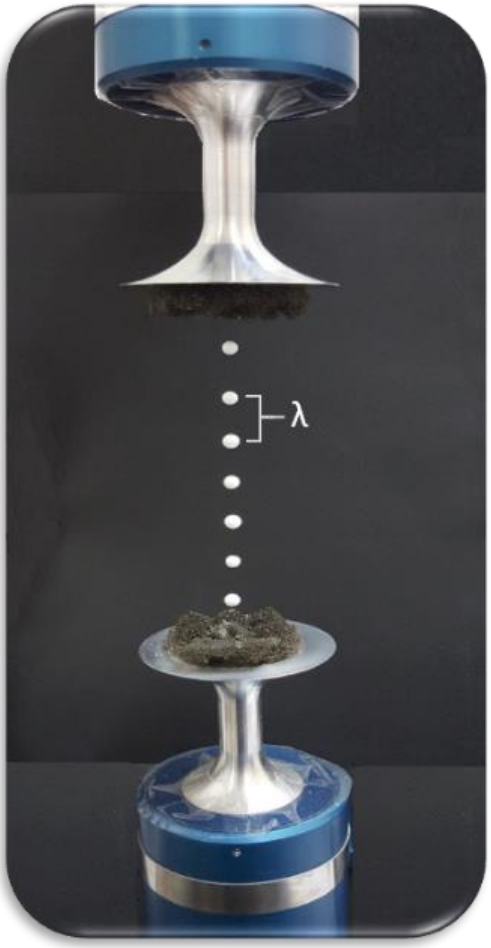

Figure 2.8. Standing waves in an acoustic levitator which furnish stable equilibrium locations for levitated particles.

Therefore, the wave intensity, emitted by an isotropic source, decreases with the inverse of the square of the distance from the source.

When an acoustic wave reflects off of a surface, the interaction between its compressions and rarefactions induces interferences, that can combine to create a standing wave. Standing acoustic waves have defined nodes, i.e., areas of minimum pressure, and antinodes, i.e., areas of maximum pressure. Figure 2.8 shows the stable equilibrium locations for levitated particles.

Two different kinds of waves are employed in acoustic levitation to generate acoustic radiation pressure, they are defined as traveling waves or Near-field Acoustic Levitation (NFAL) and standing waves or Standing Wave Acoustic Levitation (SWAL) (see Figure 2.9).

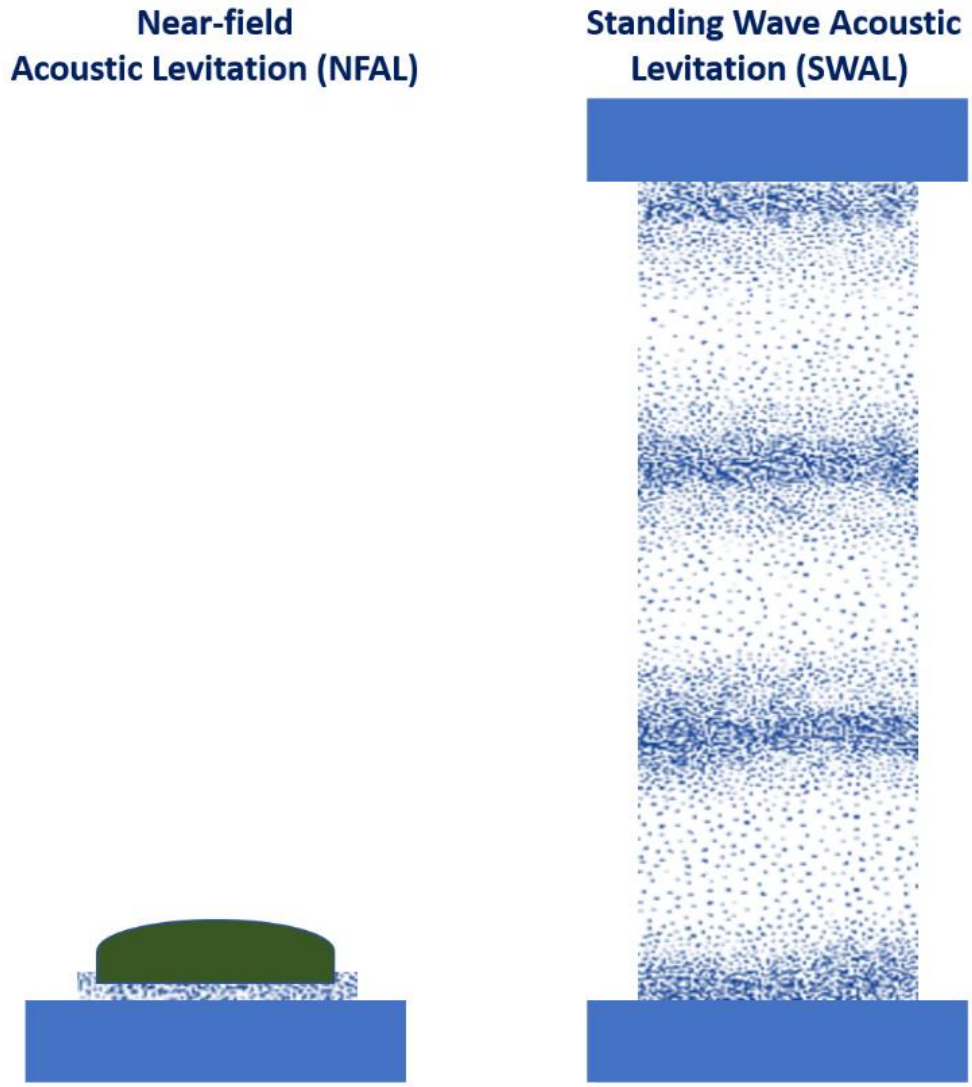

Figure 2.9. Two different kinds of waves are employed in acoustic levitation to generate acoustic radiation pressure: traveling waves or Near-field Acoustic Levitation (NFAL) (on the left) and standing waves or Standing Wave Acoustic Levitation (SWAL) (on the right).

The first ones propagate through a medium with transport of energy, the second are stationary waves, generated by two traveling waves, an incident and a reflected wave. They present pressure nodes, i.e.,

positions where the pressure is zero and antinodes, in which the pressure fluctuates between a maximum and minimum value.

In NFAL, samples are levitated and transported at a very small distance above a vibrating surface using ultrasonic Surface Acoustic Waves (SAW)s by means of squeeze film effects in near field.

In SWAL, small samples of different shape are levitated in pressure nodes. The acoustic radiation force limits the sample weight. A typical SWAL design, which has one transducer and one reflector, creates a standing wave as shown in Figure 2.10, where the acoustic radiation pressure balances the gravity.

Waves, produced by a transducer and a reflector present pressure nodes and anti-nodes along the blue vertical line. A sample is trapped at a pressure node because of the time-averaged forces of the acoustic radiation pressure. These forces at pressure antinodes push the object axially. The sample is located slightly below a pressure node due the gravitational force. In Figure 2.11, a representation of the acoustic force, the pressure wave and the acoustic potential is reported. The period of the pressure wave is the twice of that of the acoustic force wave.

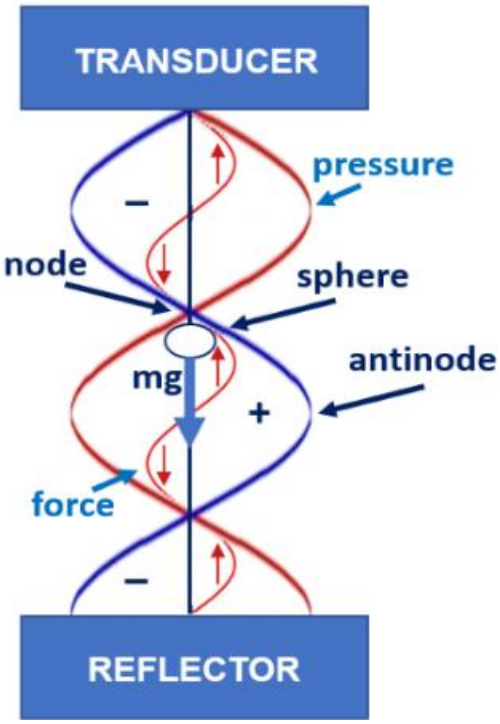

Figure 2.10. Particle suspended inside an acoustic levitator.

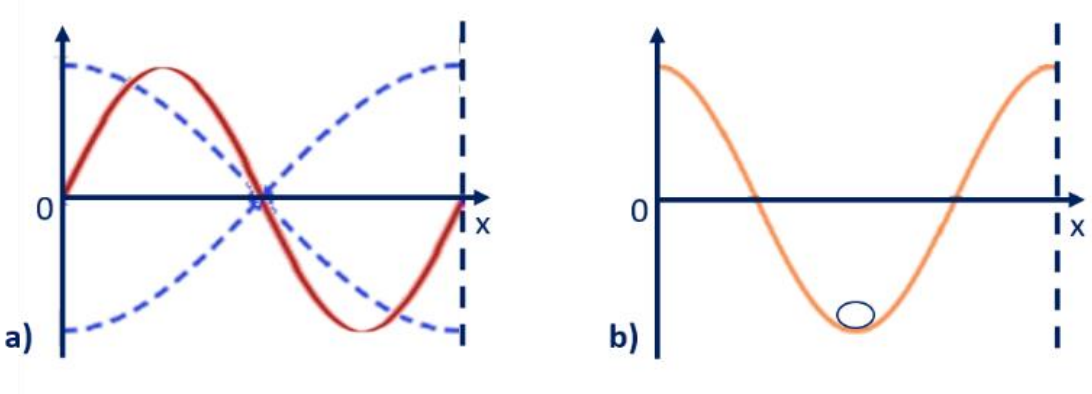

Figure 2.11. a) Sketch of the acoustic force (solid red line) and the pressure wave (dashed blue line) and b) the acoustic potential (solid orange line).

In an acoustic levitator, a standing wave is generated by a piezoelectric crystal which gives rise to a stationary acoustic radiation force when the distance between two transducers is an integral multiple of the half wavelength.

The transducers, made of aluminium alloy, are driven by piezoelectric drivers, inside an aluminium mounting tubes of 38 mm diameter. The nominal frequency of the transducers is 22 KHz. The distance of the two transducers is set to a nominal separation of 10 acoustic wavelengths, approximatively 150 mm. Two acoustic absorbing foam disks approximately 50 mm in diameter are glued onto the face of the transducer horns to reduce unwanted reflections that can cause instabilities in the levitated sample.

For a perfect gas, the equation of state, known as ideal gas law, is:

$$PV = nRT \tag{8}$$

In an adiabatic process, pressure P is a function of density ρ:

$$P = C\rho \tag{9}$$

where C is a constant.

Pressure and density can be divided into mean and total components: $C = \frac{\partial P}{\partial \rho}$:

$$P - P_0 = \left(\frac{\partial P}{\partial \rho}\right)(\rho - \rho_0) \tag{10}$$

The adiabatic bulk modulus for a fluid is defined as:

$$B = \rho_0 \left(\frac{\partial P}{\partial \rho}\right)_{adiabatic} \tag{11}$$

which give the result:

$$P - P_0 = B\left(\frac{\rho-\rho_0}{\rho_0}\right) \tag{12}$$

Condensation, s, is defined as the change in density for a given ambient fluid density.

$$s = \frac{\rho-\rho_0}{\rho_0} \tag{13}$$

The linearized equation of state becomes: $p = B_s$, where p is the acoustic pressure $(P - P_0)$.
The continuity equation for the conservation of mass is:

$$\frac{\partial P}{\partial t} + \frac{\partial}{\partial x}(\rho u) = 0 \tag{14}$$

where u is the flow velocity of the fluid. The equation can be linearized and the parameters can be divided into mean and variable components, as following:

$$\frac{\partial}{\partial t}(\rho_0 + \rho_0 s) + \frac{\partial}{\partial x}(\rho_0 u + \rho_0 s u) = 0 \tag{15}$$

Considering that ambient density changes with neither time nor position and that the condensation multiplied by the velocity is a very small number:

$$\frac{\partial s}{\partial t} + \frac{\partial}{\partial x} u = 0 \tag{16}$$

Euler's force equation for the conservation of momentum is:

$$\rho \frac{Du}{Dt} + \frac{\partial P}{\partial x} = 0 \tag{17}$$

where D/Dt is the convective, substantial or material derivative.

From the linearization of the variables:

$$(\rho_0 + \rho_0 s) + \left(\frac{\partial}{\partial t} + u\frac{\partial}{\partial x}\right)u + \frac{\partial}{\partial x}(P_0 + p) = 0 \tag{18}$$

Neglecting small terms, the equation becomes:

$$\rho_0 \frac{\partial u}{\partial t} + \frac{\partial p}{\partial x} = 0 \tag{19}$$

Considering the time derivative of the continuity equation and the spatial derivative of the force equation results in:

$$\frac{\partial^2 s}{\partial t^2} + \frac{\partial^2 u}{\partial x \partial t} = 0 \tag{20}$$

$$\rho_0 \frac{\partial^2 u}{\partial x \partial t} + \frac{\partial^2 p}{\partial x^2} = 0 \qquad (21)$$

and multiplying the first by ρ_0, subtracting the two and substituting the linearized equation of state, it becomes:

$$-\frac{\rho_0}{B}\frac{\partial^2 P}{\partial t^2} + \frac{\partial^2 p}{\partial x^2} = 0 \qquad (22)$$

The result is:

$$\frac{\partial^2 p}{\partial x^2} - \frac{1}{C^2}\frac{\partial^2 P}{\partial t^2} = 0 \qquad (23)$$

where $c = \sqrt{\frac{B}{\rho_0}}$ is is the speed of propagation.

The solution of eq. (22), can be found as:

$$p = p_0 \sin(kx) e^{-i\omega t} \qquad (24)$$

where p_0 is the pressure amplitude, $k = \omega / c_0$ the wave number, ω the angular frequency and a pressure node located at $x = 0$ is the boundary condition.

Spheres of different diameter and weight, can levitate in the pressure nodes; these nodes and anti-nodes appear at fixed points separated by a distance of $\lambda/2$. Knowing the frequency of the transducer, $f = 22KHz$ and the velocity sound, $v_s = 343\,{}^{m}/_{S}$ at the considered temperature $T = 22°C$, it is possible to determine the wavelength of the standing wave as it follows:

$$\lambda = \frac{v_s}{f} = \frac{343000}{22000} = 1{,}56cm \qquad (25)$$

In Figure 12, the forces that are responsible for compensating the gravitational force and that hold the sample in the pressure node, are sketched.

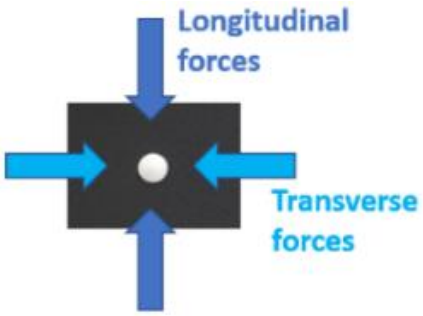

Figure 12. Levitation forces that are responsible for compensating the gravitational force and that are able to levitate the particle.

An object in the presence of a sound field will experience forces associated with the field. An acoustic force arises from the scattering of the sound wave by the body. In order to have an object suspended in the acoustic field, the acoustic force should counteract the gravity force, i.e., weight of the object.

2.2 Mechanical Models for Motion of an Acoustically Levitated Sphere

Two mechanical models will be introduced to study the damped oscillations and the motion of an acoustically levitated sphere around the node. They represent respectively longitudinal and transverse forces and are constituted by a mass-spring system and by a stretched string.

In principle, an acoustic levitator is a system in which a transducer produces an impulse, characterized by a wave-form that permits to a sample to levitate, but in unstable condition. It can be dealt as a mechanical equivalent model, constituted by a mass-spring system of elastic constant k, connected to a mass m (see Figure 2.13).

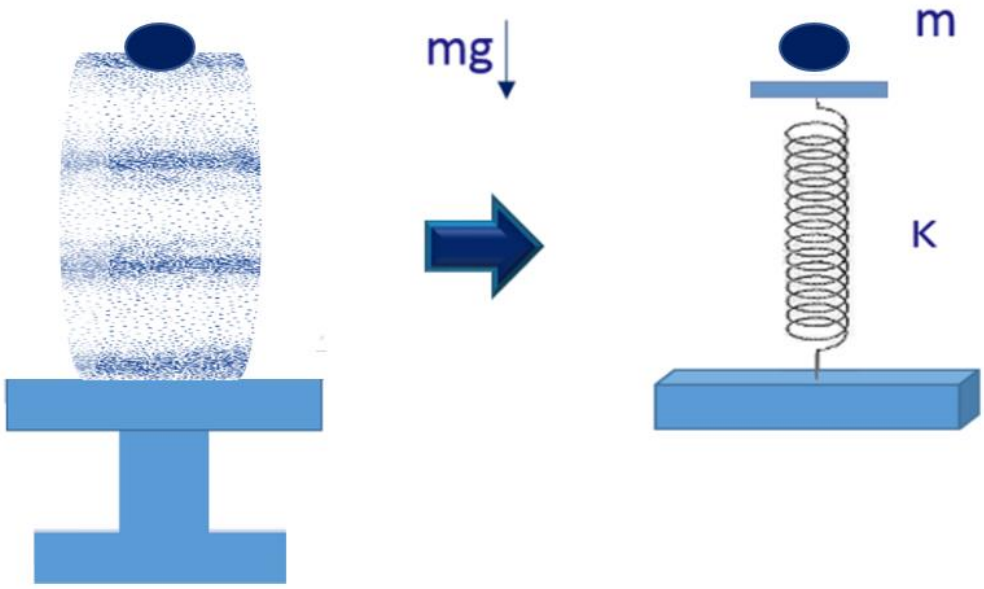

Figure 2.13. Mass-spring system of elastic constant k to study the damped oscillations of a mass around a node (longitudinal forces).

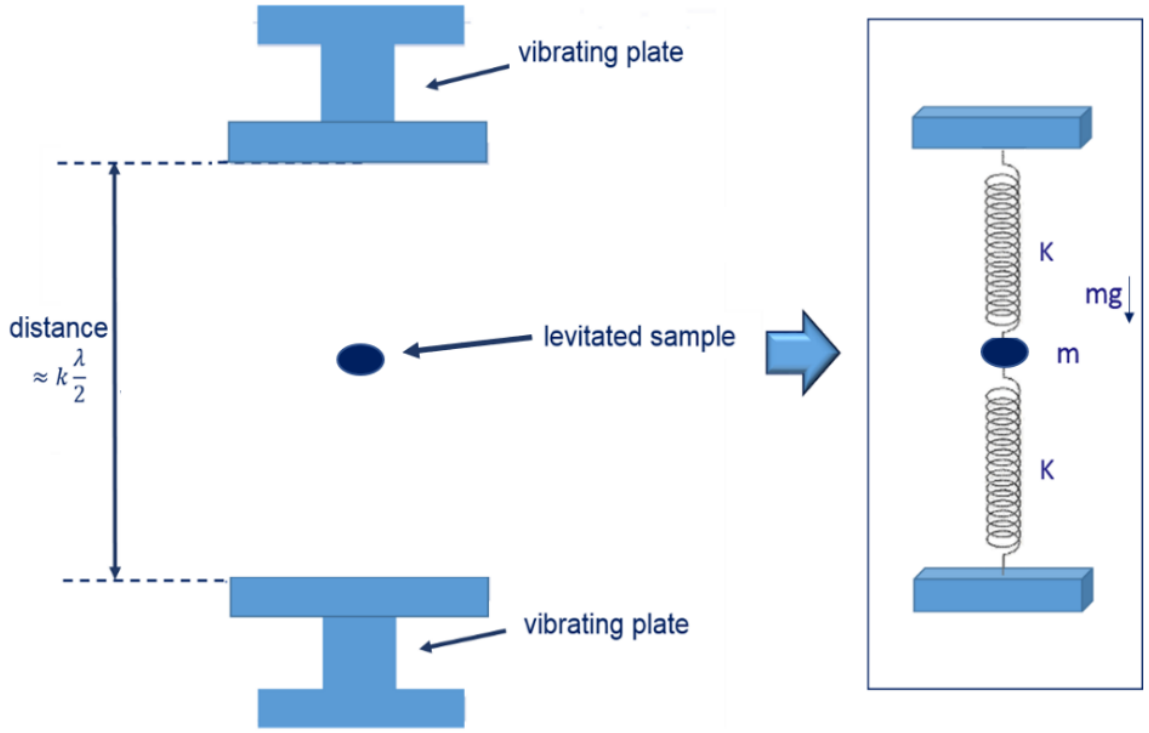

Figure 2.14. Mass-spring system of elastic constant $2k$ to study the damped oscillations of a mass around a node.

A mechanical model to study the damped oscillations of a mass around a node is constituted by two springs of equal elastic constant k, connected to the mass m and is shown in Figure 2.14.

The system can be simplified in a single mass-spring system of elastic constant 2k. The equation of the system is the following second-degree differential equation:

$$m\ddot{y} + +\gamma_L\dot{y} + 2kx = -mg \qquad (26)$$

in which m is the mass, γ_L the longitudinal damping coefficient, k the elastic constant, g the gravity acceleration, $F = -mg$ the force weight, y describes the position, $\dot{y}$ and $\ddot{y}$ are respectively the first and second derivate of y.

The solution of the equation is constituted by the sum of a solution in t, $y_h(t)$ and a particular solution, y_p:

$$\begin{cases} y_h(t) = A_L e^{-\frac{\gamma_L t}{2}} sin(\omega t + \varphi) \\ y_p = -\frac{mg}{2k} \end{cases}$$

with $\omega_L = \sqrt{\frac{2k}{m}}$ pulse or angular frequency, measured in [rad/s].

So, the solution of the equation became:

$$y(t) = A_L e^{-\frac{\gamma_L t}{2}} sin(\omega t + \varphi) - \frac{mg}{2k} \qquad (27)$$

The second mechanical model is employed to study the damped oscillations of a mass around the node (transverse forces, as shown in Figure 2.15.

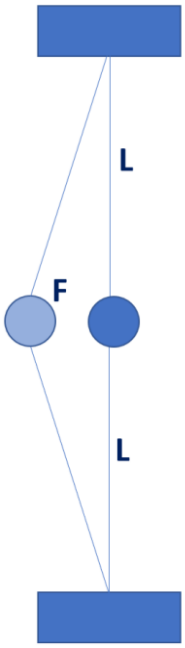

Figure 2.15. Stretched string to study the damped oscillations of a mass around a node.

Considering a mass m, connected to two equal stretched strings of length L, on which a tension T acts. If the mass is moved of a small step x in the horizontal direction, assuming that the tension T not varies appreciably, it is possible to obtain that the recall force is equal to: $F = -\left(\frac{2T}{L}\right)x$.

So, the equation of the system became in this case:

$$m\ddot{x} + +\gamma_T \dot{x} + \left(\frac{2T}{L}\right)x = 0 \qquad (28)$$

in which m is the mass, γ_T the transverse damping coefficient, k the elastic constant, T the tension on the two stretched strings, L the length, x describes the position, $\dot{x}$ and ẍ are respectively the first and second derivate of x. The solution of eq. (28) is:

$$x_h(t) = A_T e^{-\frac{\gamma_T t}{2}} sin(\omega t + \varphi) \qquad (29)$$

where for the pulsation is: $\omega_T = \sqrt{\frac{2T}{mL}}$.

2.3 EULER'S EQUATION APPROACH

Standing wave levitation approach takes in account a model which assumes enough small, incompressible and rigid sphere levitating in presence of acoustic standing wave. For fluid it assumes that effect of viscosity can be neglected and that barotropic relation p = f (ρ) holds. Because of our assumptions we can use Euler's equation:

$$\frac{\partial \vec{v}}{\partial t} + (\vec{v} \cdot \nabla)\vec{v} = -\frac{\nabla \mathrm{p}}{\rho} \tag{1}$$

assuming that the flow of fluid is irrotational, it is possible to express vector of velocity with gradient of scalar function ϕ (velocity potential): $\vec{v} = \nabla\phi$. Continuity equation holds:

$$\frac{\partial \rho}{\partial t} + \nabla \cdot (\rho \vec{v}) = 0 \tag{2}$$

which can be written as:

$$\frac{1}{\rho}\frac{\partial \rho}{\partial t} = \nabla^2 \phi \tag{3}$$

For a medium, such as air, in which from barotropic relation follows $\frac{dp}{d\rho} = f'(\rho) = const = c^2$ differential equation for ϕ exact to first order leads to wave equation for ϕ:

$$\nabla^2 \phi = \frac{1}{c^2}\frac{\partial^2 \phi}{\partial t^2}. \tag{4}$$

Eq. (1) can be written as

$$\nabla \dot{\phi} = \nabla \dot{\left(\int \frac{dp}{\rho} \right)} \tag{5}$$

from which follows non-stationary Bernoulli equation:

$$\dot{\phi} - \int \frac{dp}{\rho} = \frac{v^2}{2}. \tag{6}$$

For further derivation of integral $\int \frac{dp}{\rho}$ we expand barotropic relation into series in terms of factor $s = \frac{\rho - \rho_0}{\rho_0}$:

$$p = f(\rho_0 - s\rho_0) \approx f(\rho_0) + s\rho_0 f'(\rho_0) + \frac{1}{2}s^2 {\rho_0}^2 f''(\rho_0) + \cdots \tag{7}$$

From this expansion we can express *dp* and combine it with expression $\rho^{-1} \approx \rho_0^{-1}(1 - s + s^2 - \cdots)$.

Eliminating factor *s* and regarding $f(\rho_0) = p_0$, for pressure variation in the medium can be expressed:

$$\delta p = p - p_0 = \rho_0 \frac{\partial \phi}{\partial t} + \frac{\rho_0}{2c^2}\left(\frac{\partial \phi}{\partial t}\right)^2 - \frac{1}{2}\rho_0 v^2. \quad (8)$$

To get solutions for pressure variation it is need to calculate velocity potential from wave eq. (4). For that we need to take into consideration boundary conditions which of course sharply depend on geometry of the levitated object. Solution for ϕ from (4) will be oscillatory. For small spheres equality $\phi = |\phi| \cos(kh) \cos(\omega t)$ can be shown (h denotes position of levitated particle in z-direction). From definition of velocity potential and Bernoulli equation (6) it follows that pressure variation will also oscillate along distance between sound radiator and levitated object. It can be shown that force on enough small-levitated particle created in travelling waves is smaller for few orders of magnitude ($F \propto r_s^6$) than force created in stationary waves. This is why effect of travelling waves can be neglected. Acoustic force on a small, rigid sphere (model described before) in a standing wave is derived to be:

$$F = 8\pi r_s^2 (k r_s) \bar{E} sin(2kh) f\left(\frac{\rho_0}{\rho_s}\right). \quad (9)$$

It is expressed with wave number *k*, radius of sphere r_s, mean total energy-density of sound in a medium $\bar{E} = \frac{1}{2}\rho_0 k^2 |\phi|$, density of sphere ρ_s and so called relative density factor f which in case for stationary wave is defined as

$$f\left(\frac{\rho_0}{\rho_s}\right) = \frac{1 + \frac{2}{3}\left(1 - \frac{\rho_0}{\rho_s}\right)}{2 + \frac{\rho_0}{\rho_s}}. \quad (10)$$

Another different approach to derive force on small particle in standing wave field is with acoustic potential. The acoustic force is obtained from

$$\vec{F} = -\nabla U. \quad (11)$$

Expression for acoustic force, like (9), is of course the same, regardless which approach we use. Acoustic potential is often expressed in form

$$U = 2\pi r_s \left[f_1 \frac{\langle p_0^2 \rangle}{3\rho_0 c^2} - f_2 \frac{\rho_0}{2} \langle v_0^2 \rangle \right] \quad (12)$$

with $\langle v_0^2 \rangle$ and $\langle p_0^2 \rangle$ being time-averaged square of velocity and pressure of the acoustic wave, both considered in the point where levitated object is found. f_1 (monopole coefficient) and f_2 (dipole coefficient) are numerical factors given by

$$f_1 = 1 - \frac{\rho_0 c_0^2}{\rho_s c_s^2} \quad (13)$$

and

$$f_2 = \frac{2(\rho_0 - \rho_s)}{2\rho_s + \rho_0} \quad (14)$$

where again index 0 presents surroundings (medium) and index s particle (sphere). Eq. (12) can be presented with maybe more intuitive form:

$$U = V_s \left[f_1 \langle E_{pot} \rangle - \frac{3}{2} f_2 \langle E_{kin} \rangle \right] \tag{15}$$

with V_s as volume of a sphere and $\langle E_{pot} \rangle = \frac{1}{2\rho_0 c^2} \langle p_0^2 \rangle$ and $\langle E_{kin} \rangle = \frac{\rho_0}{2} \langle v_0^2 \rangle$ being averaged potential (of compressed medium) and kinetic (due motion of medium) energy density of acoustic wave.

Particle‘s equilibrium points are at $F_i = \frac{\partial U}{\partial x_i} = 0$. Acoustic force according to (11) depends on geometry of a chamber in which experiment is performed. With definition of acoustic potential (11) we can see that particle‘s tendency to minimal force can be seen as tendency to potential minima.

In presence of gravity, gravitational term has to be added to expression for acoustic potential (into (12) or (15)): $U = U_{acoustic} + U_{grav}$ where gravitational contribution is defined as

$$U_{grav} = (m_s - m_0) g h \tag{16}$$

where m_s and m_f are the mass of the sample and the mass of fluid, which is displaced because of presence of particle whereas h again denotes vertical position of particle.

By now viscosity of medium was neglected. This approximation is justified when there is no presence of rigid boundary in medium and wave attenuation is neglected. Otherwise viscous term $\eta \nabla^2 \vec{v}$ has to be added to Euler‘s eq. (1).

Because of viscosity acoustic attenuation is emerged, in other words, momentum of acoustic waves is transferred to the medium, resulting in net displacement of it (i.e. acoustic streaming) in space between boundaries. This net displacement creates gradient of streaming velocity and viscous force which acts as holding force. Hence, levitated object is considered stabilized.

Experimentally it was noticed that this streaming velocity is proportional to amplitude of sound radiator, by increasing amplitude, streaming velocity (and viscous force) also increases. In standing waves levitation, system different corrections are considered. Thickness of viscous boundary layer is defined as:

$$\delta = \sqrt{\frac{2\eta}{\rho_0 \omega}} \tag{17}$$

Expressed with η as coefficient of viscosity and ω frequency of sound. In standing wave levitation effect of viscosity can be neglected as long distances within a few δ are not reached. It can also be neglected for particles for which characteristic dimension exceeds characteristic dimension of viscous boudary layer ($rs >> \delta$). Since we consider model which assumes particles with $rs << \delta$ we have to regard viscous corrections.

Viscous corrections can be presented with numerical factors f_1 and f_2. Since viscosity does not affect pressure in medium but only velocity of its flow, only factor f_2 has to be redefined into

$$f_2 = \left(\frac{\rho_0}{\rho_s}, \frac{\delta}{r_s}\right) = f_2\left(\tilde{\rho}, \tilde{\delta}\right) = \frac{2(1-\gamma(\tilde{\delta}))(\tilde{\rho}-1)}{2\tilde{\rho}+1+3\gamma(\tilde{\delta})} \tag{18}$$

with factor $\gamma\left(\tilde{\delta}\right) = -\frac{3}{2}(1 + i(1 + \tilde{\delta}))\tilde{\delta}$ and taking only $Ref_2\left(\tilde{\rho}, \tilde{\delta}\right)$ in eq. (12). Contribution of viscous corrections depend on viscosity of medium, material of lifted particle and its diameter.

Acoustic levitation by standing wave has been employed for several different techniques. Main advantage of this approach is the fact that levitated object is isolated and it can not react with its surroundings any more. This is very desirable when studying or dealing with chemical reactions especially with the fact that levitated particle is easy reachable and available for handling. In physics isolating of sample is desirable when observing phase transitions, process of crystallization or to study the structure of proteins or nanoparticles. Similar use of standing wave levitation is in interesting experiment to isolate droplets of liquid and observe their evaporation process by illuminating droplet and determining its volume with help of shadows.

2.4 Surface Tension and Wettability in Complex Systems

Wettability is the feature of a solid to prefer to be in contact with one fluid rather than another and it describes the balance between adhesive and cohesive forces.

In a liquid, cohesive forces avoid contact with the surface, forming a spherical shape when all three phases, i.e. solid, liquid and gaseous, are in equilibrium, whereas between the liquid and the solid surface, adhesive forces cause the liquid to spread across the surface. If a surface of a material is attracted to a certain liquid, it is considered "-philic" for that substance; while a surface that tends to repel a certain liquid, is considered "-phobic".

Liquids possess different important properties like density, viscosity and surface tension; the latter is the only property thanks to which a solid having greater density than that of a liquid can float on to the surface of the liquid. Also the shapes of the drop are governed by the property of surface tension. More specifically, the surface tension value depends by the purity of certain liquids. Liquids are distinguished from gases, because they exhibit a free separation surface, that acts like a stretched thin membrane and possesses certain mechanical properties due to cohesion between molecules.

The property to show the tendency of contracting and then that force acting on the surface of a liquid and that tends to minimize the surface area it affects physical properties such as wettability, is defined surface tension.

In this framework, the conjunction use of acoustic levitation and InfraRed (IR) spectrocopy offers a valid approach to determine the surface tension value. It is fundamental to isolate a single drop suspended in the air and to observe the physical and chemical changes. Furthermore, it allows

obtaining very high concentrations of mixtures starting from solutions, impossible to achieve without the use of levitation.

In a liquid, the drop shape is ideally determined by surface tension; each molecule is pushed equally in all direction by neighboring molecules, then the resulting force is equal to zero. Unlike internal molecules of the bulk, the superficial molecules not present neighboring molecules in every direction to provide a balanced net force, but they are pushed inward by the neighboring molecules, creating an internal pressure, as showed in Figure 1a. So the liquid voluntarily contracts its surface area to maintain the lowest surface free energy.

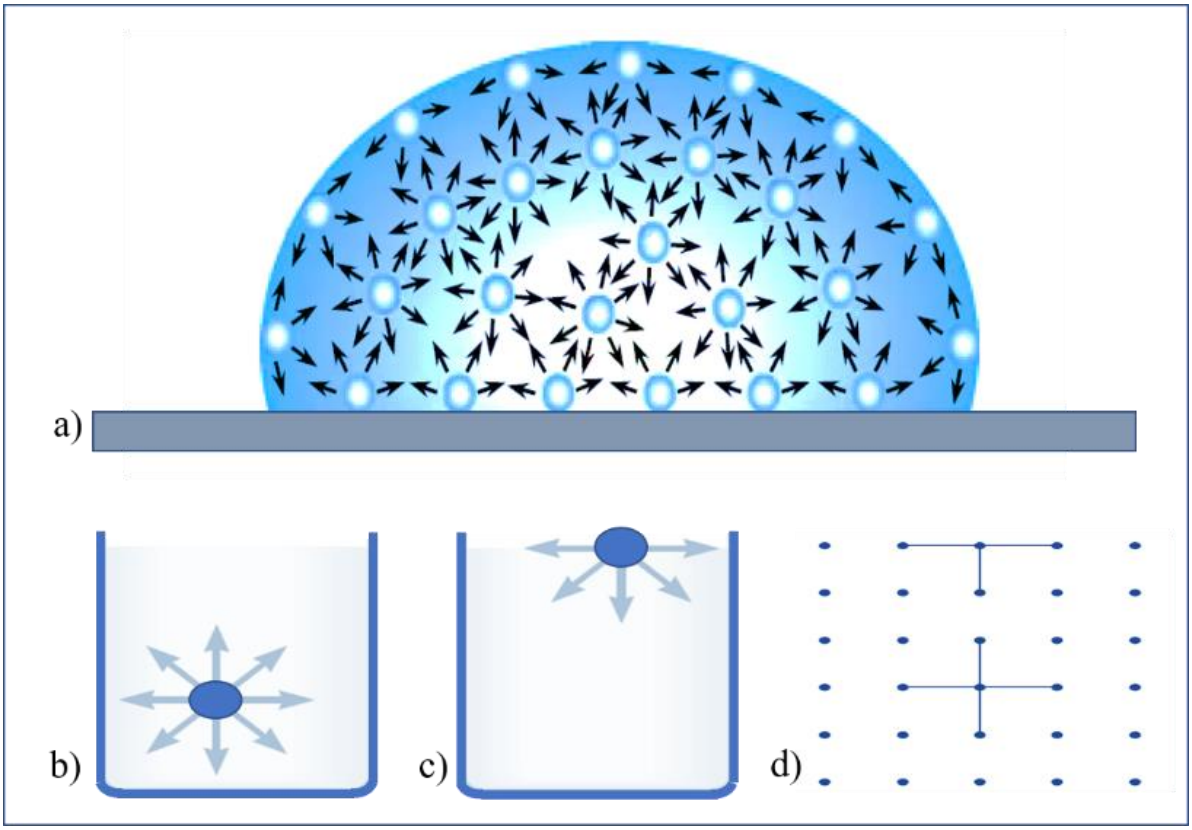

Figure 2.16. Molecules in a liquid a) Molecules in a zoom of a liquid drop, in which the surface tension is determined by the unbalanced forces of liquid molecules at the surface; b) a molecule in a liquid is surrounded on sides by other molecules that attract it equally in all directions with a net force equal to a zero; c) a molecule in the surface suffers a net force toward the interior, due to the absence of molecules above this surface; d) cross section of a primitive three-dimensional model of a molecule interfacing to vacuum.

More specifically, as showed in the below part of Figure 2.16, it is considered a molecule in a liquid, surrounded on sides by other molecules that attract the central molecule equally in all directions with a net force equal to a zero (Figure 2.16b), a molecule in the surface (Figure 2.16c) and a cubic grid, in which the molecules are located, with length equal to the molecular separation length, i.e. L_{mol}.

In Figure 2.16c, the absence of molecules above the surface, causes a net attractive force toward the interior. This force causes the liquid surface to contract toward the interior until repulsive collisional forces from the other molecules stop the contraction at the point in which the surface area is a minimum. If the liquid is not influenced by external forces, the sample forms a sphere, with minimum surface area for a given volume.

From a mathematical point of view, looking at figure 1d, each molecule has six bonds to its neighbours in the interior, while only five on surface, for which considering a total binding energy ε of a molecule, a surface molecule is linked for $\frac{5}{6}\varepsilon$. The missing binding energy corresponds to adding an extra positive energy $\frac{1}{6}\varepsilon$ for each surface molecule, therefore the binding energy can be calculated as $\varepsilon \approx h \cdot m$, where h is the specific heat of evaporation and $m = M_{mol}/N_A = \rho L_{mol}^3$ the mass of a single molecule, in which M_{mol} is the molecular mass, N_A the Avogadro's number and ρ the density. Dividing the molecular surface energy $\frac{1}{6}\varepsilon$ with the molecular area scale L_{mol}^2, it is possible to obtain the surface energy density or surface tension γ:

$$\gamma \approx \frac{\frac{1}{6}\varepsilon}{L_{mol}^2} \approx \frac{1}{6}\frac{h \cdot m}{L_{mol}^2} \approx \frac{1}{6} h \cdot \rho \cdot L_{mol} \qquad (1)$$

where ρL_{mol} is the effective surface mass density of a layer of thickness L_{mol}.

The apparatus, shown in Figure 2.17, is employed to furnish a simpler definition of surface tension.

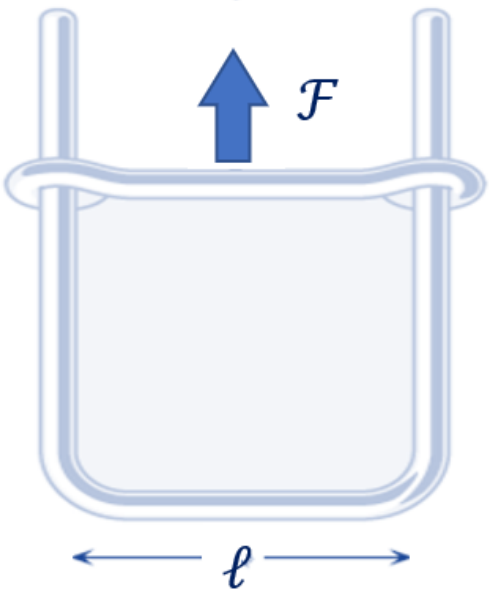

Figure 2.17. C-shaped wire frame, employed to furnish a simpler definition of surface tension. It is constituted by a frame on which is placed a wire that can slide with negligible friction, containing a thin film of liquid and can be employed to measure the surface tension of a liquid.

It is constituted by a C-shaped wire frame on which is placed a wire that can slide with negligible friction, containing a thin film of liquid. It can be also employed to measure the surface tension of a liquid. From this example, it is possible to notice how it is necessary a force $\mathcal{F}$ to move the slider to the right and extend the liquid surface that is contracted because of the surface tension.
This surface tension (γ), measured in $N \cdot m^{-1} = J \cdot m^{-2}$, can be defined as the force $\mathcal{F}$ per unit of length over which it acts, as expressed in the following equation:

$$\gamma = \frac{\mathcal{F}}{L} \qquad (2)$$

$L = 2\ell$ is a total length, where ℓ is the length of the slider and $\mathcal{F}$ acting force.

From a general point of view, the sign of γ depends on the strength of the cohesive forces holding molecules of a sample together compared to the strength of the adhesive forces between the opposing molecules of the interfacing samples.
If the surface tension of two liquids is negative, a large amount of energy can be released by maximizing the area of the interface, so the two fluids are mixed thoroughly instead of being kept separate. An example is that of alcohol and water. Immiscible fluids, such as oil and water present instead a positive surface tension that makes them seek towards minimal interface area with maximal smoothness.

2.5 MEASUREMENTS METHODS

STALAGMOMETRIC METHOD

Different measurement methods for surface tension determination are generally employed, the most common is the stalagmometric method. It consists in the measurement of weight of several liquid drops that leak out of the glass capillary of a stalagmometer (Figure 2.18). If the weight of each drop is known, it is also possible to count the drops number which leaked out for the surface tension measurement. The drops are formed slowly at the tip of the glass capillary placed in a vertical position; the pendant drop at the tip starts to break away when its weight reaches that value balancing the surface tension of the liquid.

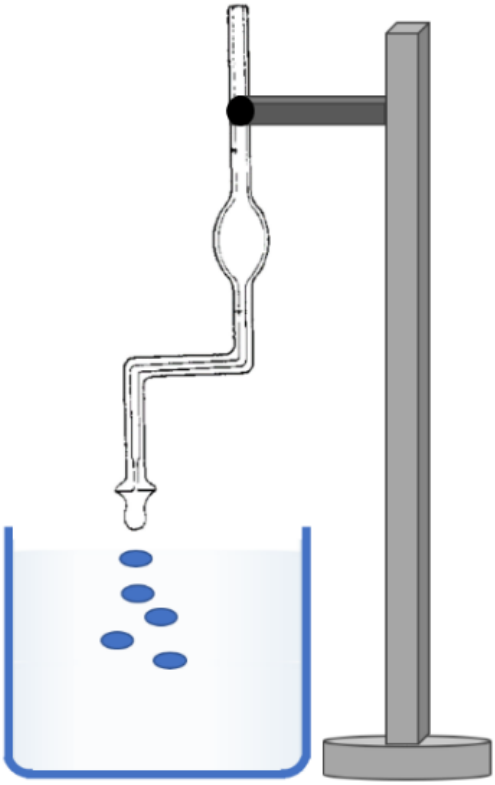

Figure 2.18. Stalagmometer instrument to determine surface tension in a liquid sample.

In practise, after having determined the water and sample mean drops number, the surface tension of this latter can be calculated as following:

$$\gamma = \gamma_0 \cdot \frac{n_0}{n} \cdot \frac{\rho}{\rho_0} \qquad (3)$$

where γ_0, n_0 and ρ_0 are the surface tension, the drops number and the density of the water, respectively, while n and ρ the drops number and the density of the sample. Each equation is calculated for a given temperature.

In order to calculate the density ρ it is possible to employ the picnometer method. After having determined the weight of the used picnometer m_1, of the water m and of the investigated sample m_2, calculated at the different temperatures, the density ρ can be calculated from the following equation:

$$\rho = \rho_0 \cdot \frac{m - m_1}{m_2 - m_1}. \qquad (4)$$

CAPILLARY RISE METHOD

Capillary rise method is the oldest method employed for surface tension determination. A capillary is a thin tube made of glass, within which there is a liquid that moves up because of a consequence of the surface tension appearance at the liquid/gas interface. From this phenomenon it is possible to

determine the surface tension value. More in detail, a thin circular capillary is dipped into the tested liquid, if the interaction forces of the liquid with the capillary walls are stronger than those between the liquid molecules, then the liquid wets the walls and rises in the capillary to a defined level and the meniscus is hemispherically concave. In the opposite situation the forces cause decrease of the liquid level in the capillary below that in the chamber and the meniscus is semispherically convex. Figure 2.19 shows the both cases.

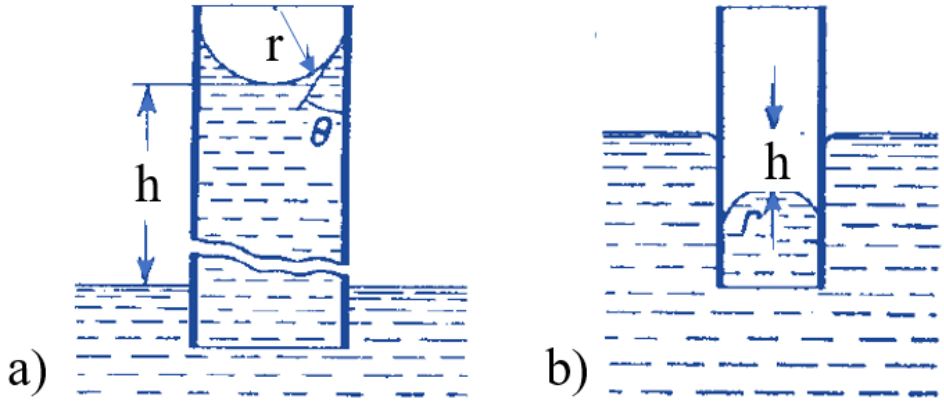

Figure 2.19. Capillary rise method representation to determine the surface tension value. a) A thin circular capillary is dipped into the tested liquid, if the interaction forces of the liquid with the capillary walls are stronger than those between the liquid molecules, then the liquid wets the walls and rises in the capillary to a defined level; b) in the opposite case, the forces cause decrease of the liquid level in the capillary below that in the chamber.

In the case in which the cross-section area of the capillary is circular and the radius is sufficiently small, it is possible to deduce that the meniscus is semi spherical. Furthermore, along the perimeter of the meniscus, acts a force f_1 because of the surface tension:

$$f_1 = 2\pi r \cdot \gamma \cdot \cos(\theta) \qquad (5)$$

where r is the capillary radius, γ the liquid surface tension and θ the wetting contact angle.
The force f_1 is equilibrated by the mass of the liquid raised in the capillary to the height h, that is the gravity force f_2. In the case of non-wetting liquid, it is lowered to a distance h, the f_2 is calculated by:

$$f_2 = \pi r^2 \cdot hdg \qquad (6)$$

where d is the liquid density, measured in g/cm^3, and g is the acceleration gravity.

In equilibrium, it is necessary that $f_1 = f_2$ and hence follows:

$$2\pi r \cdot \gamma \cdot \cos(\theta) = \pi r^2 \cdot hdg \qquad (7)$$

so:

$$\gamma = \frac{rhdg}{2\cos(\theta)}. \qquad (8)$$

If the liquid completely wets the capillary walls the contact angle $\theta = 0°$, that means $\cos(\theta) = 1$.

In such a case the surface tension can be determined from the following equation:

$$\gamma = \frac{rhdg}{2}. \qquad (9)$$

FLAT PLATE METHOD AND CONTACT ANGLE

Wettability studies usually involve a direct contact angles measurement to identify the wettability degree due to the interaction between a solid and a liquid. From a general point of view, small contact angles, i.e. ≪90°, correspond to high wettability, whereas large contact angles, i.e. ≫90°, to low wettability.

Contact angle measurements furnish an important parameter, that is the surface tension, which quantifies the wettability characteristics of a material.

It is considered a liquid drop on a flat, horizontal surface, the contact angle can be defined as that angle formed by the intersection of the liquid-solid interface and the liquid-vapor interface. The interface where solid, liquid, and vapor co-exist is referred to as the "threephase contact line". Figure 2.20 shows how it is possible to observe a small contact angle when the liquid spreads on the surface, while a large contact angle when the liquid beads on the surface.

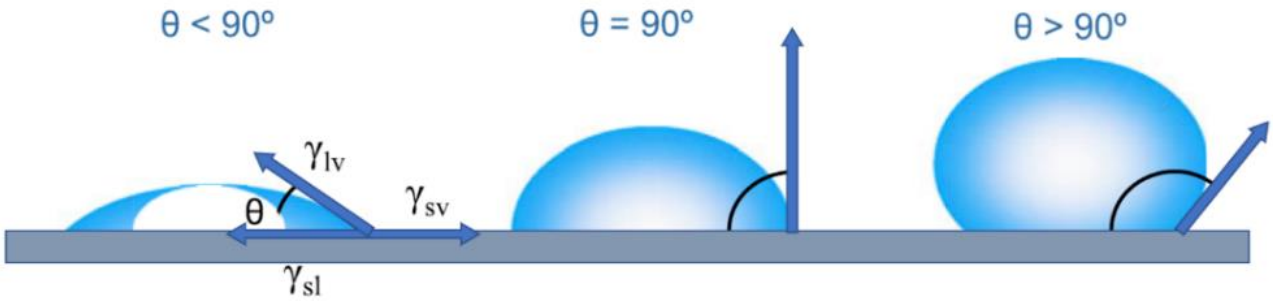

Figure 2.20. Sketch of contact angles formed by liquid drops on a flat plate.

More in detail, a contact angle less than 90° indicates that wetting of the surface is favorable, and the fluid will spread over a large area on the surface; while contact angles greater than 90° generally means that wetting of the surface is unfavorable so the fluid will minimize its contact with the surface and form a compact liquid droplet. This intermolecular force to contract the surface is called surface tension, and it is responsible for the shape of liquid droplets.

Theoretically, the contact angle is expected to be characteristic for a given solid-liquid system in a specific environment.

Contact angle of a liquid drop on an ideal solid surface is defined by the mechanical equilibrium of the drop under the action of three interfacial tensions, usually referred to as Young's equation:

$$\gamma_{lv} \cdot \cos(\theta) = \gamma_{sv} - \gamma_{sl} \qquad (10)$$

where γ_{lv}, γ_{sv} and γ_{sl} represent the liquid-vapor, solid-vapor, and solid-liquid interfacial tensions respectively, and θ is the contact angle.

From Young's equation, the three thermodynamic parameters γ_{lv}, γ_{sv} and γ_{sl}, determine a single and unique θ. However, there are metastable states of a drop and the observed contact angles are usually not equal to θ.

The wettability phenomenon is more than just a static state; in fact, the liquid moves to expose its fresh surface and to wet the fresh surface of the solid in turn. In this case, the measurement of a single static contact angle to characterize wetting behaviour is no longer adequate.

TILTED PLANE METHOD AND DYNAMIC CONTACT ANGLE

If the three-phase contact line is in motion, the contact angle is named dynamic contact angle and the employed method to determine surface tension is that of the tilted plane. More in detail, the dynamic contact angles are precisely two: the advancing contact angle θ_a and the receding contact angle θ_r. The first is formed by the expansion of the liquid, while the second by the contraction.

These angles belong to a specific range, with the advancing angles tending to a maximum value θ_{max} and the receding angles to a minimum value θ_{min}.

The difference between the advancing angle and the receding angle is called Hysteresis (H):

$$H = \theta_{max} - \theta_{min}. \qquad (11)$$

Dynamic contact angles at a low speed, should be equal to the measured static contact angle. The measurement of H furnishes an approach of evaluation of the substrate surface quality. A tilted plane method (Figure 2.21) was introduced to obtain both advancing and receding contact angles by tilting the solid surface until the drop just begins to move.

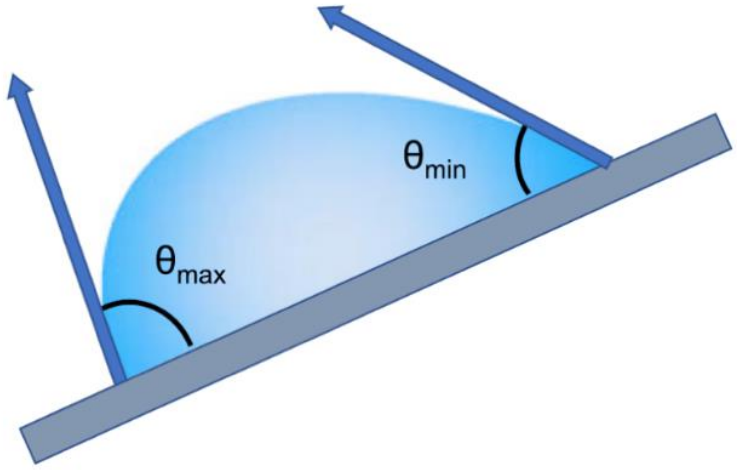

Figure 2.21. Tilted plane method for surface tension measurement.

The contact angles obtained at the lowest point θ_{max} and the highest point θ_{min} are considered as the advancing and receding contact angles, respectively.

The surface tension can be calculated as the inversion of the H coefficient:

$$\gamma = \frac{1}{H} = \frac{1}{\theta_{max} - \theta_{min}}. \qquad (12)$$

INVESTIGATED SAMPLES

1. ETHYLENE-GLYCOL (EG) AND POLYETHYLENE-GLYCOL (PEG) AQUEOUS SOLUTIONS

EG, chemical formula: HO-CH_2-CH_2-OH, and PEG, chemical formula: HO-$(CH_2$-CH_2-$O)_m$ H are colorless, low-volatility, low viscosity and hygroscopic substances. The first is fully miscible in water and its hydroxyl give rise to a wide variety of derivatives, while the seconds are used as an inactive ingredients in the pharmaceutical industry as solvent, plasticizer, surfactant, ointments, and suppository base, tablet and capsule lubricant. PEGs are considered inert (they do not react with other materials). They has low toxicity with systemic absorption less than 0.5%.

The study includes ancillary surface tension and density data determinations of aqueous solutions of EG and PEGs, with molecular weights of 200, and 600 in water, in the 293-338 K temperature range and at atmospheric pressure.

EG and PEGs with number-average molecular weights of 200 and 600, manufactured by Aldrich-Chemie were used in this study. Double-distilled water was used in making the solutions. The investigated systems were aqueous solutions as a function of weight fraction, i.e. ϕ = (grams of EG or PEG)/(grams of EG or PEG + grams of H_2O), at values of concentration for EG of ϕ=0.00, 0.50, 0.60 and 0.80, while for PEG200 and PEG600 at a weight fraction of ϕ= 0.50. The solutions were prepared by mass, using an analytical balance with ± 0.01mg accuracy. PEGs are hydrophilic oligomers or polymers synthesized from ethylene oxide, its formula is HO-$(CH_2$-CH_2-$O)_n$-H, with 'n' that indicates the average number of oxyethylene groups. These polymers are synthesized in a wide range of molecular weights; a defined PEG chain size and molecular weight are called monodispersed polymers, while polydispersed, when there is a Gaussian distribution of chain lengths and molecular weights. So far a significant experimental material has been accumulated on the properties of PEG aqueous solutions, obtained by inelastic light diffusion [54], incoherent neutron dispersion [55] etc.

The benefits of PEGs are due to the possibility to chemically attack many reactive functional groups to the terminal sites of the polymer. They are easily miscible with water at the liquid state, but less soluble in the solid state, with their solubility that decrease with the increases of the molecular weight.

Furthermore, other important characteristics of these polymers are their biocompatibility, the high structure flexibility, the amphiphilicity, low toxicity, solubility in water and their lubricating properties.

Table 2 reports the infrared adsorption frequencies and assignments of PolyEthyleneOxide (PEO) in the crystalline and molten states (3, 4, 7) with vs: very strong; s: strong; m: medium; w: weak; sh: shoulder. “trans” and “gauche” indicate – CH_2 – CH_2 – groups.

The wide range of PEGs provides flexibility in choosing properties to meet the requirements of many different applications, particularly in pharmaceuticals, cosmetics and foodstuffs, the physiological safety of the PEGs is of crucial importance. All polyethylene glycols, in combination with other products, are employed in cosmetics products, such as toothpastes, moisturizers, shampoos, breath fresheners and mouthwashes, including anti-plaque and antiseptic mouth rinses (listed in Table 3). They are also used to keep all ingredients in solution and increase the shelf life and stability of the products.

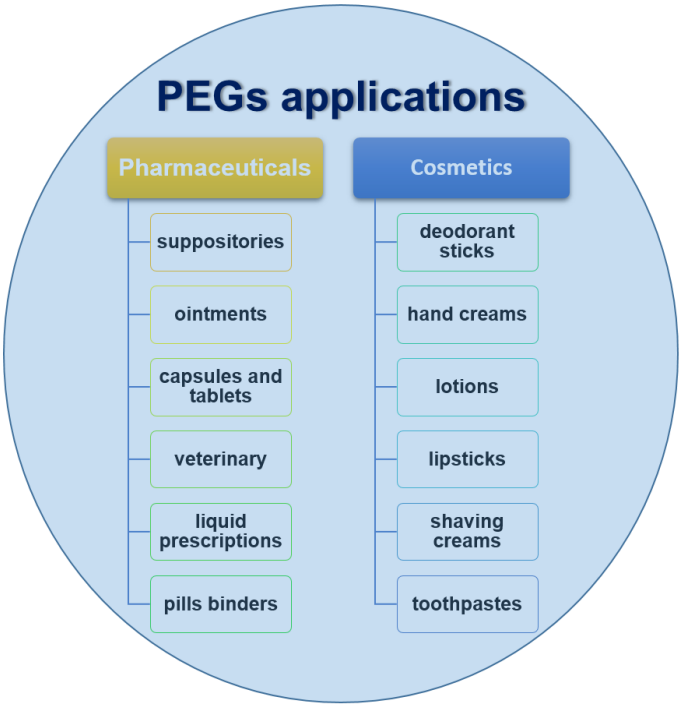

Figure 3: Pharmaceuticals and cosmetics PEGs applications. They are also used to keep all ingredients in solution and increase the shelf life and stability of the products.

Poly-Ethylene Glycols (PEG)s and their aqueous solutions are interesting systems both for the scientific point of view and for the practical applications. They react with other materials and has low toxicity with systemic absorption less than 0.5%. Thanks to their colorless, low-volatility, low viscosity and hygroscopic substances, they are used as protectant.

PEGs [83-123] with number-average molecular weights of 200 and 600 Da, manufactured by

Aldrich-Chemie, were investigated. Double-distilled water was used in making the solutions. In particular, the investigated systems were aqueous solutions as a function of PEG weight fraction, i.e. ϕ = (grams of PEG)/(grams of PEG + grams of H_2O), at values of concentration of ϕ=0.50. The solutions were prepared by mass, using an analytical balance with ± 0.01mg accuracy. PEGs are hydrophilic oligomers or polymers synthesized from ethylene oxide, its formula is HO-(CH_2-CH_2-O)$_n$-H, with 'n' that indicates the average number of oxyethylene groups. These polymers are synthesized in a wide range of molecular weights; a defined PEG chain size and molecular weight are called "monodispersed polymers", while "polydispersed", when there is a Gaussian distribution of chain lengths and molecular weights. So far a significant experimental material has been accumulated on the properties of PEG aqueous solutions, obtained by inelastic light diffusion [54], incoherent neutron dispersion [138-143] etc.

The benefits of PEGs are due to the possibility to chemically attack many reactive functional groups to the terminal sites of the polymer. They are easily miscible with water at the liquid state, but less soluble in the solid state, with their solubility that decrease with the increases of the molecular weight. Furthermore, other important characteristics of these polymers are their biocompatibility, the high structure flexibility, the amphiphilicity, low toxicity, solubility in water and their lubricating properties.

2. Disaccharides Aqueous Solutions: Trehalose, Sucrose and Maltose Mixtures

The investigated samples are diluted aqueous solutions of trehalose (known as α-D-glucopyranosyl-α-D glucopyranoside) and of sucrose (known as α-D-glucopyranosyl- β-D-fructofuranose) in a concentration range of 50% water and 50% pure sample, with a chemical structure shown in Figure 2.

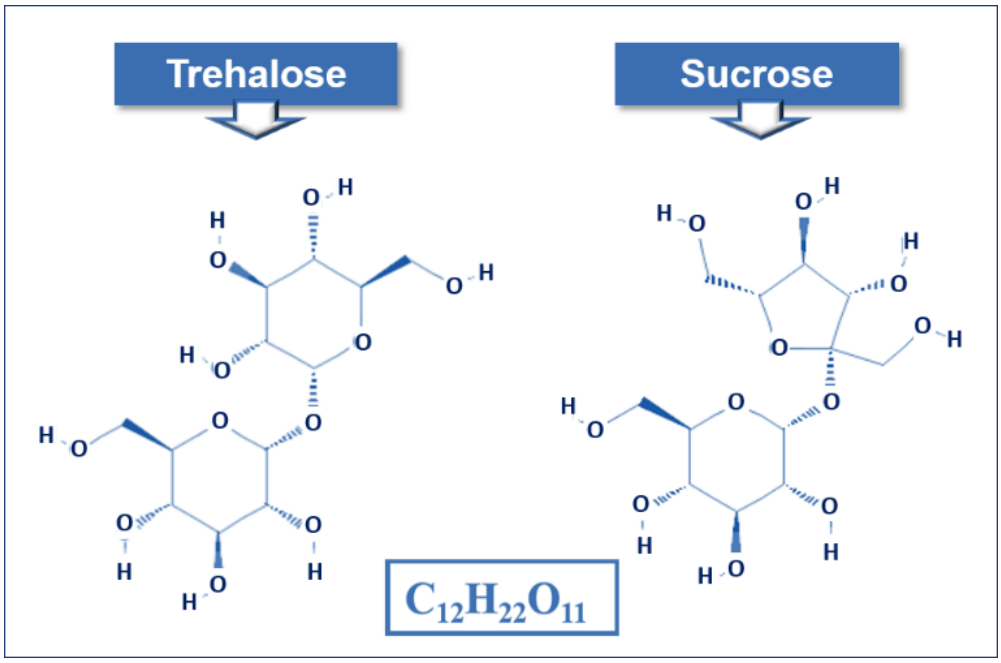

Figure 2. Molecular structure of trehalose, also known as α-D-glucopyranosyl-α-D glucopyranoside and sucrose, known as α-D-glucopyranosyl- β-D-fructofuranose. They have the same molecular formula $C_{12}H_{22}O_{11}$ and same molecular weight of 342.30 g/mol.

Trehalose is a not reducing disaccharide of glucose, due to the linkage that occur between the two-glucopyranose rings at the reducing end of the glycosylic residues, while sucrose is a disaccharide of D-fructose and D-glucose connected at their reducing groups. By understanding the particular interplays that occur between sugars, water and biological systems, it is possible to explain the reason for which disaccharides are good protectants. Furthermore, from the study of the properties of different sugars, it is possible to know the reason for which some disaccharides are more valid than others. In this context, trehalose and sucrose are the most widely employed disaccharides to stabilize the biological materials, such as cells, proteins and membranes. They have the same chemical formula ($C_{12}O_{11}H_{22}$) and molecular weight of 342.30 g/mol, but different structures. In fact, trehalose owns two symmetrical connected glucose rings, while sucrose only a rigid fructose ring. From a general point of view, sucrose is one the most studied sugars over the last hundred years, as evidenced by the famous work published in 1906 by Einstein about the Brownian motion. A large number of studies

on the effects of sucrose have been carried out for over a hundred years and this number continues to grow each year. Several recent empirical studies have examined the thermo-physical properties and the structure of aqueous solutions of trehalose and sucrose, proving the benefits obtained by the addition of these two disaccharides to biological systems, besides the hydrogen-bonding capabilities. Comparisons of their relative efficacy have often found trehalose to be the more effective protectant. Notwithstanding the abundance of data and the extraordinary bioprotective and osmoregulative properties of trehalose are well empirically defined, the underlying molecular mechanisms remain cryptic and the understanding of this disaccharide remains inadequate.

MATERIALS AND METHODS

1. ACOUSTIC LEVITATOR

Acoustic levitation of droplets is a new tool for containerless material processing. It is employed in studies of drying processes and as theoretical model testing, in addition to the directly measure performed by means of a video camera.

In particular, the levitation device, shown in figure 3, is composed by a levitation apparatus, an ultrasonic power amplifier, an acoustic controller circuit and a video camera. The levitation apparatus, placed inside a preconditioned process chamber for the moisture and temperature control, is constituted by two transducers, mounted on a rigid vertical axis in opposite position, generating two standing acoustic waves of 22 KHz. They can levitate liquid droplets in each node formed by the conjunction of the two sinusoidal waves, thanks to a pressure gradients and interferences. The acoustic waves are generated by a piezoelectric crystal, which gives rise to a stationary acoustic radiation force, irradiated by the transducers, when the distance between them is an integral multiple of the half wavelength. Furthermore, two acoustic absorbing foam disks are glued onto the face of each transducer to reduce instabilities in the levitated sample. The droplet is introduced in the middle of the transducers using a micropipette injection. The ultrasonic power amplifier, consisting of a capacitive load for the two transducers, variable as function of frequency and it is powered by a power supply of ± 40 V. There is also an oscilloscope to monitor the amplitude of the waves and to measure the current to the transducers. The acoustic controller circuit, furnishes the drive signal to the ultrasonic power amplifier. It hooks the resonant frequency of the transducers with a phase lock loop and maintains near zero the phase angle between the drive current and the voltage. Finally, a video camera is employed for video recordings and images and for the sample positioning. It also allows the diameter determination by a direct monitoring. The second device of the instrumental set-up is an IR Spectrometer Vertex 70v, by Bruker Optics. It operates in conjunction with the levitator to collect absorption spectra in an off-line status. The spectra are constituted by 128 interferograms, ensuring a spectral resolution of 4 cm^{-1} and each spectrum is corrected for atmospheric water background, baseline and area normalization. Furthermore, a toughbook PC is employed for recording all video, images and data and for measuring the diameter, throughout a specific software.

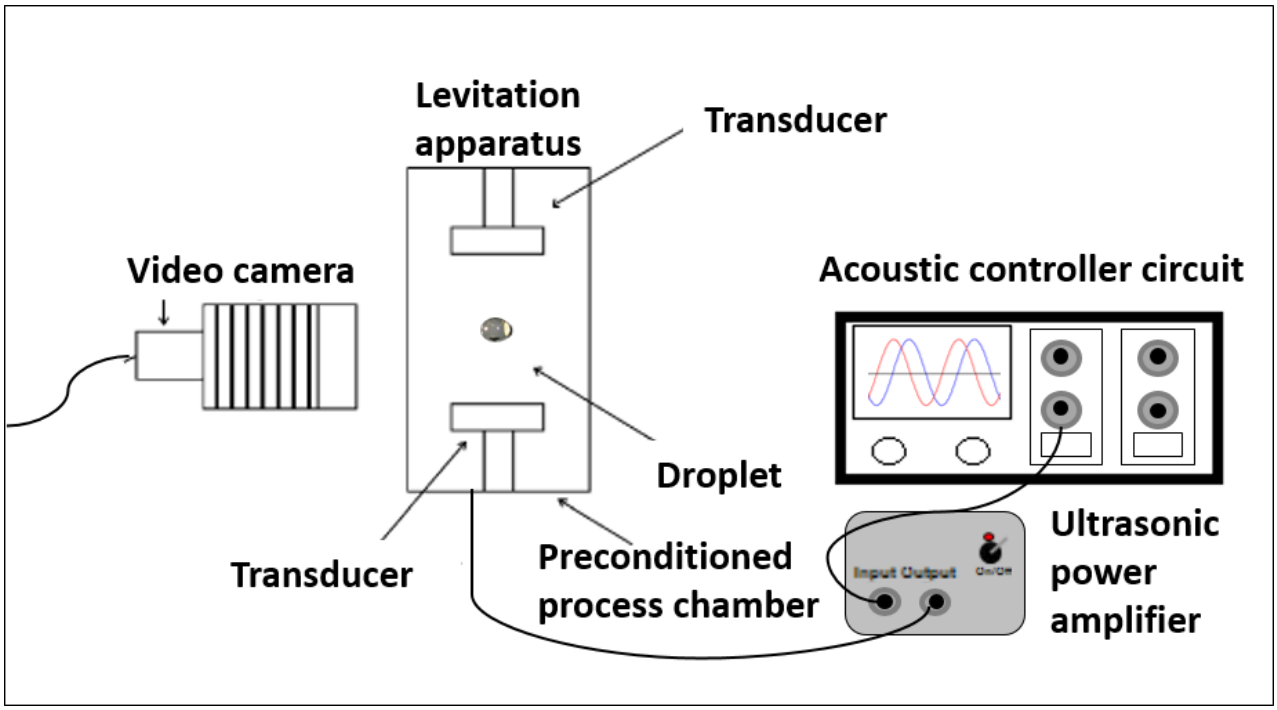

Figure 3: Levitation device scheme, constituted by a levitation apparatus, placed inside a preconditioned process chamber, an ultrasonic power amplifier, an acoustic controller circuit and a video camera.

The measurement of the droplet diameter as a function of time, i.e. the drying process of a single levitated droplet within of an acoustic levitator, can be performed with three different procedures: a mathematical theoretical formulation and a direct measurement. More specifically, the theoretical formulation is the one already discussed in section 1.1. The direct measurement consists in a monitoring of the droplet in time with a video camera, connected to a PC that records and measures the droplet dimensions in real time.

Fig. 3 reports the acoustic levitation system. It has dimensions of 30 x 45 x 60 cm, a total weight of 30 Kg, works at sound pressure levels lower than 160 dB and has a transducers distance of 15 cm.

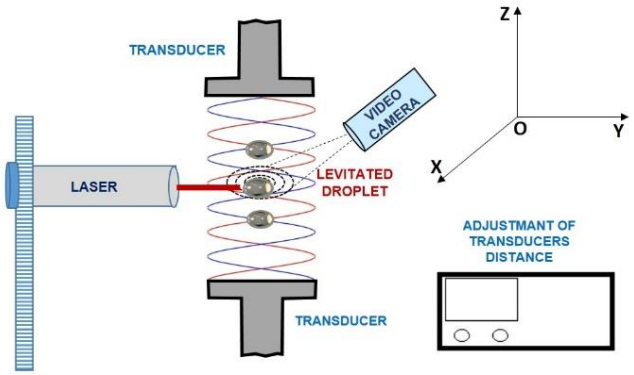

Figure 3. Single-axis Acoustic Levitator (SAL) system. A direct droplet diameter evaluation was performed by a video camera and a laser pointer.

RESULTS AND DISCUSSION

1. EXPERIMENTAL RESULTS FOR THEORETICAL MODEL TESTING FOR DISACCHARIDES SOLUTIONS

The drying process theoretical model is tested by a direct measurement, performed on disaccharide solutions that were analyzed as substances with high solubility in water in order to achieve a high solid content in the sample solutions. The solubility of the disaccharide in water is ca. 200g/100ml at 25°C. In this study, the investigated systems were trehalose and sucrose aqueous solutions, manufactured by Sigma-Aldrich, as a function of disaccharide weight fraction percentage. The solutions were prepared by mass, using an analytical balance with ± 0.01mg accuracy. Levitated solutions were also analyzed in this study. Double-distilled water was used in making the solutions.

Surface tension measurements were carried out using a standard thermostated stalagmometer, calibrated with distilled water (σ = 72.8 mN/m at T = 20°C). A constant temperature bath was used to control the temperature of the solutions to an accuracy of ± 0.1°C. Density measurements were performed by standard picnometer technique. Measurements for each solution were repeated four times. The surface tension of a liquid mixture is an important property, which plays an important role in affecting the mass and heat transfer at the interface.

Droplets of 1.5 mm of radius were inserted into the pressure node of the sound field using a micropipette injection. The Sound Pressure Level (SPL) was set up between 155 and 160 dB and the experiments were performed three times.

The direct measurement was performed by means of a Hitachi KP-HD20A video camera, with a resolution of 1944 H x 1092 V (2.1 megapixels), studying the D^2 vs t data of trehalose and sucrose aqueous solutions as a function of time, that follow a linear trend for 20 minutes, showing an ability to avoid total water evaporation since a percentage of water is strongly bonded with the disaccharide. The agreement between the two data-set is satisfactory. Finally, by using density data it is possible to determine the diameter evolution as a function of time and hence to test the D^2 versus time law of the drying process theoretical model.

Figure 6 shows the D^2 (t) curve of trehalose (on the left) and of sucrose (on the right) aqueous solutions. In particular, a linear decrease of the radius squared until the critical point appears where a crust form. The transition is not a sharp break, but changes over a long time form a bend in the curve.

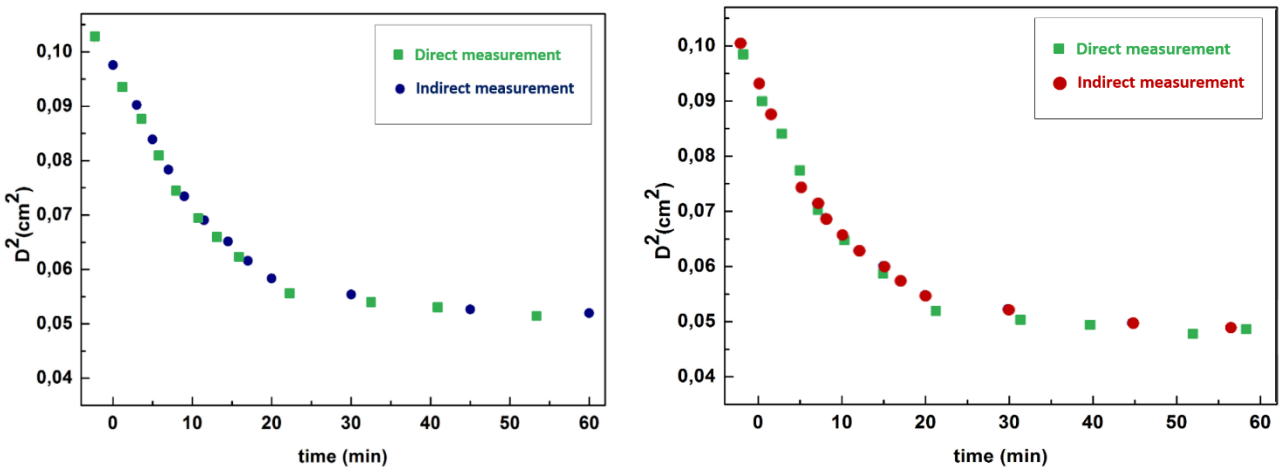

Figure 6: Drying behaviour of trehalose (on the left) and of sucrose (on the right) solutions droplets at 25°C dependent on the disaccharide content (D^2(t)). The blue points represent the trend of indirect measurement, while the green points, the trend of the direct measurement, that are in accord.

The experimental results show as, both in the case of trehalose and sucrose aqueous solutions, the drying model prediction is in accord in the first trend. The variation of the droplet diameter, as a function of time, is equal both in the theoretical model, that in direct and undirect measurement.

The experimental findings, obtained by the two independent employed approaches, reveal, for both the samples, a good agreement with the theoretical model previsions for the initial time trend. Furthermore, they furnish a value of the surface tension which is higher for trehalose in respect to sucrose.

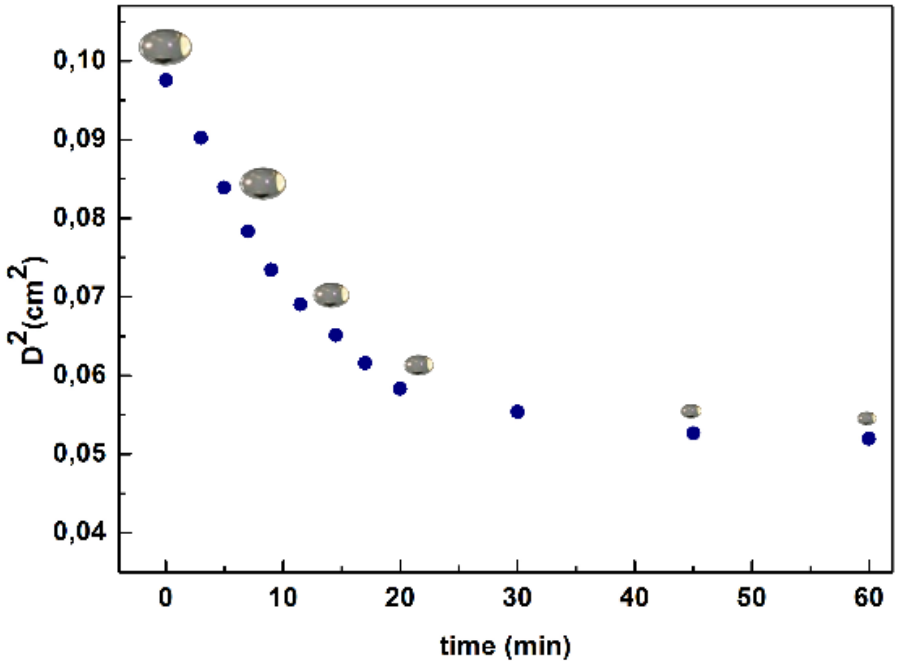

Figure 7. Measured D^2-Law as a function of time. Droplets: diameter values as evaluated by means of the video camera. Blue dots: diameter values as evaluated by a video camera monitoring. As it can be seen D^2 versus t decreases linearly in in the initial stage.

Figure 7 reports the D^2 data, droplets as a function of time, obtained by a direct measure with a video camera. As it can be seen, D^2 vs t follows a linear trend for about 20 minutes, reaching a plateau at longer time.

This result shows how trehalose is able to avoid total water evaporation since a percentage of water is strongly bonded with the disaccharide. Such a property plays a key role in bio-protection.

In conclusion, the experimental results for testing a theoretical model describing the drying process of an acoustically levitated droplet of a solution following an approach was reported. In particular, the so-called D^2 versus time law was tested on trehalose and sucrose aqueous solutions. The theoretical model showed experimental evidence both for the diameter determination, performed by the direct monitoring with the video camera. It was shown how acoustic levitation allowed to explore a wide disaccharide concentration range and to test the dependence of the diameter law as a function of lag time, i.e. D^2 versus time. By these analyses, it emerged that the behaviour of D^2 vs t follows a linear trend for about 20 minutes, reaching then a plateau at longer time. The result shows that trehalose is more able to avoid total water evaporation than sucrose, this result showed that trehalose owns more protectant properties. Furthermore, they furnished a value of the surface tension which is higher for trehalose in respect to sucrose. The study of trehalose is particularly important for a better understanding of extremophiles, organisms that can survive in harsh conditions. It is shown how acoustic levitation allows to explore a wide disaccharide concentration range and to test the

dependence of the diameter law as a function of lag time, i.e. D^2 versus time. By these analyses, it emerges that the behaviour of D^2 vs t follows a linear trend for about 20 minutes, reaching then a plateau at longer time. The result is confirmed by the experimental results, showing that trehalose is able to avoid total water evaporation, this property being essential forable to survive under extreme environmental conditions thanks to the synthesis of trehalose. These extreme environments are characterized, for example, by high aridity, very hot and low temperatures, high salinity and high values of pH. Just to report some example, the *Atacama Desert* (Chile, USA), is one the most arid place on Earth, with a year average rain fall lower than 0.08 mm, where it is possible to find *Selaginella lepidophylla*; such a plant adapts itself to a condition of prolonged òt in this environment. Another extreme environment is furnished by the *Death Valley* (USA), this region holding the record for the World highest air temperature equal to 56.7 ° C in July 1913; concerning the extremophiles that are present in this extreme environment, it is possible to mention *Bacillus Vallismortis* which ferments trehalose.

The obtained results put into evidence that trehalose molecules are capable to strongly bond themselves to water molecules, so avoiding water evaporation under high temperature and drought conditions.

2. Experimental Results for Mechanical Models for Motion of an Acoustically Levitated Sphere

The results of the damped oscillations of an acoustically levitated sphere of 4 mm of diameter and 2,19 mg of weight are discussed in this section. The measurements were performed, considering for the two transducers an instrument (SAL™ Materials Development Inc.) *Amplitude control*, A, ranging between 3,5 and 6,25 and a frequency of 22 KHz. In the following, only the study with A equal to 6 is reported. The initial amplitude of the oscillation was set-up by approaching the sphere with a wood stick.

Figure 16 shows the measured signal and the fitting result performed by using the following formula:

$$s(t) = 0.7e^{-2.5t}\sin(2\pi \cdot 6.289t) \qquad (30)$$

As it can be seen from the figure, significative oscillations occur within about 1,56 s; these oscillations are to be connected with the acoustic transverse forces.

In order to investigate the dependence of oscillation frequency on the instrument *Amplitude control*, A, different measurements were performed by varying A between 3.50 and 6.25. The results are reported in Figure 17.

Finally, a dynamic measure was performed by varying in time the instrument *Amplitude control*, A, and hence the pulsation of the signal. Figure 18 shows the time behaviour of $\omega(t)$.

In order to analyze the frequency variation of the registered signal, in the following we perform a comparative Fourier and Wavelet analysis [163-172].

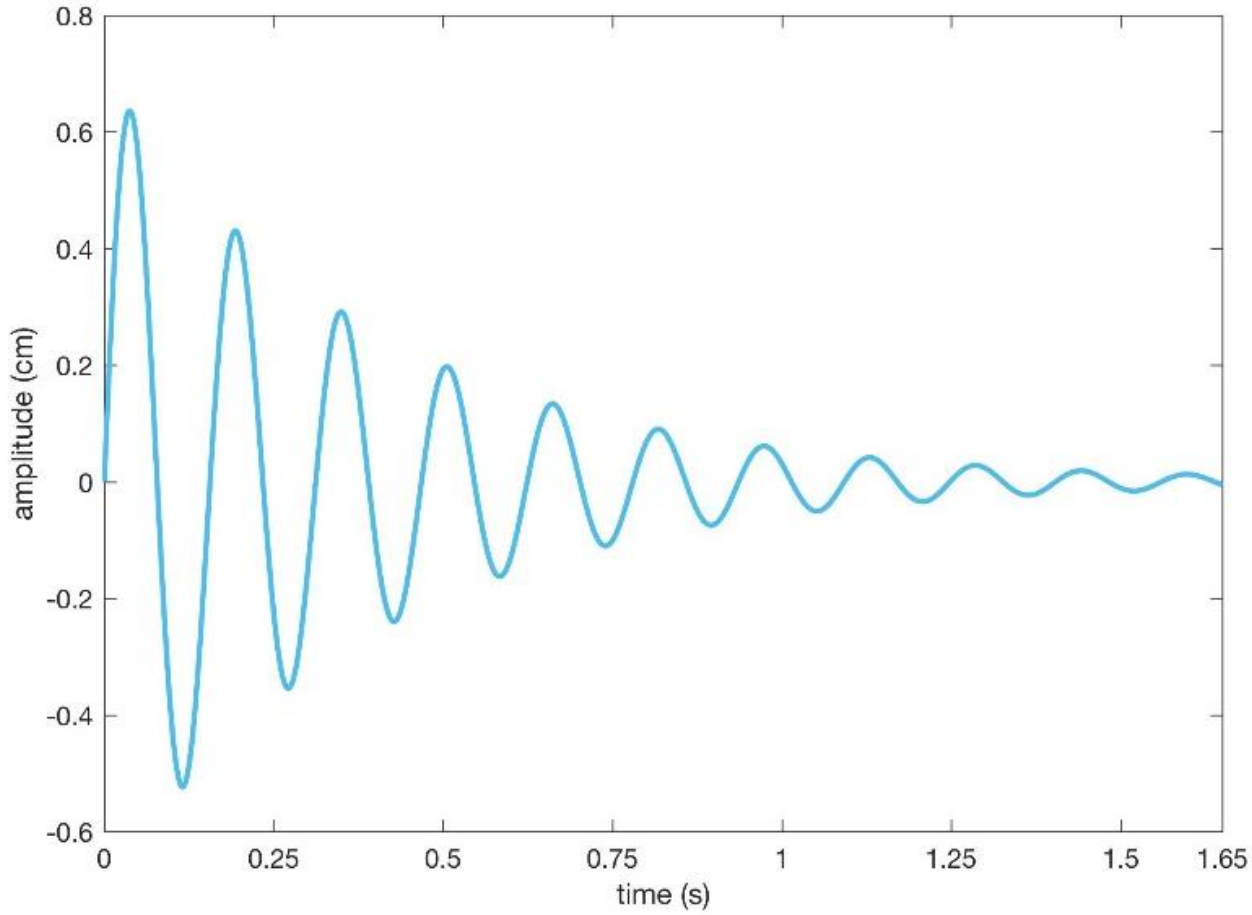

Figure 16. Registered signal of the transversal motion of an acoustically levitated sphere of 4 mm of diameter and 2,19 mg of weigh.

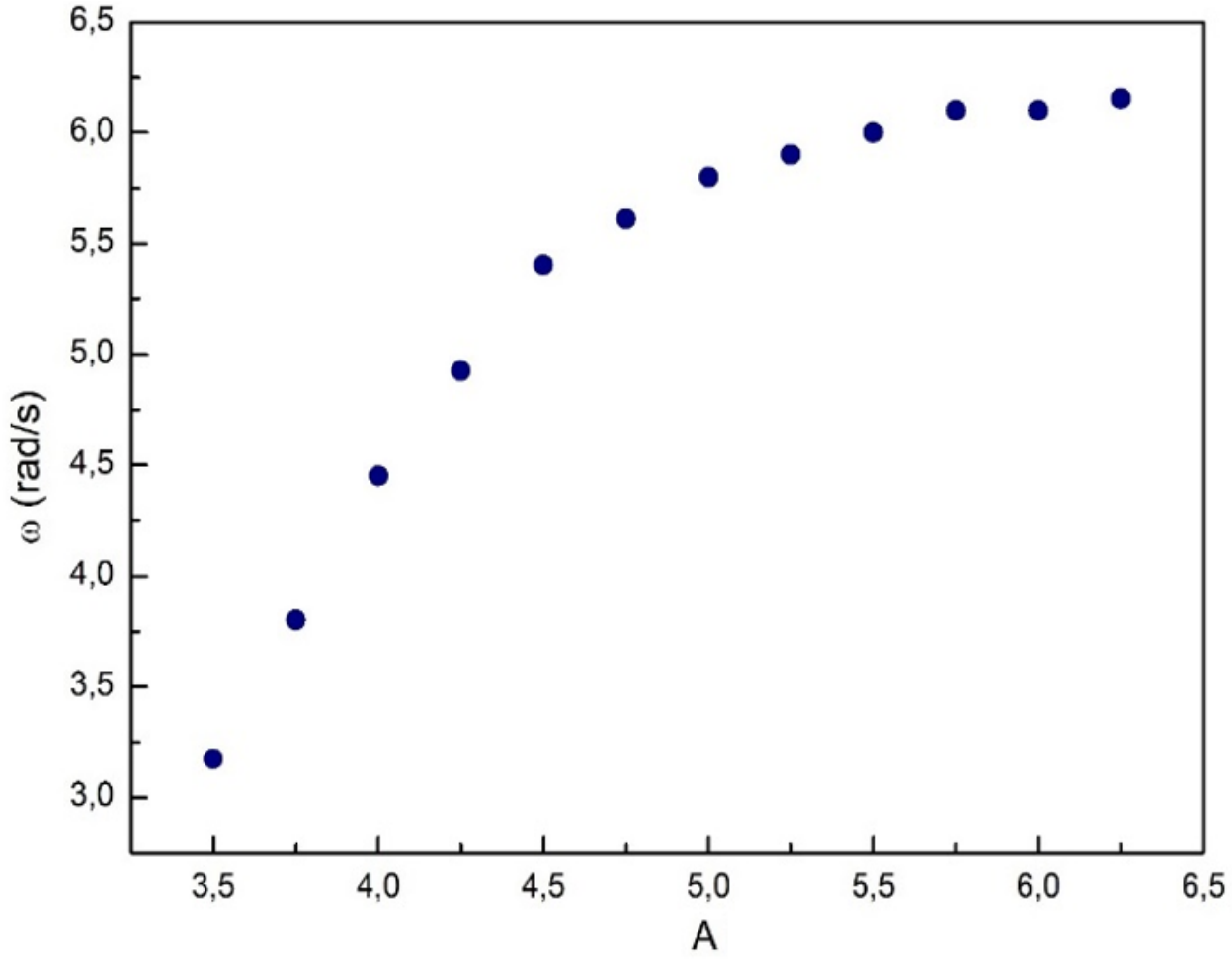

Figure 17. Dependence of the pulsation of the signals on instrument *Amplitude control*, A, when it increases between 3,50 and 6,25.

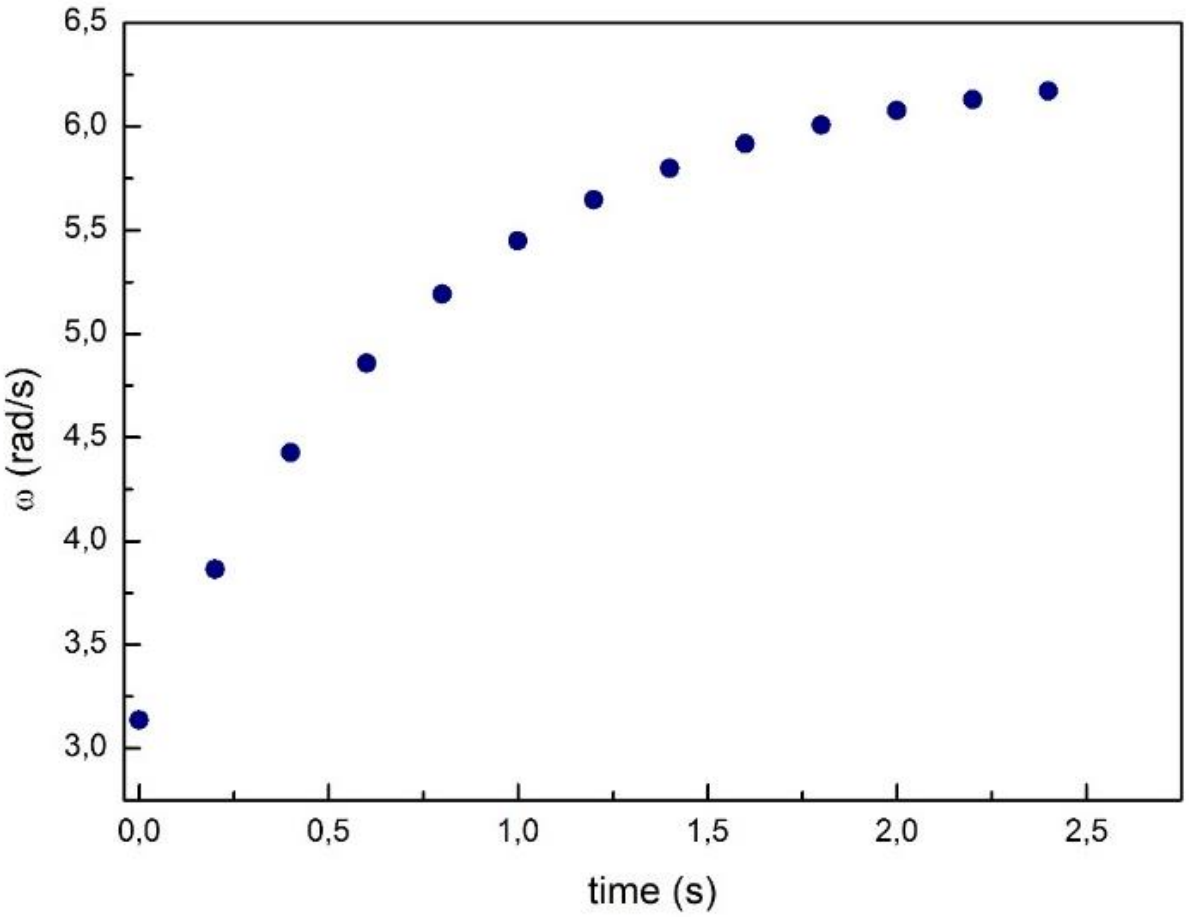

Figure 18. Pulsations of the analyzed signal that vary as a function of time following a square root trend.

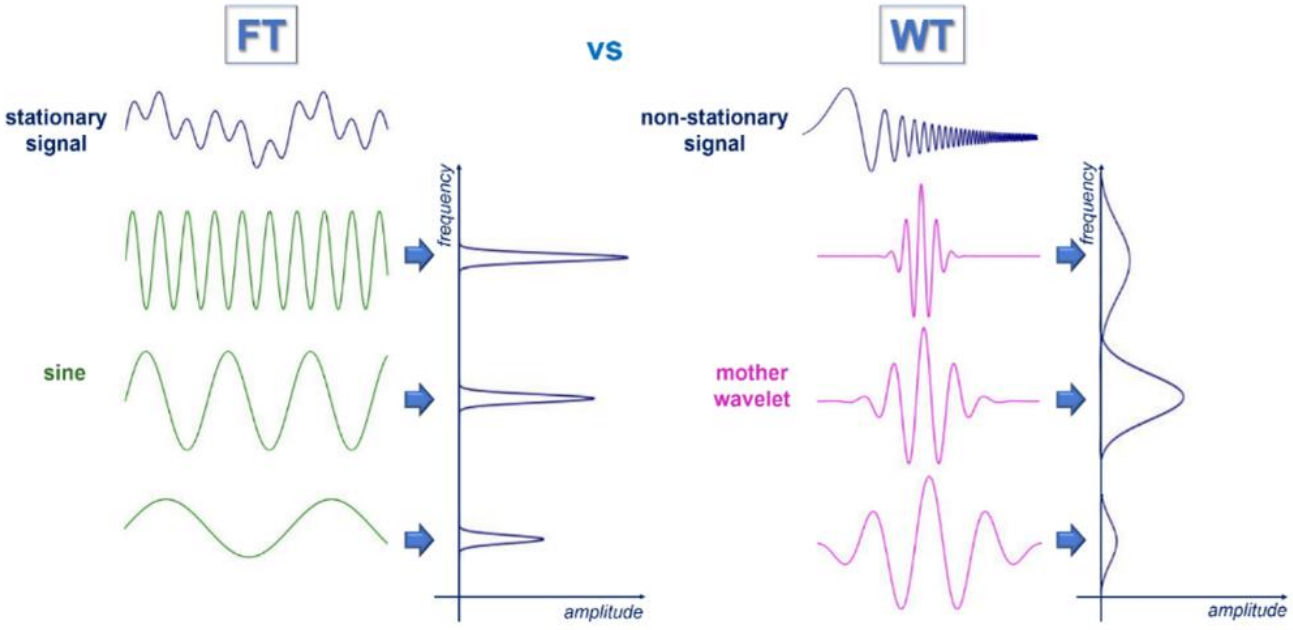

Figure 19. Comparison between Fourier Transform (FT) and Wavelet Transform (WT).

Figure 19 shows a comparison between the Fourier Transform (FT) and the Wavelet Transform (WT). In particular on the left, FT decomposes a stationary signal $f(t) = \sin(0.5t) + \sin(t) + \sin(3t)$ into three sinusoids of different frequencies, which sum to the original waveform; here the spectral power identifies their respective amplitudes.

In contrast to the FT, WT can be considered locally periodic wave-trains. As shown on the right of Figure 19, a family of wavelets is obtained by shifting and scaling a prototype mother wavelet, such that this set of functions adequately sample all the frequencies present in the non-stationary signal. All these wavelets present the same number of cycles for different frequency bands and they result in different wavelet durations. The convolution gives time-varying amplitudes of the signal in frequency and time, because it expresses the amount of overlap between the signal and this family of functions. Figure 20 shows on the top the registered signal together with the WT scalogram and FT spectrum. In particular it is shown how WT allows to follow the square root trend of the pulsations as a function of time.

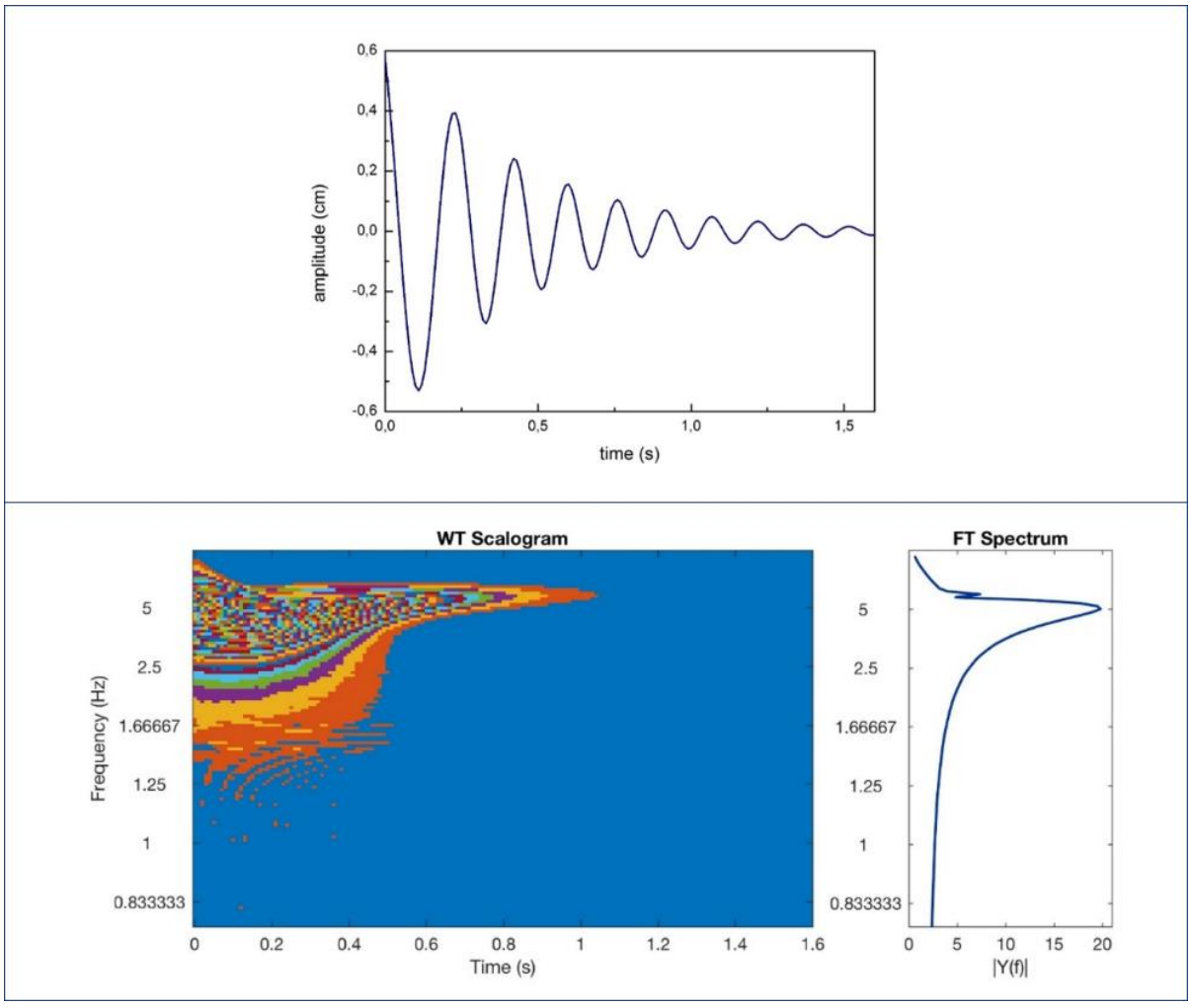

Figure 20. Registered signal (on the top); WT scalogram and FT spectrum.

From the WT and FT analysis it is possible to follow the trend of the pulsations of the analysed signal as function of time. The obtained results show in an effective way that by increasing the amplitude value the oscillation frequency of the levitated particle increases.

In conclusion, the experimental results show an approach to explain the standing waves by means of an acoustic levitator is presented. In particular, thanks to the employment of an acoustic levitator, an effective and straightforward method to visually show the nodes of acoustic standing waves is shown. Two mechanical models to study the damped oscillation of a sphere around a single node are introduced. By means of the WT analysis it is possible to follow the trend of the pulsations of the analysed signal as function of time. The obtained results show in an effective way that by increasing the instrument Amplitude control value the oscillation frequency of the levitated particle increases.

3. Experimental Results for Surface Tension and Wettability in Complex Systems

The employment of acoustic levitation technique furnishes a valid approach to evaluate surface tension in disaccharides aqueous mixtures.

The measurements were performed on trehalose and maltose aqueous solutions, manufactured by Sigma-Aldrich, in a concentration range of 50% water and 50% pure sample, that were analyzed as substances with high solubility in water in order to achieve a high solid content in the sample solutions. The solubility of the disaccharides in water is ca. 200g/100ml at 25°C.

The solutions were prepared by mass, using an analytical balance with ± 0.01mg accuracy. Double-distilled water was used in making the solutions.

A constant temperature bath was employed to control the temperature of the solutions to an accuracy of ± 0.1°C. Density measurements were performed by standard picnometer technique. Measurements for each solution were repeated five times.

Droplets of 1.5 mm of radius were inserted into the pressure node of the sound field using a micropipette injection.

The D^2 -law was applied to calculate the evaporation rate coefficient, i.e. the angular coefficient of the straight line, that is inversely proportional to surface tension value.

$$D^2 = D_0^2 - \beta t \qquad (16)$$

so:

$$\beta = -\frac{D^2 - D_0^2}{t} = \frac{C}{\tau}. \qquad (17)$$

Figure 8 shows the obtained results.

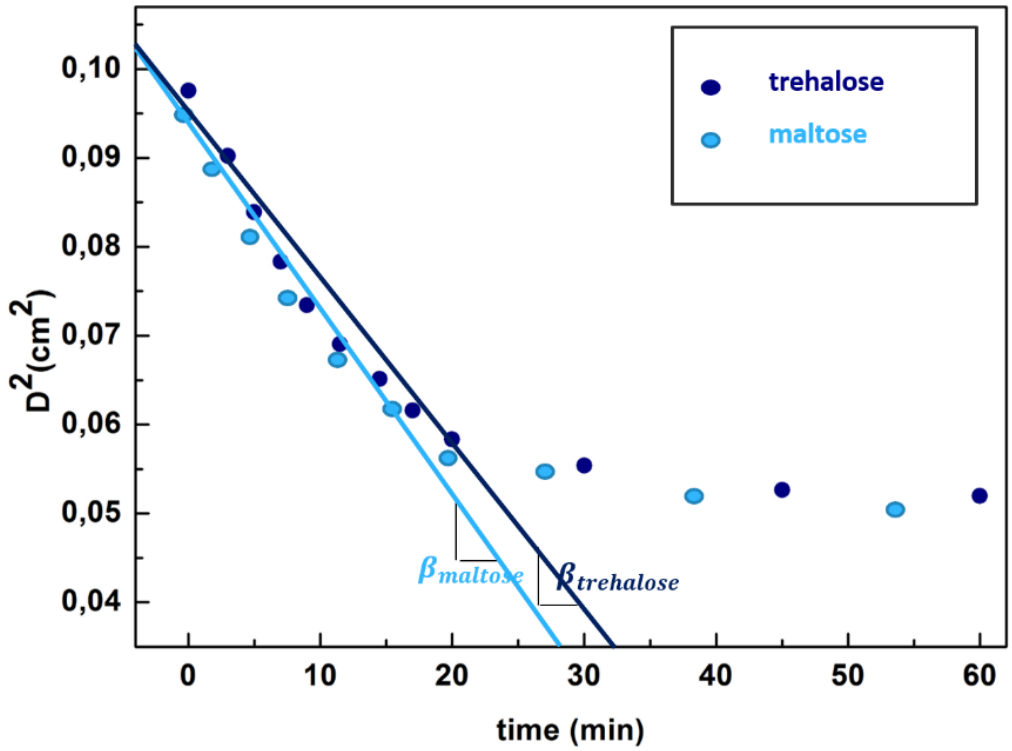

Figure 8. D^2 -law versus time representing the square diameter calculated as function of the evaporation time.

It follows that:

$$\beta_{\text{trehalose}} < \beta_{\text{maltose}} \qquad (18)$$

Surface tension is calculated as follows:

$$\tau = \frac{C}{\beta} = -\frac{C \cdot t}{D^2 - D_0^2}. \qquad (19)$$

From the β calculation for acoustically levitated trehalose and maltose aqueous solutions, results that the surface tension is higher for trehalose in respect to maltose:

$$\tau_{\text{trehalose}} = 82.94 > \tau_{\text{maltose}} = 79.22\ [\text{mN/m}] \qquad (20)$$

In order to analyse the spectra, wavelet analysis was also employed [180-185].

This evaluation approach was tested by the flat plate method, shown in Figure 9. Contact angles measurements were performed, so to determine the surface tension and to verify the previous obtained results.

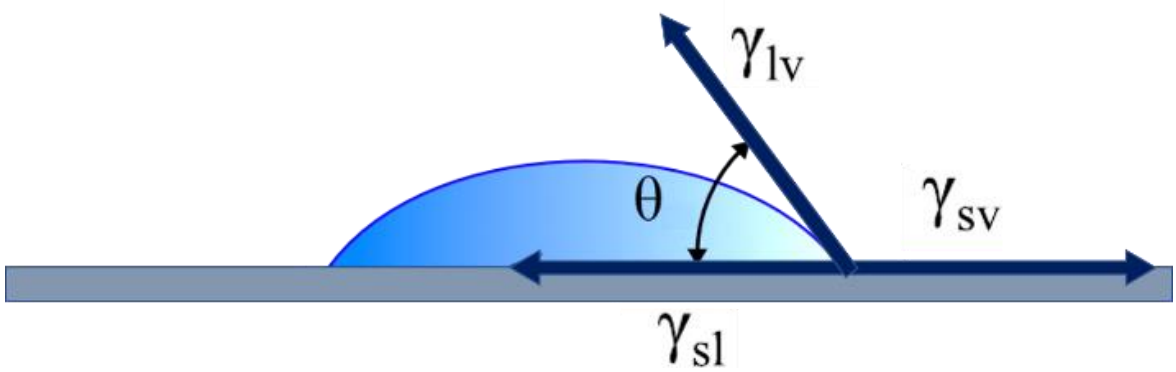

Figure 9. Flat plate method employed to test the evaluation approach of acoustic levitation and IR spectroscopy.

For this purpose, Zisman plot was employed, in which the cosine of the contact angle was plotted versus surface tension for some homologous liquid drops on a surface of glass substrate, resulting in a straight-line. The line can be extrapolated to $\cos(\theta) = 1$, corresponding to a contact angle equal to zero, i.e. complete wetting. Surface tension at $\cos(\theta) = 1$ was given the term critical surface tension γ_c. This term is considered as a wettability index.

Table 1 reports the known contact angle and $\cos(\theta)$ corresponding to the surface tension of some liquids measured at $T = 25°C$, so to represent the Zisman plot and to determine the unknown surface tension with a direct contact angle measurement.

Table 1. Surface tension (γ), contact angles (θ) and $\cos(\theta)$ for water, glycerol and formamide at $T = 25°C$. These values permit to represent the Zisman plot and to determine the unknown surface tensions by a direct measurement of the contact angle.

	surface tension γ	contact angle θ	$\cos(\theta)$
water	72,80	32,75	0,841
glycerol	64,00	29,77	0,868
formamide	58,20	28,23	0,881

By calculating the contact angles of the known liquids and the corresponding surface tension, it was possible to determine also the surface tension values of trehalose and maltose aqueous mixtures in a concentration range of 50% water and 50% pure sample. The measured contact angles for trehalose and maltose (Figure 10) were 36,0° and 34,5°, respectively. These angles correspond to the previous calculated values for surface tension.

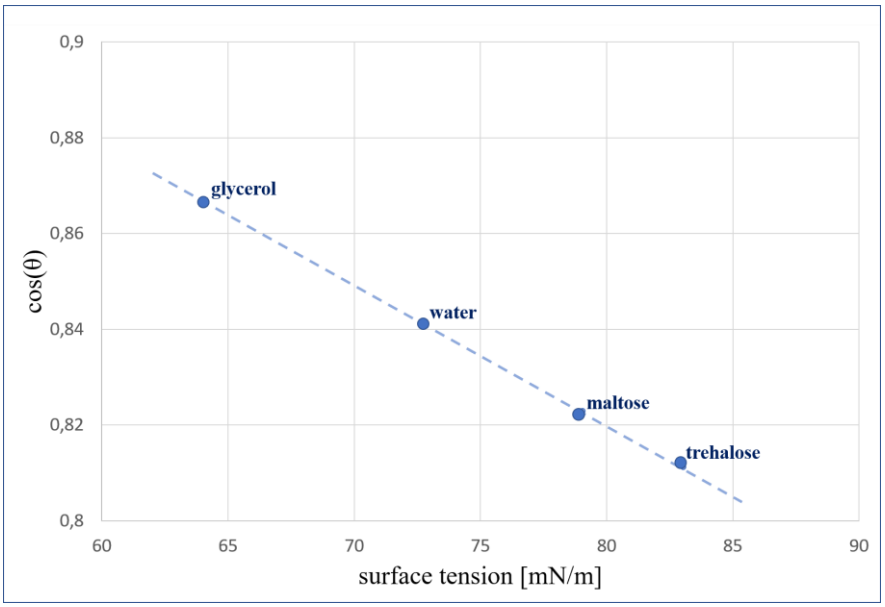

Figure 10. Zisman plot reporting the surface tension, measured in $[mN/m]$ and $\cos(\theta)$ of glycerol, water, trehalose and maltose aqueous solutions.

The obtained results were in accord with the previous results and this confirms that the conjunction use of acoustic levitation and IR spectroscopy techniques was revealed a valid approach to characterize surface tension in acoustically levitated disaccharides aqueous mixtures. Furthermore, it confirms that, also in this case, the surface tension is higher for trehalose in respect to maltose.

In conclusion, the experimental results show an approach to characterize surface tension in acoustically levitated drops is presented and tested. The investigated systems are trehalose and maltose aqueous solutions which show different surface tension values. For these systems, contact angle measurements with the flat plate method are performed to test the evaluation approach. It is demonstrated to be a valid method to determine the surface tension values. Furthermore, the experimental results show how the surface tension is higher for trehalose in respect to maltose. In conclusion, it results more able to avoid total water evaporation, showing that trehalose owns more protectant properties than maltose.

CHAPTER 3

Neutron sources are increasingly employed in a wide range of research fields. For some specific purposes an alternative to existing large-scale neutron scattering facilities, can be offered by the new generation of portable neutron devices. This chapter reports a neutron generator mainly addressed to biophysics applications with specific reference to portable non-stationary neutron generators applied in Neutron Activation Analysis (NAA). Deuterium-Deuterium pulsed neutron sources able to generate 2.5 MeV neutrons, with a neutron yield of 1.0 x 10^6 n/s, a pulse rate of 250 Hz to 20 kHz and a duty factor varying from 5% to 100%, when combined with solid-state photon detectors, show that this kind of compact devices allow rapid and user-friendly elemental analysis. The findings obtained by several simulations with the MCNP Monte Carlo code, necessary for the realization of a shield for indoor measurements, are presented. Furthermore, an evaluation of the neutron spectrum modification caused by the shielding is reported.

Nowadays neutrons are used in different fields of science, including elemental analysis, art and archaeology, environmental and geological fields, electronics, medicine and especially in biophysics applications [1-15].

The use of neutrons in some of these fields has been limited by the large amount of sample required, however neutrons furnish many advantages in the study of the structure and dynamics of biological samples, since these systems have a high hydrogen content and so neutrons allow the visualization of hydrogen atoms [16-33]. For solution structures of macromolecular complexes that can often not be crystallized for structure determination, neutron scattering take advantage of contrast variation by changing the isotopic composition of both the solvent and the individual macromolecular components to clarify these structures at intermediate resolution [34-56]. More specifically, neutrons can be used as probe for biological systems for the atomic and molecular detail, to image processes at the organism level under realistic conditions. In this case, the advantage is the high penetrating power, in

contrast between light elements and lack of radiation damage. Neutron imaging is useful to study the water uptake in plant roots, a process of obvious agricultural importance that is difficult to image with light microscopy.

Reactor technology, developed in 1940s reached a plateau in performance in 1970s with the construction of ILL (in France) and HFIR (in USA). The spallation process, developed in the 1970s, opened the opportunity to produce brighter beams. Currently operating high-flux spallation sources include ISIS (UK), SNS (USA) and the MLF at J-PARC (J).

In this framework, the European Spallation Source (ESS), in construction to Lund, Sweden, will have a long pulse, particularly well-suited for a number of neutron techniques relevant for biological systems [57-70]. In combination with modern isotope labelling techniques, it will allow experiments with a far larger number of biologically interesting samples. Detailed studies are dependent on how many neutrons can be produced by a neutron source. This is a significant limitation for existing sources based on nuclear reactors. As a result, scientists and engineers have developed a new generation of neutron sources based on particle accelerators and spallation technology, a much more efficient approach. ESS, for example, will provide up to 100 times brighter neutron beams than existing facilities today.

For some specific purposes an alternative to existing large-scale neutron scattering facilities, can be offered by the new generation of portable neutron devices [71-104]. In the following paper an overview of new generation portable neutron generators, mainly addressed to biophysics applications is presented [105-122]. In particular, the employment of portable non-stationary neutron generators in Neutron Activation Analysis (NAA) is discussed [123-155]. Finally, some relevant examples of biophysics applications are reported, as obtained by a deuterium-deuterium pulsed neutron source able to generate 2.5 MeV neutrons, with a neutron yield of 1.0×10^6 n/s, a pulse rate of 250 Hz to 20 kHz and a duty factor varying from 5% to 100%; when combined with solid-state photon detectors it allows rapid and user-friendly elemental analysis and some examples of data analysis.

3.1 Portable Neutron Generators

In the last fifty years, neutron generators were developed and then employed in several fields of application.-The potentiality and the advantages of the portable neutron generators, based on fusion reactions, to produce easily fast neutrons, instead of spallation sources, radioactive decay neutron sources and spontaneous fission sources were well know already in 1961. In the last years, neutron generators were developed and then employed in several fields of application. Nowadays, neutron generators are diffusely employed, ranging from imaging techniques, to material characterization,

from geological field to electronics (testing of devices), in non-destructive methods, in research activities thank to their simple structure and their simple functioning and most in biophysics. Among the various light-ion accelerators, compact devices designed as hermetic, sealed tubes that use Deuterium–Deuterium (D–D) and Deuterium–Tritium (D–T) reactions have found the most widespread use in industry:

$$\boldsymbol{D + D \rightarrow {}^{3}_{2}He + {}^{1}_{0}n + 3.270MeV}$$

$$\boldsymbol{D + T \rightarrow {}^{4}_{2}He + {}^{1}_{0}n + 17.590MeV}$$

These accelerators generate neutrons of ~2.5 and ~14.1 MeV, respectively. They consist of a source able to generate positively charged ions; one or more devices to accelerate the ions; a metal hydride target loaded with either Deuterium, Tritium, or a mixture of the two; and a gas-control reservoir, also made of a metal hydride material. The most common ion source used in neutron generators is a cold-cathode, or Penning ion source, which is a derivative of the Penning trap, used in Penning ion gauges.

As far as the elemental analysis is concerned, a low neutron flux of $10^7 \div 10^8$ n/s is required, that furnishes the advantage to measure easily prompt gamma from (n,γ) and (n,n',γ) reaction and allows to work safer, both in steady and in pulse mode, compared to radioactive neutron sources. In order to produce this neutron flux an ion source is used, such as Deuterium ions, of a few tens of microamperes and more than 80 keV energy, which produce neutrons of $10^6 \div 10^8$ n/s from D-D or D-T reactions.

In these last years, Portable Fast Neutrons Generators (NG)s are becoming a valid alternative to nuclear reactors in many industrial applications, in fields of neutron science, medical research and various elemental analysis applications, ranging from art and archaeology to environmental and geological fields, from the research to electronics, medicine and especially in biophysics applications. Such a technological development has widened the horizons of Portable Fast Neutron Generators in a variety of fields. Fig. 1.1 and Table 1.1 resumes the most significant applications.

Another relevant application of neutron portable sources is represented by Neutron Stimulated Emission Computed Tomography (NSECT) [156-172], which is being developed as a non-invasive imaging technique to determine element concentrations also in the living organisms. NSECT uses a neutron beam, which scatters inelastically from atomic nuclei, generating characteristic gamma photons that can be detected and identified. From the gamma photons energy, it is possible to infer the elemental composition of the target.

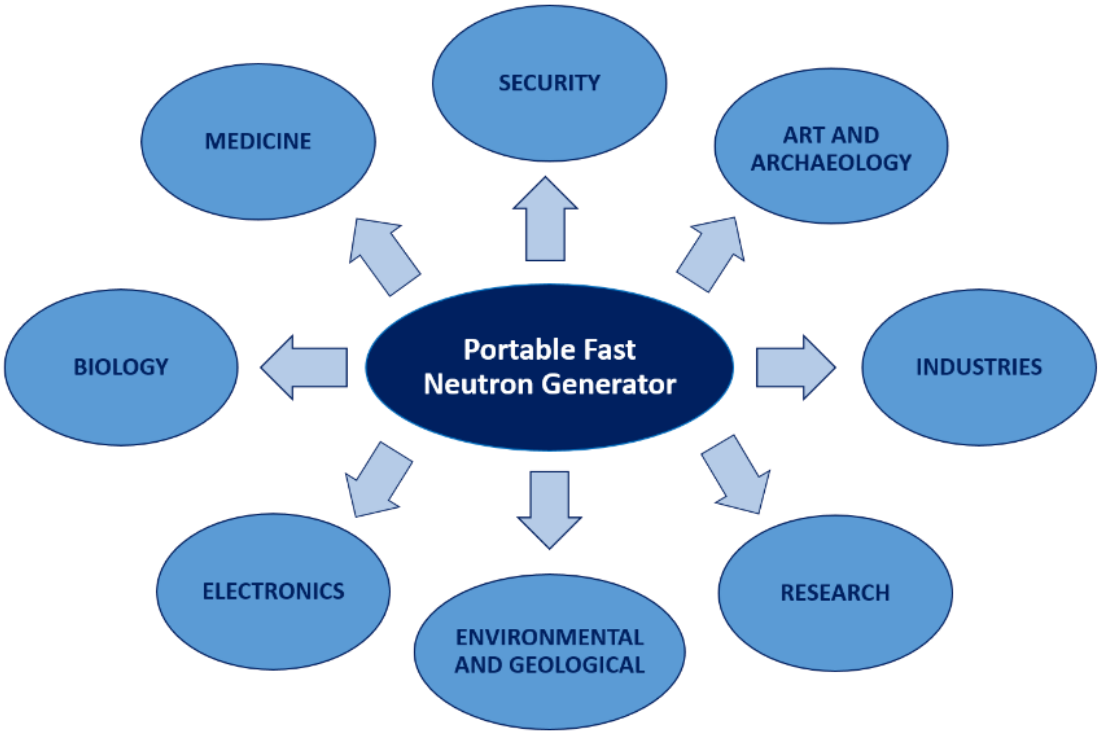

Figure 1.1. Possible application fields of a Portable Fast Neutron Generator, in particular in security, in art and archaeology, in industries, in research, in environmental and geological field, in electronics, biology and medicine.

Table 1.1

Applications of Portable Fast Neutron Generator in different fields: security, art and archaeology, industries, research, environmental and geological field, electronics, biology and medicine.

Security	detection of explosive material, illegal drugs, chemical and nuclear weapons, luggage or cargo inspections	[173-176]
Arts and Archaeology	art objects and archaeological artefacts typically not permitted to investigate with destructive techniques	[177-179]
Industries	on-line analyzers of raw materials transported on conveyor belts, especially in cement factories; analysis of minerals or materials with similar compositions (glass, cement, coal)	[180-182]
Research	reaction cross-sections and interfering reactions	[183-185]

Educational	training of young scientists in various aspects of neutron generation and diagnostics and a wide spectrum of modern technologies, such as those related to ion sources, particle acceleration techniques, beam handling and diagnostics, magnet technology, vacuum techniques, detector technology, nuclear electronics, data acquisition as well as processing techniques	[186-187]
Environmental and Geological	environmental studies focused on elements of interest such as Hg, Cd, As, Cu; recycled material (metals, plastics or mixtures thereof), waste rock piles, mine tailings, etc…; in agriculture it is useful for detecting pesticide residues on crops	[188-190]
Electronics	measure of impurities in silicon semiconductors and neutrons testing on electronic devices	[191-195]
Biology and Medicine	living material is composed mainly of carbon, hydrogen, oxygen, and nitrogen, the presence or absence of other elements can have a profound effect on the well being of an organism. Thus, it is being used in several laboratories to measure the concentrations of magnesium, copper, zinc and other metals in human blood	[196-200]

Table 1.2

Characteristics of some commercial Portable Fast Neutron Generator, in particular Thermo Scientific, Sodern, Adelphi tech. and VNIIA.

Thermo Fisher Scientific, Inc.

Model	**Applications**	**Maximum Neutron Yield [n/s]**	**Typical Tube Lifetime**	**Operating Mode**
API 120 NG	Explosive detection, Buried land mines, Chemical weapons, UXO analysis, Drugs detenction, In-Vivo body composition	2.00E+07	1,200 hours @ 10^7 n/s	Continuous only

D 711 NG	Large object imaging in cargo, Radiation effects research, Fast neutron radiography, Neutron activation analysis	2.00E+10	1,000 hours @ 10^{10} n/s	Continuous only
MP 320 NG	Explosive detection, Buried land mines, Chemical weapons, UXO analysis, Drug detection, In-Vivo body composition, Minerals mining and exploration, Bulk materials (coal, cement)	1.00E+08	1,200 hours @ 10^{8} n/s	Continuous and pulsed
P 211 NG	Transuranic waste assay, Fissionable Materials	1.00E+08	Up to 500 hours or greater	Continuous and pulsed
P 385 NG	Explosives detection, Bulk materials analysis, WMD detection, UXO analysis, Contraband detection, Vehicle inspection	5.00E+08	4,500 hours @ 10^{8} n/s	Continuous and pulsed

Sodern

Model	**Applications**	**Maximum Neutron Yield [n/s]**	**Typical Tube Lifetime**	**Operating Mode**
GENIE 16	Neutron analysis for scientific education, Neutron analysis for research, Industrial on line analysis	2,00E+08	8,000 hours @ 5x107 n/s	Continuous and pulsed
GENIE 35	Neutron analysis for scientific education, Neutron analysis for research, Industrial on line analysis	1010/4π n/s/sr	2,000 hours @ 1010/4π n/s/sr	Continuous and pulsed

Adelphi Technology, Inc.

Model	Applications	Maximum Neutron Yield [n/s]	Typical Tube Lifetime	Operating Mode
DD108	Prompt Gamma Neutron Activation Analysis (PGNAA), Neutron Activation Analysis (NAA)	1,00E+08	2,000 hours	Continuous and pulsed
DD109.1	Prompt Gamma Neutron Activation Analysis (PGNAA), Neutron Activation Analysis (NAA), fast neutron radiography.	1,00E+09	2,000 hours	Continuous and pulsed
DD109.4	Prompt Gamma Neutron Activation Analysis (PGNAA), Neutron Activation Analysis (NAA), fast neutron radiography.	4,00E+09	2,000 hours	Continuous and pulsed
DD-109M	Prompt Gamma Neutron Activation Analysis (PGNAA), Neutron Activation Analysis (NAA), fast neutron radiography.	4,00E+09	2,000 hours	Continuous
DD110MB	Prompt Gamma Neutron Activation Analysis (PGNAA), Neutron Activation Analysis (NAA), determining the concentrations of elements in many materials.	2,00E+10		Continuous
DT108API	High resolution imaging	1,00E+08		Continuous
DT110-14 MeV Neutron Generator	Security, baggage and container screening for the detection of explosives or contraband and for the detection of special nuclear materials, imaging and elemental analysis.	1,00E+10		Continuous

All-Russia Research Institute of Automatics – VNIIA

Model	Applications	Maximum Neutron Yield [n/s]	Typical Tube Lifetime	Operating Mode
ING-013	Elemental Analysis	5,00E+09	1,600 hours @ 10^8 n/s	Pulsed
ING-03	Elemental Analysis	3,00E+09	1,600 hours @ 10^8 n/s	Pulsed
ING-031	Elemental Analysis	2,00E+10	1,600 hours @ 10^8 n/s	Pulsed
ING-07	Elemental Analysis	1,00E+09		Continuous and pulsed
ING-17	Elemental Analysis	3,00E+08		Continuous and pulsed
ING-27	Elemental Analysis	1,00E+08		Continuous
NG-14	Elemental Analysis	2,00E+10		Continuous
ING-10	Research Activities	5,00E+08		Pulsed
ING-12	Research Activities	2,00E+09		Pulsed

3.2 ELEMENTAL ANALYSIS

Elemental analysis is of basic importance in life sciences since neutrons allow determining of the different components of a sample resulting, in many cases, more sensitive in respect to other analytical methods [123-134]. One of the forms of interaction between neutrons and matter is the neutron capture; in this process (Fig. 1.3), a target, via a non-elastic collision in the atomic nucleus, absorbs a neutron and a compound nucleus in an excited state is formed [135-146]. Then, the compound nucleus will de-excite into a more stable configuration through emission of one or more characteristic prompt γ-rays. The process ends when the ground state formed during the de-excitation, is stable; this occurs when an isotope of the same element, with a mass number increased by one, is produced. Generally, every chemical element has at least one isotope that produces a radioactive one

in neutron capture. They typically emit β particles and γ radiation with a given half-life [147-155]. The energies of the prompt and delayed γ-rays allow identifying the emitter nuclide and their intensity is proportional to its amount. Neutron Activation Analysis (NAA), as also known as Instrumental Neutron Activation Analysis (INAA), Prompt-Gamma Neutron Activation Analysis (PGNAA) and Delayed Neutron Activation Analysis (DNAA), are analytical sensitive techniques useful for qualitative and quantitative multi-element analysis of major, minor, and trace elements [123-129].

Hevesy and Levi, who first noticed how samples exposed to a source of neutrons, became highly radioactive, discovered NAA in 1936 and so they apply neutron irradiation for the qualitative and quantitative identification of the elements present within a sample. NAA is used to determine the concentration of elements in a variety of matrices and is based upon the conversion of stable nuclei to other mostly radioactive nuclei via nuclear reactions. The nuclear reactions occur by irradiating the sample with neutrons. In particular, a neutron is captured by a target, transmuting it into an unstable nucleus, which then decays by fission or by the release of some particle or photon. NAA uses low-energy thermal neutrons to transmute a wide range of nuclei into unstable isotopes; irradiation can take many hours while measurement of the decay energies and rates of the unstable transmuted isotopes can require days. By analyzing the spectrum of prompt or delayed γ-rays and after comparing with tabulated nuclear data for γ-ray emission, one may trace back the elements of which the test sample consists. Fast NAA is also a possibility, requiring, however, considerably more energetic neutrons than a Deuterium filled DPF can produce.

The NAA reaches a detection limit as low as $1{:}10^{15}$. For this reason this technique is applied not only in a wide range of scientific applications covering as different fields of study as geology, biology or cultural heritage but it is equally interesting for quality control or environmental supervision in an industrial context. There are several types of neutron sources for NAA, such as accelerators, radio-isotopic neutron emitters, reactors and portable neutron generators.

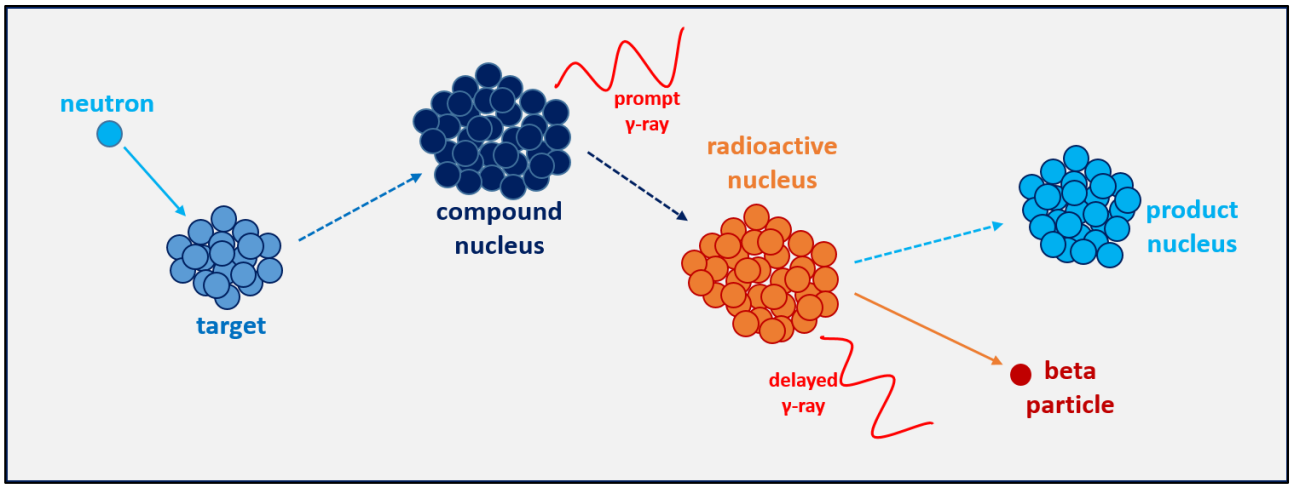

Figure 1.3. Principle of function of NAA for elemental analysis. A target, via a non-elastic collision in the atomic nucleus, absorbs a neutron and a compound nucleus in an excited state is formed. Then the compound nucleus will de-excite into a more stable configuration through emission of one or more characteristic prompt γ-rays. The process ends, when the ground state formed during the de-excitation, is stable. This occurs, when an isotope of the same element, with a mass number increased by one, is produced.

3.3 Fast Neutron Generator and Shielding Design Calculations

Fast NGs are valid and interesting available sources of neutrons, increasingly employed in a wide range of research fields, such as science and engineering. The Thermo Scientific MP 320 is an example of very lightweight portable fast NG. It can be used in different applications like explosive, weapon detection, or drug detection and it can be employed in laboratories for different kind of research applications because it is a relatively compact system that requires a very low power. It is possible to operate with either a D-T or a D-D neutron tube, simply changing the target inside the neutron tube. In fact, in "D-T mode", the source is able to generate a neutron yield of 1.0×10^8 n/s with an energy of 14.1 MeV, while in "D-D mode" it generates a neutron yield of 2.0×10^6 n/s with an energy of 2.5 MeV. The NG can be modulated varying the pulse rate from 250 Hz to 20 kHz, varying respectively from 5% to 100% the duty factor. It can be also used in conjunction with an ORTEC PINS-GMX solid-state photon detector, made of n-type high-purity germanium. For indoor application, such as research activities, the NG needs the realization of a specific bunker necessary to avoid damage from radiation exposition for users and instrumentation. Neutrons interact with nuclei in a variety of ways, for instance, if the nucleus is unchanged in either isotopic composition or internal energy after interacting with a neutron, the process is called elastic scattering. On the other hand, if the nucleus, still unchanged in composition, is left in an excited state, the process is called inelastic scattering. Generally, two or more neutrons are emitted when a nucleus is struck by a high energy

neutron. There are three different procedures for the calculation of the shielding, which are neutrons transport equation, the Monte Carlo simulation and the removal cross section method.

Neutrons transport theory is relatively simple in principle and it is possible to determine an exact equation for transport phenomena, i.e. Boltzmann equation, also known as transport equation. Unfortunately, it is much easier to derive the Boltzmann equation than it is to solve it, though under some specific conditions, such as uniform materials and same energy for the neutrons, the equation simplifies considerably the problem and it can be calculated in a rather straightforward way. This simplified transport theory is known as neutron diffusion equation and it is shown in the following:

$$D\,\nabla^2\phi - \Sigma_a\phi + s = \frac{1}{v}\frac{\partial\phi}{\partial t}. \quad (3)$$

However, many diffusion problems can not be solved by the analytical techniques; they have need of numerical computation methods [11].

Another different method shielding calculation is the Monte Carlo simulation. It consists of simulating individual particles and recording some aspects of their average behavior, using the central limit theorem. Monte Carlo simulation can be employed to duplicate theoretically a statistical process for complex problems that can not be modeled by computer codes, using deterministic methods. The individual probabilistic events of a process are simulated sequentially and the probability distributions, which govern the events, are statistically sampled to describe the total phenomenon.

Finally, the removal cross section method takes into account the ability of materials to remove neutrons of different energies from the primary beam. The interactions that slow neutrons down and cause their eventual removal from a beam are probabilistic, whereby a flux of neutrons of intensity *I* will be diminished in a thickness x of absorber proportionally to the intensity of the neutron source and the neutron removal coefficient Σ_{nr}, of the absorbing material:

$$-\frac{dI}{dx} = \Sigma_{nr} I. \quad (4)$$

The solution of the equation is:

$$I(x) = I_0 e^{-\Sigma_{nr} x} \quad (5)$$

in which, I_0 is the initial intensity, $I(x)$ refers to those neutrons that penetrate a distance x in the absorber without a collision, $e^{-\Sigma_{nr} x}$ is the probability that a given neutron travels at a distance x without any interaction. From a conceptual point of view, Σ_{nr} can be considered as the probability per unit path length that a neutron will undergo an interaction as it moves through an absorber and it will be removed from the beam by either absorption or scattering [11].

3.4 BIOPHYSICAL AND ELECTRONIC APPLICATIONS

The indoor MP320 NG can be employed both for biophysical and electronic applications, some examples are elemental analysis and testing of devices. Elemental analysis, known as Neutron Activation Analysis (NAA) is an analytical technique for qualitative and quantitative multi-elemental analysis of major, minor and trace elements. For example, with this technique, it is possible to trace heavy metals in samples of biophysical interest that contain aqueous solutions [17-21], disaccharides [22-39] or polymers [40-47] and which have already been studied with other spectroscopic techniques [48-51]. In NAA, a target, after a non-elastic collision in the atomic nucleus, absorbs a neutron and forms a compound in an excited state. When the compound nucleus de-excites into a more stable configuration, an emission of one or more characteristic prompt gamma rays occurs. The process ends when the ground state formed during the de-excitation, is stable, i.e. at the moment in which an isotope of the same element, with a mass number increased by one, is produced. Generally, every chemical element has at least one isotope that produces a radioactive one in neutron capture. They typically emit β particles and γ radiation with a given half-life. The energies of the prompt and delayed gamma rays allow to identify the emitter nuclide and their intensity is proportional to its amount.

The Earth's atmosphere acts as a shield against ionizing radiation coming from deep space. However, the interaction of galactic cosmic rays with the terrestrial atmosphere produces a "shower" of secondary particles, mainly neutrons, which come down to sea level [52]. Thus, all electronic devices are exposed to this "natural" radiation environment. Despite the neutron flux is quite low (especially at sea level) even a single neutron, under certain conditions, can cause a failure into electronic devices: this case is known as Single Event Effects (SEE)s [53]. SEEs are related to the charge generated in the semiconductor, through ionization realized by the incident particle. In the case of neutrons, this mechanism is activated by the emission of secondary charged particles, after a nuclear reaction, radioactive decay or spallation [54]. If the ionization takes place near a reverse biased pn junction, the electron-hole pairs are separated by the electric field and then collected by the electrodes, generating a transient current. This microscopic mechanism can lead to different macroscopic effects, as for example, Single Event Upset (SEU) in a memory [55] or Single Event Burnout (SEB) affecting power MOSFETs [56]. In order to characterize a device's sensitivity to terrestrial neutrons, it is necessary to perform accelerated tests with dedicated neutron facilities. The procedures to carry out such tests and the required featured of the facilities are regulated by international standards such as the JESD89A. The scope of these tests is to assess the failure rate associated with terrestrial neutron SEE.

Spallation and mono-energetic sources are suggested for testing devices with high-energy neutrons. Spallation sources produce a “white” neutron spectrum, which mimics the natural terrestrial neutron environment. A valid alternative could be represented by mono-energetic facilities. There are only few mono-energetic neutron sources: D-T and D-D facilities, respectively at 14 MeV and 2.45 MeV. According with the standard JESD89A. In this context, the proposed neutron facility could be used for accelerated SEE testing of electronic devices.

EXPERIMENTAL SET-UP FOR NAA

A portable neutron source, a shield-moderator, a gamma-ray spectrometer, and a computer form the experimental set-up, aligned by a fixed support (Fig. 2.1) [71-87].

A neutron source is located at the front edge of a polyethylene moderator that slows down the neutrons. The source emits fast neutrons toward the sample. Fast neutrons excite nuclei by inelastic scattering, while some neutrons suffer capture reactions. A neutron generator produces one million neutrons per second omni-directionally.

A tungsten shadow shield is interposed between moderator and spectrometer, to protect germanium crystal from neutron damage. A collimator of annular bismuth surrounds the crystal, for excluding the background of gamma rays and for maximizing the signal/noise ratio of the gamma-ray spectrum.

The γ-ray detector is a Portable Isotopic Neutron Spectroscopy (PINS), a non-destructive assessment system that analyses and provides on-site identification information. The PINS spectrometer probes the investigated sample with neutrons; these excite the atomic nuclei within, producing γ-rays. The spectrum of the γ-rays energy intensity is characteristic of the chemical element. The PINS software permits to identify each element inside the sample and determines its composition. PINS uses neutrons produced by a portable deuterium-deuterium neutron generator, with a kinetic energy of approximately 2.5 MeV, to excite nuclei inside the testing sample [88-104].

The spectrometer includes a High-Purity Germanium (HPGe) detector, used to detect γ-rays emitted from the sample, a digital signal processing multichannel analyser, an internal battery, and an electrical-powered refrigerator. The detector is connected to a computer, which acts as control panel, through an Ethernet. The PC allows the analysis of the instrument, start and stop data acquisition, such as display of the spectrum resulting and interlock for the neutron generator. The support aligns the experimental set-up in an optimal geometry for measurements. The system allows to identify chemicals inside a container without the need for disassembly, contact, physical sampling.

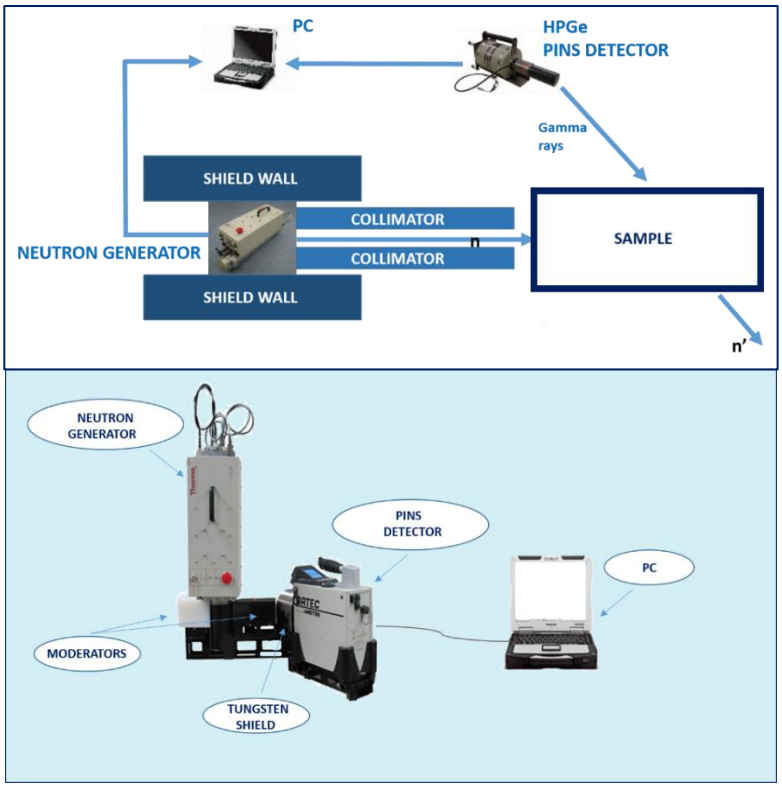

Figure 2.1. Experimental set-up for NAA: a portable neutron source, a shield-moderator, a γ - ray spectrometer, and a computer form the experimental set-up, aligned by a fixed support.

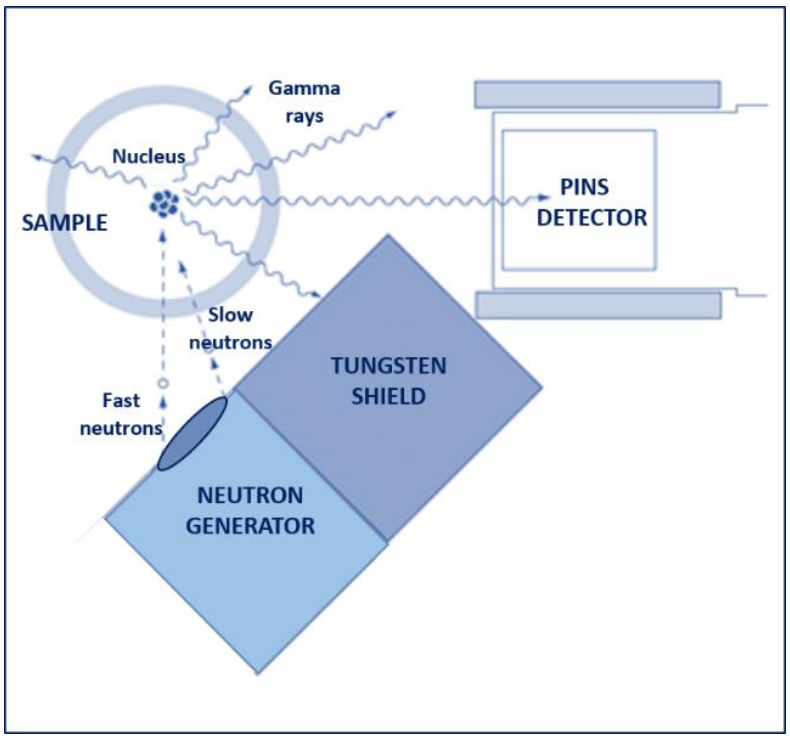

Figure 2.2. The PINS moderator block and shadow shield aligned with the *γ*-ray detector.

RESULTS AND DISCUSSION

3.5 EXPERIMENTAL RESULTS FOR THERMO SCIENTIFIC MP320 NG SHIELDING

For the design of the MP320 NG shielding, the features in table 1 were taken as a reference.

Table 1. Features for the design of the MP320 NG shielding.

reaction	D-D
max neutron energy [MeV]	2.45
neutron yield [n s^{-1}]	2.00E+06

In order to perform a preliminarily evaluation of the shielding thicknesses was used the method of removal cross section. In a second moment, data preliminarily obtained were verified with MCNP Monte Carlo code simulations. The removal cross sections for different materials are available in several handbooks for shielding dimensioning, in particular, the employed materials for neutron shielding and their Σ_r are reported in table 2 [12-14].

Table 2. Materials employed for neutron shielding.

material	**ρ [g cm^{-3}]**	**Σ_r [cm^{-1}]**
borated silicone (Elmahroug et al, 2013)	1.59	0.1007
30% borated PE (Elmahroug et al, 2013)	1.19	0.1191
iron (Kaye and Laby, 2005)	7.86	0.168
lead (Kaye and Laby, 2005)	11.35	0.116
barite concrete (NBS, 1957)	3.491	0.0945

In order to optimize the shielding size it is necessary to select materials that offer a good shielding power, i.e. an high Σ_r. It is also important to utilize the interactions of neutrons with the different materials in order to optimize the processes of slowing down and capture. Therefore, the shielding is made of successive layers of different materials. The exponential attenuation law is valid only for collimated neutron beam, while in the case in which the source can be considered as a point source, the spatial dependence of the neutron flux has to be considered. Therefore, the attenuation law becomes the following:

$$\acute{\Phi} = \frac{\varphi_0 e^{-\Sigma_r \cdot t}}{4\pi d^2} \tag{6}$$

where φ_0 is the initial neutron yield (n s^{-1}), d is the distance at which neutron flux is calculated respect to the source position, Φ is the neutron flux at distance d from the source and t is the thickness of shielding material. The method of removal cross section allows to obtain realistic estimations of the neutrons attenuation. Further evaluations can be performed using numerical codes based on the Monte Carlo method. The aim of the shielding is to reduce the neutron flux up to make the dose rate lower than the project limit. The evaluation of the different materials thickness was made considering their characteristics (Σ_r and weight). Therefore, the materials and thickness in table 3 were chosen.

Table 3. Materials and thickness for Neutron Generator MP320 shielding.

material	**Σ_r [cm^{-1}]**	**t [cm]**
30% borated PE	0.1191	15
barite concrete	0.0945	15

Neutron flux was calculated on the external surfaces at the end of the shielding, taking in consideration the distance between the source, considered a point source, the internal surface of the shielding and the entire shielding thickness. The values of neutron flux obtained for the different surfaces are shown in table 4.

Table 4. Neutron flux values obtained for the different surfaces of the shielding.

	shielding							
	up		**lateral**		**back**		**front**	
material	**t [cm]**	**$\acute{\Phi}$ [n cm^{-2} s^{-1}]**	**t [cm]**	**$\acute{\Phi}$ [n cm^{-2} s^{-1}]**	**t [cm]**	**$\acute{\Phi}$ [n cm^{-2} s^{-1}]**	**t [cm]**	**$\acute{\Phi}$ [n cm^{-2} s^{-1}]**
air	33	146.15	15	397.89	23	300.86	57	48.99
30% borated PE	15	11.57	15	21.77	15	18.47	30	0.59
barite concrete	15	1.63	15	2.59	15	2.30	0	0.59

In figure 1, it is possible to see the different thicknesses of the shielding: the green part represents the 30% borated PE, while the grey part, barite concrete.

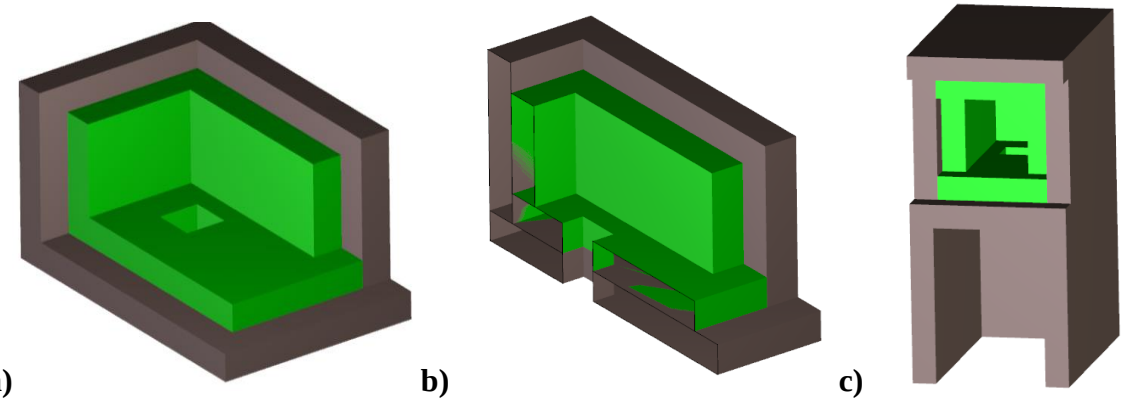

Figure 1. Representation of shielding thicknesses (a), shielding section view (b) and shielding structure (c).

In the section view, it is possible to identify the window for the samples irradiation. NG will be located inside the shielding, with the neutron emitting target in correspondence of the window. The entire shielding will be sustained by a concrete structure as shows in figure 1 (c). Figure 2 shows the shielding inside the laboratory and the comparison between the shielding and a user.

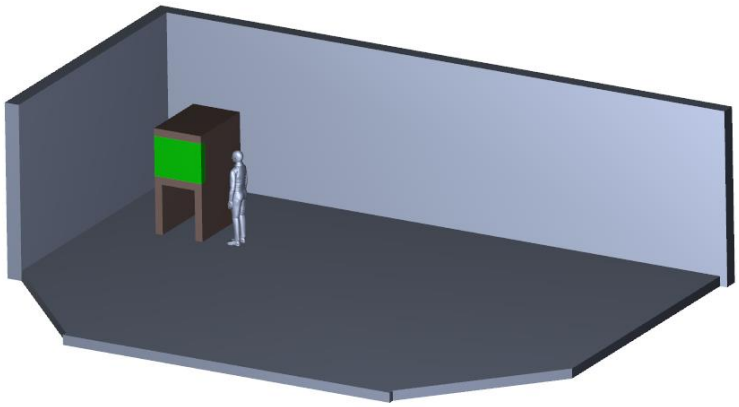

a)

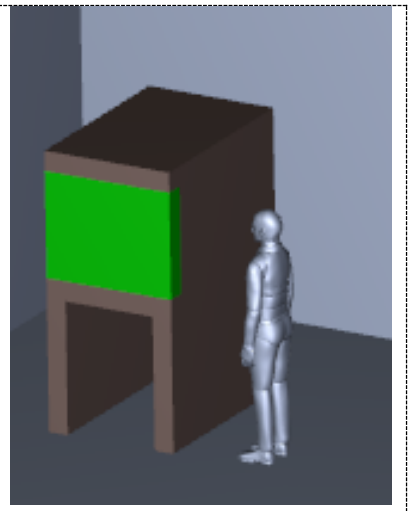

b)

Figure 2. Shielding representation inside the laboratory (a) and comparison between the shielding and a user.

Several simulations were performed with a software based on Monte Carlo method, in order to verify the values obtained with the application of removal cross section. The code used was MCNP5. The code includes information relatively to the geometry, materials and source characteristics. The cells in which evaluate the neutron flux were also specified. These were placed on the external surfaces of the shielding in correspondence of the specification addressed in the design phase. For neutron flux evaluation was chosen the Track Length Estimate of Cell Flux (F4) that allow to obtain the average neutron flux in a volume V, as described in following formulation:

$$\overline{\phi_V} = \frac{1}{V} \int dE \int dV \int ds\, N(\vec{r}, E, t) \qquad (7)$$

where $N(\vec{r}, E, t)$ is the density of particles, regardless of their trajectories, at a point.

Thus, the code studies the life of the particles generated into the source and then evaluates their average behavior in the volume V. Therefore, taking into consideration the complexity of the problem, it will be necessary to simulate an adequate number of particles in order to reduce the uncertainty on the flux values.

Two sections of the shielding are reported in figure 3: the blue part represents 30% Borate PE, the yellow part, barite concrete and the green part, the cells in which neutron flux was calculated. The cross in the two figures shows the point at which the “neutron source” is located.

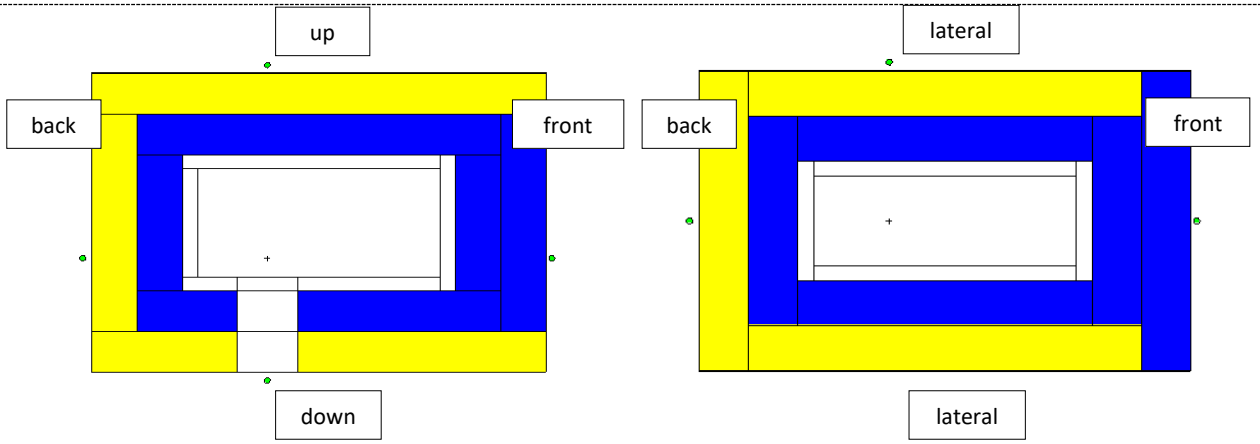

Figure 3. Shielding sections from MCNP simulations.

Simulations were performed considering the life of $2 \cdot 10^9$ neutrons, in order to evaluate the flux in the green cells and in order to obtain a standard deviation under the 10%. The values obtained by the simulation represent the average flux into the cells volume for every neutron started from the source. They must be handled in order to obtain the value of the mean flow in the cells. After handling the values, the results in table 5 were obtained.

Table 5. Neutron flux values obtained by Monte Carlo simulation.

	shielding			
	up	**lateral**	**back**	**front**
energy [MeV]	$\dot{\Phi}$ **[n cm^{-2} s^{-1}]**	$\dot{\Phi}$ **[n cm^{-2} s^{-1}]**	$\dot{\Phi}$ **[n cm^{-2} s^{-1}]**	$\dot{\Phi}$ **[n cm^{-2} s^{-1}]**
2.45	0.349	0.103	0.252	8.87x10^{-3}
total	3.75	1.61	2.63	0.145

Comparing the values obtained from the simulation with those obtained by the removal cross section method, as shown in table 6, it is possible to verify that this method allows to obtain the realistic values of the neutron flux and it represents a valid approach to determine neutron shielding thicknesses.

Table 6. Comparison between Removal Cross Section Method and Monte Carlo Method.

	shielding			
	up	**lateral**	**back**	**front**
	$\dot{\Phi}$ **[n cm^{-2} s^{-1}]**	$\dot{\Phi}$ **[n cm^{-2} s^{-1}]**	$\dot{\Phi}$ **[n cm^{-2} s^{-1}]**	$\dot{\Phi}$ **[n cm^{-2} s^{-1}]**
Σ_r **method**	1.63	2.59	2.30	0.59
MCNP total	3.75	1.61	2.63	0.145

In order to evaluate the effect of shielding, it is possible to calculate the neutron dose rate. The following parameters were taken into account as references for the dose rate limits evaluation:

• Project Equivalent Dose [mSv/y] 0.5;

• Annual duty hours [h/y] 1.200.

The project neutron dose rate was chosen as half of the annual limit for the population in order to consider also the photons contribute to the total dose rate. The annual duty hours were chosen as the typical lifetime of the target. Taking into account of the set parameters, the reference value for the dose rate is equal to:

$$\frac{0.5\left[\frac{mSv}{y}\right]}{1{,}200\left[\frac{h}{y}\right]} = 4.2 \cdot 10^{-4}\left[\frac{mSv}{h}\right]. \quad (8)$$

In order to evaluate the neutron dose rate, it is necessary to know the neutron spectrum and to apply the flow-to-dose rate energy-dependent conversion factors. Considering the neutron spectrum obtained with MCNP simulations and applying the conversion factors, the dose rate values, shown in table 7, were obtained [15-16].

Table 7. Equivalent Dose Rate values outside the neutron shielding.

	shielding			
	up	**lateral**	**back**	**front**
equivalent dose rate [mSv/h]	1.51×10^{-3}	2.81×10^{-2}	$4.0E \times 10^{-2}$	1.62×10^{-2}
equivalent dose rate @ 0.1 m from the shielding [mSv/h]	1.20×10^{-8}	2.23×10^{-7}	3.18×10^{-7}	1.29×10^{-7}

The obtained values of neutron dose rate are over the limit of $4.2 \cdot 10^{-4}[mSv/h]$, however, taking into account the geometric attenuation is possible to evaluate that the neutron dose rate goes down rapidly below the limit.

Every application field of neutron sources needs particular characteristics of irradiation and it is necessary to evaluate if the source is suitable for the tests. The shielding or other structural materials cause the modification of the energy spectrum of a neutron source and, hence, of the exposed samples. Therefore it is necessary to evaluate the modified energy spectrum in order to define the real characteristics of the neutron source. Several simulations were performed to this aim, using MCNP. The neutron spectrum was evaluated in correspondence to the window for the irradiation of the samples, outside the shielding, as shown in figure 4.

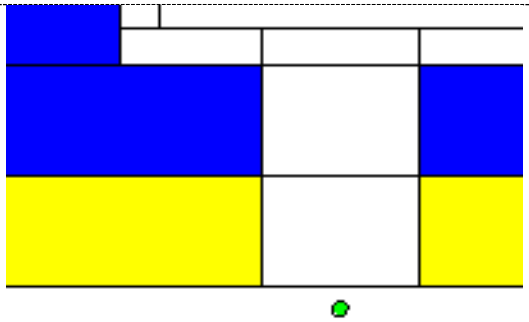

Figure 4. Detail of spectrum evaluation point.

The simulations were performed both for the D-D and D-T mode in order to evaluate the effect of shielding on the two different energy neutron beams.

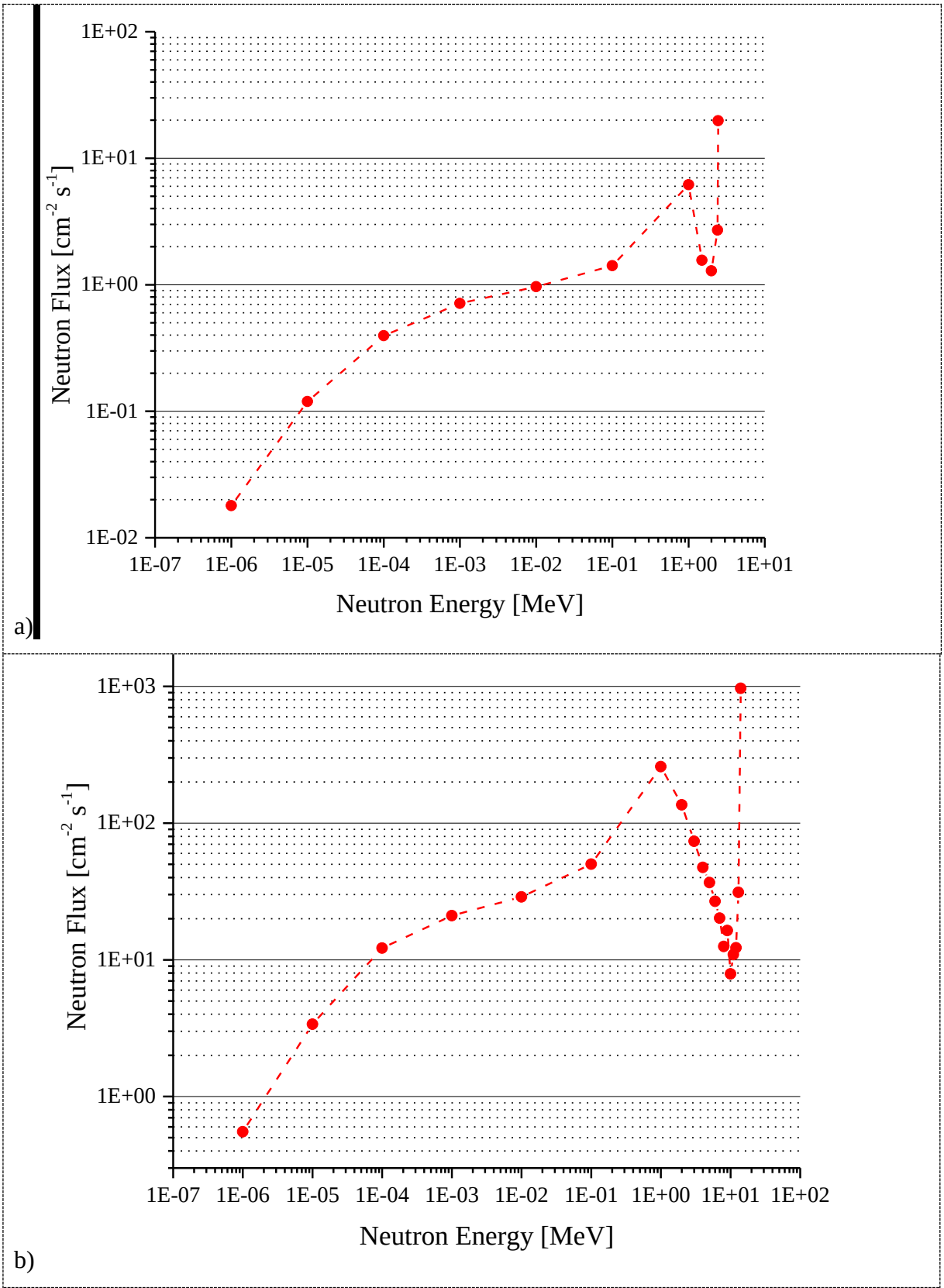

Figure 5. a) D-D neutron spectrum; b) D-T neutron spectrum.

The graphics in figure 5 show how the presence of the shielding contributes to the spectrum change to which the samples will be exposed.

In conclusion, the data obtained with the method of removal cross section and through simulations with MCNP represent a fundamental aid in the design of the shield, necessary for the indoor use of the neutron source. This work is therefore a starting point for the construction of the shield and the obtained data will be verified experimentally. The project could be subjected to modifications in order to optimize the irradiation characteristics of the samples. The employed predictive tools will be so critical to the optimization process and will allow to intervene on the shielding before its construction. The whole device represents a valid research tool and the areas where it can be used are numerous and biophysics and electronics represent only two examples of the many possible uses of this facility. The reduced operating costs, the compactness and the possibility of varying the duty factor make the neutron generator a very competitive device within the panorama of the available neutron sources.

3.6 Experimental Results for NAA System

Neutrons, produced by the portable source, excite the nuclei they encounter by inelastic scattering and neutron capture; the excited nuclei decay to ground states because of γ-ray emission, and these rays are characteristic of the emitting nucleus. The Fig. 2.3 shows, as an example, the full energy-range PINS gamma-ray spectrum for the chlorine nucleus (Cl) with an energy of about 6 MeV. More precisely, a PINS spectrum contains many vertical peaks, which represent the identification of the chemical inside the investigated sample. The peaks are labelled with the emitting chemical element symbol and the gamma ray peak energy.

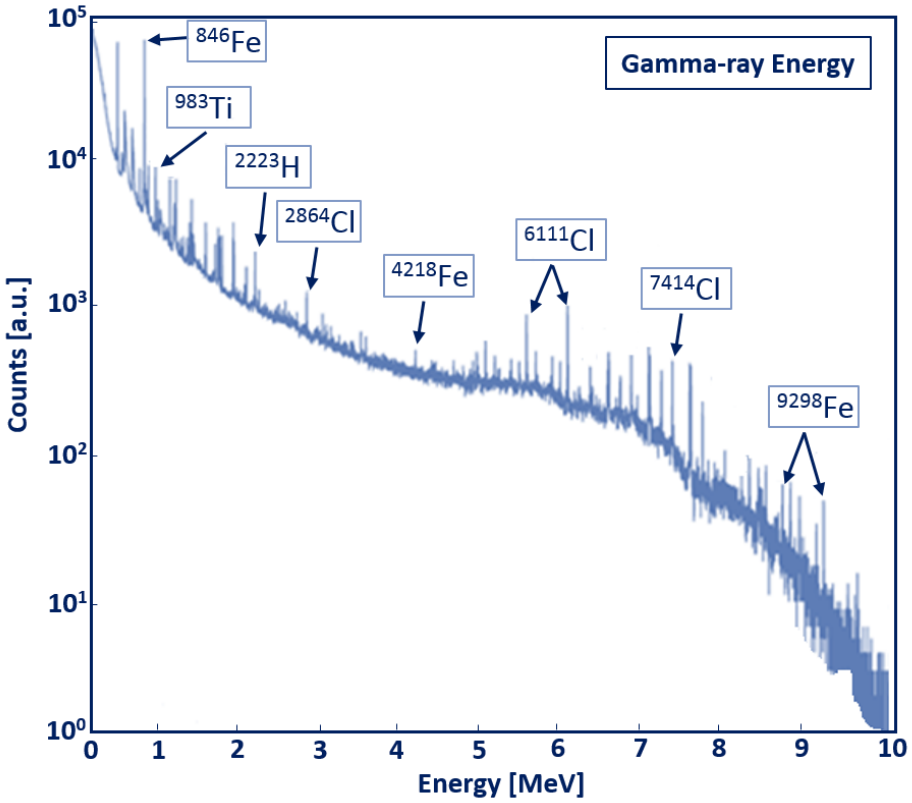

Figure 2.3. Full energy-range PINS γ-ray spectrum for the chlorine nucleus (Cl) with an energy of about 6 MeV. The peaks, labelled with the emitting chemical element symbol and the gamma ray peak energy, represent the identification of the chemical inside the investigated sample.

The Figure 2.3 shows the data analysis. In general, γ-ray energy and intensity vary from one nucleus to another, such as in the case of hydrogen nucleus that emits a gamma ray at 2.2 MeV and phosphorus nucleus that emits at 1.3 MeV. The HPGe detector measures these γ-rays and displayed they in a spectrum, in which are identified the chemical elements excited by the neutrons. The PINS software records and displays the incoming spectra measurements, every 10 seconds, fitting the peaks of interest, re-calibrating the energy scale, and performing a chemical analysis.

In order to determine the peaks in the full energy-range PINS γ-ray spectrum, i.e. the values for which "kinks" and/or anomalies in the trends occur, a wavelet method can be used.

It's well known that wavelet analysis represents an innovative and powerful tool to investigate non-stationary signal processing such as trends, drift, and, in particular, beginnings and ends of events, abrupt spectral changes and first order discontinuities which, in the framework of this work, identify with a great precision peak positions, especially in the presence of complex spectral features. Wavelet analysis has recently found a wide range of applications in various fields, such as, engineering, physics, mathematics and neutron scattering. In particular, wavelet analysis allows to perform a local

analysis of the signal, to de-noise a signal without appreciable degradation and to highlight aspects of data such as aspects like trends, anomalies, discontinuities in higher derivatives, and self-similarity features… In figure X, as an example, a signal with a sudden spike, at top, is shown; at bottom the wavelet analysis, WT reveals the spike of the signal.

Differently from what occurs for Fourier Transform (FT), which decomposes the signal into big waves, i.e. the sinusoids, Wavelet Transform(WT) decomposes the signal by means of shifted and scaled mother wavelet:

$$W(a,b) = \frac{1}{\sqrt{a}} \int_{-\infty}^{+\infty} f(t)\psi^* \left(\frac{t-b}{a}\right) dt$$

Where, $f(t)$ is the signal, a (being $a > 0$) represents the scale or the scaling parameter that refers to the width of the wavele; more precisely , if $|a| < 1$, ψ is compressed (high frequenciy), , if $|a| > 1$ ψ is dilated (low frequencies). The parameter b is the shift or translation parameter, which take into account the time location of the wavelet, finally the term, ψ^* is the conjugate.

WT furnishes the *scalogram*

$$P_W(a,b) = |W(a,b)|^2$$

that represents the wavelet coefficients defining a local time–frequency energy density.

The NAA spectra can be analyzed by means of a wavelet analysis that allows to de-noising the registered signal and to identify the peak positions [201-205].

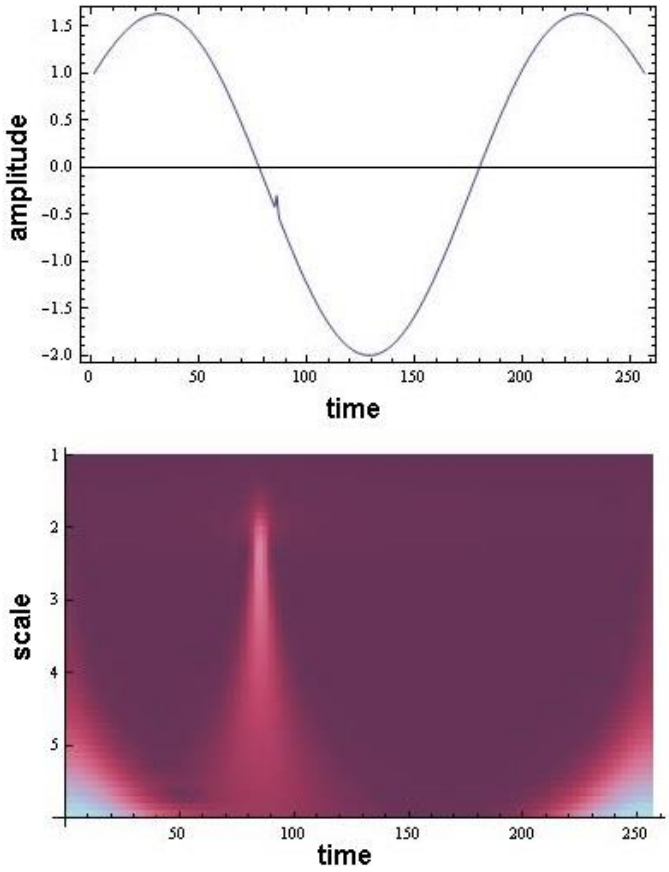

Figure 2.4. An example of signal with a sudden spike (on the top) and its scalogram plot (on the bottom). The wavelet transform clearly reveals the spike of the signal.

In Figure 2.4, as an example, a signal with a sudden spike, at top, is shown; at bottom the wavelet analysis, WT reveals the spike of the signal. It is possible to notice that wavelet analysis allows decomposing the signal into shifted and scaled versions of the mother wavelet.

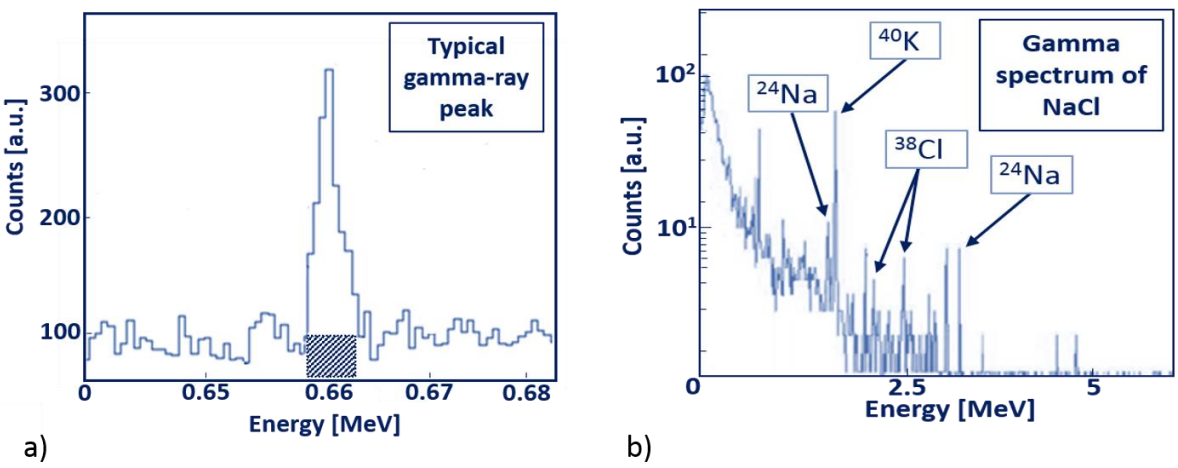

Figure 2.5. Some relevant examples of NAA are reported. a) Typical γ-ray peak. The PINS instrument analyses γ-ray peaks individually or in small groups. In the figure, some particular attributes of the ^{137}Cs γ-ray peak: the centroid, the height, the width and the area, are reported. The peak centroid energy is at 0.662 MeV. b) A γ-spectrum obtained from the D-D NG with a NaCl sample irradiated by a neutron yield of ~10^6 n/s from the D-D NG. In particular, the energy peak reports the presence of ^{24}Na, ^{40}K, ^{38}Cl in the NaCl investigated sample.

The Figure 2.5 reports some particular attributes of the ^{137}Cs γ-ray peak: the centroid, the height, the width and the area. The centroid is the midpoint of count distribution of peaks; which represents the energy peak of the γ-ray, and identifies each chemical element. The peak area is calculated from the sum between the number of counts and the edge of the lower peak energy to the upper energy edge, while the net peak area from the difference between the peak area and the background area under the peak. The net peak areas are directly proportional to the mass of the chemical element present in the investigated sample. About the determination of the areas, the related uncertainties are the most critical information of a spectrum: there is a background called the Compton continuum. The blue part highlights the background area under a peak. It can be subtracted from the gross peak area to determine the net peak area. Alternatively, a Gaussian fit for the peak atop a line segment that represents the average Compton background is possible. An example is for the ^{137}Cs that presents a peak centroid energy of 0.662 MeV. The uncertainty ratio of the net peak area is t = (826.9/45.1) = 18.3 that is certainly a real peak. In fact, as a rule, a peak with a ratio of value 3 have a high statistical, while peak value major to 5 are certainly true peaks. Candidate peaks with t values less than 1 are likely fluctuations in the Compton background. By this test, the small spike near 0.651 MeV is a fluctuation.

Another example, that demonstrate the validity of a simple and intuitive system of elemental analysis, as well as portable too, is the gamma spectrum obtained from the D-D generator with a NaCl sample.

The Fig. 2.5 b) shows the result of a γ spectra obtained with NaCl sample irradiated by a neutron yield of ~10^6 n/s from the D-D NG. In particular, the energy peak reports the presence of ^{24}Na, ^{40}K, ^{38}Cl in the NaCl investigated sample.

In conclusion, chapter 3 reports an overview of the new generation of portable neutron sources specifically addressed to biophysics applications. After an introduction on the importance of neutrons for the study of biophysical samples and a description of the typical experimental set-up for the analysis of biophysics samples, an overview of applications with specific reference to elementals analysis is furnished. More specifically some example of NAA results obtained by using a portable non-stationary Deuterium-Deuterium pulsed neutron generator are presented. Such device is able to generate 2.5 MeV neutrons with a neutron yield of 1.0 x 10^6 n/s, with a pulse rate of 250 Hz to 20 kHz, and a duty factor varying from 5% to 100%; in combination with a solid-state photon detector, such as PINS spectrometer, allows a rapid and user-friendly elemental analysis. Finally, some examples are reported.

CONCLUSIONS

In conclusion, the thesis work focuses its attention on issues concerning sample-environment devices for biophysical applications and neutron spectroscopy. In particular, acoustic levitation technique and a portable neutron source for biophysical and electronic applications are treated. The work is divided into two section, one inherent to a single-axis acoustic levitator, the other to the neutron source with the following experimental results. The investigated sample are principally polymers and disaccharides aqueous solutions, the results show how trehalose is able to avoid total water evaporation since a percentage of water is strongly bonded with the disaccharide. Such a property plays a key role in bio-protection. Furthermore, a test of a theoretical model describing the drying process of an acoustically levitated droplet of a solution following an approach is reported. In particular, the so-called D^2 versus time law is tested on trehalose and sucrose aqueous solutions. The theoretical model showed experimental evidence both for the diameter determination, performed by the direct monitoring with the video camera. It was shown how acoustic levitation allowed to explore a wide disaccharide concentration range and to test the dependence of the diameter law as a function of lag time, i.e. D^2 versus time. By these analyses, it emerged that the behaviour of D^2 vs t follows a linear trend for about 20 minutes, reaching then a plateau at longer time. The result showed that trehalose is more able to avoid total water evaporation than sucrose and maltose, this result showed that trehalose owns more protectant properties. Furthermore, they furnished a value of the surface tension which is higher for trehalose in respect to sucrose and

maltose. The study of trehalose is particularly important for a better understanding of extremophiles, organisms that can survive in harsh conditions.

In addition, the experimental results showed an approach to explain the standing waves by means of an acoustic levitator. In particular, thanks to the employment of an acoustic levitator, an effective and straightforward method to visually show the nodes of acoustic standing waves is shown. Two mechanical models to study the damped oscillation of a sphere around a single node are introduced. By means of the WT analysis it is possible to follow the trend of the pulsations of the analysed signal as function of time. The obtained results show in an effective way that by increasing the instrument Amplitude control value the oscillation frequency of the levitated particle increases.

The second section reports the data obtained with the method of removal cross section and through simulations with MCNP represent a fundamental aid in the design of the shield, necessary for the indoor use of the neutron source. This work is therefore a starting point for the construction of the shield and the obtained data will be verified experimentally. The project could be subjected to modifications in order to optimize the irradiation characteristics of the samples. The employed predictive tools will be so critical to the optimization process and will allow to intervene on the shielding before its construction. The whole device represents a valid research tool and the areas where it can be used are numerous and biophysics and electronics represent only two examples of the many possible uses of this facility. The reduced operating costs, the

compactness and the possibility of varying the duty factor make the neutron generator a very competitive device within the panorama of the available neutron sources.

Furthermore, an overview of the new generation of portable neutron sources specifically addressed to biophysics applications is presented. After an introduction on the importance of neutrons for the study of biophysical samples and a description of the typical experimental set-up for the analysis of biophysics samples, an overview of applications with specific reference to elementals analysis is furnished. More specifically some example of NAA results obtained by using a portable non-stationary Deuterium-Deuterium pulsed neutron generator are presented. Such device is able to generate 2.5 MeV neutrons with a neutron yield of 1.0×10^6 n/s, with a pulse rate of 250 Hz to 20 kHz, and a duty factor varying from 5% to 100%; in combination with a solid-state photon detector, such as PINS spectrometer, allows a rapid and user-friendly elemental analysis. Finally, some examples are reported.

In conclusions, the acoustic levitator and the portable neutron source represent to valid and intuitive sample-environment devices for biophysical applications and neutron spectroscopy.

REFERENCES

SINGLE-AXIS ACOUSTIC LEVITATOR

[1] Kundt, A. 1866. "Ueber Eine Neue Art Akustischer Staubfiguren Und Über Die Anwendung Derselben Zur Bestimmung Der Shallgeschwindigkeit in Festen Körpern Und Gasen. Annalen Der Physik." *Annalen Der Physik* 127 (4): 497–523.

[2] Bücks, K., Müller, H. 1933. "Über Einige Beobachtungen an Und Piezoquarzen Schwingenden Ihrem Shallfeld." *Zeitschrift Für Physik* 84: 75–86.

[3] Barmatz M., Collas P. 1985. "Acoustic Radiation Potential on a Sphere in Plane, Cylindrical, and Spherical Standing Wave Fields." *Journal of the Acoustical Society of America* 77 (3): 928–45.

[4] Cuello, G. J., Cristiglio, V., Hennet, L., Puente-Orench I. 2014. "Neutron Scattering at High Temperature and Levitation Techniques." In *Journal of Physics: Conference Series, 549*.

[5] Ashkin, A., J. M. Dziedzic, J. E. Bjorkholm, and Steven Chu. 1986. "Observation of a Single-Beam Gradient Force Optical Trap for Dielectric Particles." *Optics Letters* 11 (5): 288.

[6] Neuman, K. C., and Block S. M. 2004. "Optical Trapping." *Rev Sci Instrum* 75 (9): 2787–2809.

[7] Jacobs, G., Egry, I., Maier, K., Platzek, D., Reske, J. and Frahm, R. 1996. "Extended X-Ray-Absorption Fine Structure Studies of Levitated Undercooled Metallic Melts." *Review of Scientific Instruments* 67 (10): 3683.

[8] Egry, I., Diefenbach, A., Dreier, W. and Piller, J. 2001. "Containerless Processing in Space—Thermophysical Property Measurements Using Electromagnetic Levitation." *International Journal of Thermophysics* 22: 569-578.

[9] Muck, O. 1923. ElectroMagnetic Levitation, issued 1923.

[10] Holland-Moritz, D., Schenk, T., Convert, P., Hansen, T. and Herlach D. M. 2005. "Electromagnetic Levitation Apparatus for Diffraction Investigations on the Short-Range Order of Undercooled Metallic Melts." *Measurement Science and Technology* 16: 372–80.

[11] Rhim, Won Kyu, Chung, Sang K., Barber, D., Man, Kin F., Gary Gutt, Aaron Rulison, and Erik, Spjut R.. 1993. "An Electrostatic Levitator for High-Temperature Containerless Materials Processing in 1-G." *Review of Scientific Instruments* 64 (10): 2961–70.

[12] Paradis, Paul Francois, Takehiko Ishikawa, Jianding Yu, and Shinichi Yoda. 2001. "Hybrid Electrostatic-Aerodynamic Levitation Furnace for the High-Temperature Processing of Oxide Materials on the Ground." *Review of Scientific Instruments* 72 (6): 2811–15.

[13] Gangopadhyay, A. K., Lee, G. W., Kelton, K. F., Rogers, J. R., Goldman, A. I., Robinson, D. S., Rathz, T. J. and Hyers, R. W. 2005. "Beamline Electrostatic Levitator for in Situ High Energy X-Ray Diffraction Studies of Levitated Solids and Liquids." *Review of Scientific Instruments* 76 (7).

[14] Granier, J., Potard, C. 1987. "Elaboration et Moulage Sans Conteneur Par La Methode Dp.S Films de Gaz Demonstration et Modelisation Preliminaires." In *6th European Symposium Microgravity. Bordeaux, France, ESA SP-256*, 421–25.

[15] Parayre, C., Daniel, M., Papoular, M. and Kernevez, N. 1999. "High-Temperature Containerless Viscosity." *International Journal of Thermophysics* 20 (4): 1071–83.

[16] Nordine, P. C., Atkins, R. M. 1982. "Aerodynamic Levitation of Laser-Heated Solids in Gas Jets." *Review Scientific Instruments* 53: 1456.

[17] Drewitt, James W. E., Louis Hennet, Anita Zeidler, Sandro Jahn, Philip S. Salmon, Daniel R. Neuville, and Henry E. Fischer. 2012. "Structural Transformations on Vitrification in the Fragile Glass-Forming System $CaAl_2O_4$." *Physical Review Letters* 109 (23).

[18] Kozaily, J., Hennet, L., Fischer, H. E., Koza, M., Brassamin, S., Magazù, S., Kargl, F. 2011. "Time-of-Flight Neutron Spectroscopy: A New Application of Aerodynamic Sample Levitation." *Physica Status Solidi (C) Current Topics in Solid State Physics* 8: 3155–3158.

[19] Hennet, L., Cristiglio, V., Kozaily, J., Pozdnyakova, I., Fischer, H. E., Bytchkov, A., Drewitt, J. W. E., Leydier, M., Thiaudière, D., Gruner, S., Brassamin, S., Zanghi, D., Cuello, G. J., Koza, M., Magazù, S., Greaves, G. N., Price, D. L. 2011. "Aerodynamic Levitation and Laser Heating: Applications at Synchrotron and Neutron Sources." *European Physical Journal: Special Topics* 196: 151–165.

[20] Hennet, L., Pozdnyakova, I., Bytchkov, A., Cristiglio, V., Zanghi, D., Brassamin, S., Brun, J. F., Leydier, M. and Price, D. L. 2008. "Fast X-Ray Scattering Measurements on High Temperature Levitated Liquids." *Journal of Non-Crystalline Solids* 354 (47–51): 5104–7.

[21] Hennet, L., Pozdnyakova, I., Cristiglio, V., Cuello, G. J., Jahn, S., Krishnan, S., Saboungi, M. L. and Price, D. L. 2007. "Short- and Intermediate-Range Order in Levitated Liquid Aluminates." *Journal of Physics: Condensed Matter* 19 (45): 455210.

[22] Hennet, L., Krishnan, S., Pozdnyakova, I., Cristiglio, V., Cuello, G. J., Fischer, H. E., Bytchkov, A., Albergamo, F., Zanghi, D., Brun, J. F., Brassamin, S., Saboungi, M. L., Price, D. L. 2007.

"Structure and Dynamics of Levitated Liquid Materials." *Pure and Applied Chemistry* 79: 1643–52.

[23] Cristiglio, V., L. Hennet, G. J. Cuello, I. Pozdnyakova, A. Bytchkov, P. Palleau, H. E. Fischer, D. Zanghi, M. L. Saboungi, and D. L. Price. 2007. "Structural Study of Levitated Liquid Y_2O_3 Using Neutron Scattering." *Journal of Non-Crystalline Solids* 353 (8–10): 993–95.

[24] Hennet, L., Pozdnyakova, I., Cristiglio, V., Krishnan, S., Bytchkov, A., Albergamo, F., Cuello, G. J. et al. 2007. "Structure and Dynamics of Levitated Liquid Aluminates." *Journal of Non-Crystalline Solids* 353 (18–21): 1705–12.

[25] Mathiak, Gerhard, Juergen Brillo, Ivan Egry, Irina Pozdnyakova, Louis Hennet, Didier Zanghi, Aleksei Bytchkov, David L Price, and Dominique Thiaudiere. 2006. "Versatile Levitation Facility for Structural Investigations of Liquid Metals." *Microgravity Science and Technology* 18 (3–4): 67–72.

[26] Hennet, Louis, Irina Pozdnyakova, Aleksei Bytchkov, Viviana Cristiglio, Pierre Palleau, Henry E. Fischer, Gabriel J. Cuello, et al. 2006. "Levitation Apparatus for Neutron Diffraction Investigations on High Temperature Liquids." *Review of Scientific Instruments* 77 (5).

[27] Mathiak, G., I. Egry, L. Hennet, D. Thiaudière, I. Pozdnyakova, and D. Price. 2005. "Aerodynamic Levitation and Inductive Heating - A New Concept for Structural Investigations of Undercooled Melts." In *International Journal of Thermophysics*, 26:1151–66.

[28] Krishnan, S., Nordine, P. C., Weber, J. K. R., Schiffman, R. A. 1991. "Optical Properties and Melting Point of Pure Boron." *High Temperature Science* 31: 45.

[29] Winborne, David A., Paul C. Nordine, Daniel E. Rosner, and Neil F. Marley. 1976. "Aerodynamic Levitation Technique for Containerless High Temperature Studies on Liquid and Solid Samples." *Metallurgical Transactions B* 7 (4): 711–13.

[30] Weber, J. K. R., Krishnan, S., Ansell, S., Hixson, A. D., and Nordine, P. C., 2000. "Structure of Liquid $Y_3Al_5O_{12}$ (YAG)." *Physical Review Letters* 84 (16): 3622–25.

[31] Wang, T. G., Anilkumar, A. V., Lee C. P. 1996. "Oscillations of Liquid Drops: Results from USML-1 Experiments in Space." *Journal of Fluid Mechanics* 308: 1–14.

[32] Cristiglio, V., Grillo, I., Fomina, M., Wien, F. Shalaev, E. Novikov, A. Brassamin, S., Réfrégiers, M., Pérez, J. and Hennet, L. 2017. "Combination of Acoustic Levitation with Small Angle Scattering Techniques and Synchrotron Radiation Circular Dichroism. Application to the Study of Protein Solutions." *Biochimica et Biophysica Acta - General Subjects* 1861 (1).

[33] Weber, J. K. R., Krishnan, S., Schiffman, R. A., Nordine P. C. 1990. "Containerless Processing of Amorphous Ceramics." In *Containerless Experimentation in Microgravity Workshop, JPL, Pasadena, CA*, 385–90.

[34] Weber, J. K. R., Krishnan, S., Nordine P. C. 1991. "The Use of Containerless Processing in Researching Reactive Materials." *Journal of the Minerals, Metals, and Materials Society* 43: 8–14.

[35] DeVos, J. K., Hampton, D. S., Merkley, D. R., Rey, C. A., Weber, J. K. R. 1992. "No Title." *International Journal of Microgravity Science and Application* 9: 146–61.

[36] Weber, J. K., Richard, D. Scott Hampton, Dennis R. Merkley, Charles A. Rey, Mark M. Zatarski, and Paul C. Nordine. 1994. "Aero-Acoustic Levitation: A Method for Containerless Liquid-Phase Processing at High Temperatures." *Review of Scientific Instruments* 65 (2): 456–65.

[37] Biswas, A., Weber J. K. R., Nordine, P. C. 1995. "Removal of Residual Chromium from Aluminum Oxide by Containerless Liquid-Phase Processing." *Journal of Materials Research* 10: 1823–27.

[38] Weber J. K. R., Nordine P. C. 1995. "Containerless Liquid-Phase Processing at High Temperatures." *Microgravity Science and Technology* 7: 279–82.

[39] Biswas, A. B., Weber J. K. R., Nordine P. C. 1995. "Cr_{3+} Fluorescence in Containerless Melt-Purified Aluminum Oxide." *Journal of Materials Research* 10: 1823–27.

[40] Weber, J. K Richard. 1995. "Containerless Property Measurements on Molten Aluminum Oxide and Alumino-Silicate Binary Mixtures." In *4th Asian Thermophysical Properties Conference, Tokyo, Ed. A. Nagashima*, 873–76.

[41] Weber, J. K. R., Felten, J. J., Cho, B., Nordine P. C. 1996. "Design and Performance of the Aero-Acoustic Levitator." *International Journal of Microgravity Science and Application* 13: 27–35.

[42] Weber, J. K. R. 1996. "The Status of Containerless Processing for Materials Research and Development." In *Space '96, Tokyo, Japan*, 91–118.

[43] Weber, J. K. R. 1997. "Behavior of Molten Oxides under Containerless Conditions." *European Journal of Solid State and Inorganical Chemistry* 34: 847–59.

[44] Nordine, Paul C., Richard Weber, J. K. and Johan, G. Abadie. 2000. "Properties of High-Temperature Melts Using Levitation." *Pure and Applied Chemistry* 72 (11): 2127–36.

[45] Weber, J. K. R., Rix, J. E., Benmore, C. J., Hart, R. T., Hiera, K. J., Tangeman, J. A., Siewenie, J. E., Santodonato L. J. 2006. "Combined Levitation and Neutron Diffraction to Investigate Liquids and Solids at High Temperatures." In *ICANS-XVII, Santa Fe, New Mexico, III*, 1102–9.

[46] Weber, J. K. R., Rey, C. A., Neuefeind, J. and Benmore, C. J. 2009. "Acoustic Levitator for Structure Measurements on Low Temperature Liquid Droplets." *Review of Scientific Instruments* 80 (8).

[47] Weber, J. K. Richard. 2010. "The Containerless Synthesis of Glass." *International Journal of Applied Glass Science* 1: 248–256.

[48] Benmore, C. J., Weber J. K. R. 2011. "Amorphization of Molecular Liquids of Pharmaceutical Drugs by Acoustic Levitation." *Physical Review X* 1 (1).

[49] Weber, Richard J. K., Chris J. Benmore, Sonia K. Tumber, Amit N. Tailor, Charles A. Rey, Lynne S. Taylor, and Stephen R. Byrn. 2012. "Acoustic Levitation: Recent Developments and Emerging Opportunities in Biomaterials Research." *European Biophysics Journal* 41 (4): 397–403.

[50] Benmore, Chris J., Weber, J. K. R., Amit N. Tailor, Brian R. Cherry, Jeffery L. Yarger, Qiushi Mou, Warner Weber, Joerg Neuefeind, and Stephen R. Byrn. 2013. "Structural Characterization and Aging of Glassy Pharmaceuticals Made Using Acoustic Levitation." *Journal of Pharmaceutical Sciences* 102 (4): 1290–1300.

[51] Weber, J. K. R., Benmore, C. J., Tailor, A. N., Tumber, S. K., Neuefeind, J., Cherry, B., Yarger, J. L., Mou, Q., Weber, W. and Byrn, S. R. 2013. "A Neutron-X-Ray, NMR and Calorimetric Study of Glassy Probucol Synthesized Using Containerless Techniques." *Chemical Physics* 424: 89–92.

[52] Weber, J. K. R., Benmore, C. J., Suthar, K. J., Tamalonis, A. J., Alderman, O. L. G., Sendelbach, S., Kondev, V., Yarger, J., Rey, C. A. and Byrn, S. R. 2017. "Using Containerless Methods to Develop Amorphous Pharmaceuticals." *Biochimica et Biophysica Acta - General Subjects* 1861 (1): 3686–92.

[53] Caccamo, M. T., Cannuli, A., Calabrò, E. and Magazù, S. 2017. "Acoustic Levitator Power Device: Study of Ethylene-Glycol Water Mixtures." In *IOP Conference Series: Materials Science and Engineering*. 199:12119.

[54] Caccamo, M. T., Cannuli, A. 2018. "PEG Acoustic Levitation Treatment for Historic Wood Preservation Investigated by Means of FTIR Spectroscopy." In Press on *Current Chemical Biology*.

[55] Cannuli A., Caccamo M. T., Castorina G., Colombo F., Magazù, S. 2018. "Laser Techniques on Acoustically Levitated Droplets." *EPJ Web of Conferences* 167: 05010.

[56] Lokotosh, T. V., S. Magazù, G. Maisano, and N. P. Malomuzh. 2000. "Nature of Self-Diffusion and Viscosity in Supercooled Liquid Water." *Physical Review E - Statistical Physics, Plasmas, Fluids, and Related Interdisciplinary Topics* 62 (3 A): 3572–3580.

[57] Magazù, S. 1996. "IQENS - Dynamic Light Scattering Complementarity on Hydrogenous Systems." *Physica B* 226: 92–106.

[58] Magazù, S., Maisano, G., Mallamace, F., Micali, N. 1989. "Growth of Fractal Aggregates in Water Solutions of Macromolecules by Light-Scattering." *Physical Review A* 39: 4195–4200.

[59] Jannelli M. P., Magazù S., Migliardo P., Aliotta, F., Tettamanti, E. 1996. "Transport Properties of Liquid Alcohols Investigated by IQENS, NMR and DLS Studies." *Journal of Physics: Condensed Matter* 8 (43): 8157-8171.

[60] Magazù, S., Migliardo, F., Telling, M. T. F. 2008. "Structural and Dynamical Properties of Water in Sugar Mixtures." *Food Chemistry* 106 (4 SPEC. ISS.): 1460–1466.

[61] Magazù, S., Calabrò, E., Caccamo, M. T. and Cannuli, A. 2016. "The Shielding Action of Disaccharides for Typical Proteins in Aqueous Solution against Static, 50 Hz and 1800 MHz Frequencies Electromagnetic Fields." *Current Chemical Biology* 10 (1).

[62] Branca, C., Magazù, S., Maisano, G., Migliardo, P., Villari, V. and Sokolov, A P. 1999. "The Fragile Character and Structure-Breaker Role of Alpha, Alpha-Trehalose: Viscosity and Raman Scattering Findings." *Journal of Physics-Condensed Matter* 11 (19): 3823–3832.

[63] Magazù, S., Maisano, G., Migliardo, P. Middendorf, H. D. Villari, V. 1998. "Hydration and Transport Properties of Aqueous Solutions of α-α Trehalose." *Journal of Chemical Physics* 109: 1170–1174.

[64] Ballone, P., Marchi, M., Branca, C. and Magazù, S. 2000. "Structural and Vibrational Properties of Trehalose: A Density Functional Study." *Journal of Physical Chemistry B* 104 (26): 6313–6317.

[65] Magazù, S., Maisano, G., Migliardo, P., Tettamanti, E. and Villari, V. 1999. "Transport Phenomena and Anomalous Glass-Forming Behaviour in Alpha, Alpha-Trehalose Aqueous Solutions." *Molecular Physics* 96 (3): 381–387.

[66] Magazù, S., Maisano, G., Middendorf, H. D., Migliardo, P., Musolino, A. M. and Villari, V. 1998. "Alpha,alpha-Trehalose-Water Solutions. II. Influence of Hydrogen Bond Connectivity on Transport Properties." *Journal of Physical Chemistry B* 102 (11): 2060–2063.

[67] Minutoli, L., Altavilla, D., Bitto, A., Polito, F., Bellocco, E., Laganà, G., Fiumara, T., Magazù, S., Migliardo, F., Venuti, F. and Squadrito, F. 2008. "Trehalose: A Biophysics Approach to Modulate the Inflammatory Response during Endotoxic Shock." *European Journal of Pharmacology* 589 (1–3): 272–280.

[68] Pagnotta, S. E., Ricci, M. A., Bruni, F., McLain, S. and Magazù, S. 2008. "Water Structure around Trehalose." *Chemical Physics* 345 (2–3): 159–163.

[69] Magazù, S., Migliardo, F. and Telling, M. T. F. 2007. "Study of the Dynamical Properties of Water in Disaccharide Solutions." *European Biophysics Journal* 36 (2): 163–171.

[70] Branca, C., Magazù, S., Maisano, G. and Migliardo, P. 1999. "Alpha,alpha-Trehalose-Water Solutions. 3. Vibrational Dynamics Studies by Inelastic Light Scattering." *Journal of Physical Chemistry B* 103 (8): 1347–53.

[71] Magazù, S., Maisano, G., Migliardo, P. and Villari, V. 1999. "Experimental Simulation of Macromolecules in Trehalose Aqueous Solutions: A Photon Correlation Spectroscopy Study." *Journal of Chemical Physics* 111 (19): 9086–9092.

[72] Minutoli, L., Altavilla, D., Bitto, A., Polito, F., Bellocco, E., Laganà, G., Giuliani, D., Fiumara, T., Magazù, S., Ruggeri, P., Guarini, S. and Squadrito F. 2007. "The Disaccharide Trehalose Inhibits Proinflammatory Phenotype Activation in Macrophages and Prevents Mortality in Experimental Septic Shock." *Shock Society* 27 (1): 91–96.

[73] Magazù, S., Calabrò, E. and Campo, S. 2010. "FTIR Spectroscopy Studies on the Bioprotective Effectiveness of Trehalose on Human Hemoglobin Aqueous Solutions under 50 Hz Electromagnetic Field Exposure." *Journal of Physical Chemistry B* 114 (37): 12144–12149.

[74] Barreca, D., Laganà, G., Ficarra, S., Tellone, E., Leuzzi, U., Magazù, S., Galtieri, A. and Bellocco, E. 2010. "Anti-Aggregation Properties of Trehalose on Heat-Induced Secondary Structure and Conformation Changes of Bovine Serum Albumin." *Biophysical Chemistry* 147 (3): 146–152.

[75] Magazù, S., Migliardo, F., Affouard, F., Descamps, M. and Telling, M. T. F. 2010. "Study of the Relaxational and Vibrational Dynamics of Bioprotectant Glass-Forming Mixtures by Neutron Scattering and Molecular Dynamics Simulation." *Journal of Chemical Physics* 132 (18):184512.

[76] Varga, B., Migliardo, F., Takacs, E., Vertessy, B., Magazù, S. and Mondelli, C. 2008. "Neutron Scattering Studies on dUTPase Complex in the Presence of Bioprotectant Systems." *Chemical Physics* 345 (2–3): 250–258.

[77] Migliardo F., Caccamo, M. T., Magazù, S. 2014. "Thermal Analysis on Bioprotectant Disaccharides by Elastic Incoherent Neutron Scattering." *Food Biophysics* 9: 99–104.

[78] Magazù, S., Migliardo, F., Benedetto, A., Calabrò, E., La Torre, R., Caccamo, M. T. 2013. *"Bioprotective Effects of Sucrose and Trehalose on Proteins in Sucrose."* Nova Science Publishers, 35–46.

[79] Branca, C., Maccarrone, S., Magazù, S., Maisano, G., Bennington, S. M., Taylor, J. 2005. "Tetrahedral Order in Homologous Disaccharide-Water Mixtures." *Journal of Chemical Physics* 122: 174513-1 - 174513-6.

[80] Branca, C., Magazù, S., Migliardo, F., Migliardo, P. 2002. "Destructuring Effect of Trehalose on the Tetrahedral Network of Water: A Raman and Neutron Diffraction Comparison." *Physical Review A* 304 (1–2): 314–318.

[81] Condello, S., Calabrò, E., Caccamo, D., Currò, M., Ferlazzo, N., Satriano, J., Magazù, S., Ientile, R. 2012. "Protective Effects of Agmatine in Rotenone-Induced Damage of Human SH-SY5Y Neuroblastoma Cells: Fourier Transform Infrared Spectroscopy Analysis in a Model of Parkinson's Disease." *Amino Acids* 42 (2–3): 775–781.

[82] Magazù, S., Migliardo, F., Vertessy, B. G. and Caccamo, M. T. 2013. "Investigations of Homologous Disaccharides by Elastic Incoherent Neutron Scattering and Wavelet Multiresolution Analysis." *Chemical Physics* 424: 56–61.

[83] Migliardo, F., Caccamo, M. T., Magazù, S. 2013. "Elastic Incoherent Neutron Scatterings Wavevector and Thermal Analysis on Glass-Forming Homologous Disaccharides." *Journal of Non-Crystalline Solids* 378: 144–151.

[84] Branca, C., Magazù, S., Maisano, G., Bennington, S. M. and Fåk, B. 2003. "Vibrational Studies on Disaccharide/H_2O Systems by Inelastic Neutron Scattering, Raman, and IR Spectroscopy." *The Journal of Physical Chemistry B* 107 (6): 1444–1451.

[85] Magazù, S., Migliardo, F., Benedetto, A. 2010. "Mean Square Displacements from Elastic Incoherent Neutron Scattering Evaluated by Spectrometers Working with Different Energy Resolution on Dry and Hydrated (H_2O and D_2O) Lysozyme." *Journal of Physical Chemistry B* 114: 9268–9274.

[86] Fenimore, Paul W., Frauenfelder, H., Magazù, S., Benjamin H. McMahon, Mezei, F., Migliardo, F., Young, Robert D. and Stroe, I. 2013. "Concepts and Problems in Protein Dynamics." *Chemical Physics* 424: 2–6.

[87] Barreca, D., Lagana, G., Bruno, G., Magazù, S., Bellocco E. Diosmin Binding to Human Serum Albumin and its Preventive Action Against Degradation Due to Oxidative Injuries. *Biochimie*. 2013;95(11):2042-2049.

[88] Magazù, S., Migliardo, F., Benedetto, A, Mondelli, C., Gonzalez, M. A. 2011. "Thermal Behaviour of Hydrated Lysozyme in the Presence of Sucrose and Trehalose by EINS." In *Journal of Non-Crystalline Solids*, 357:664–670.

[89] Magazù, S. 2000. "NMR, Static and Dynamic Light and Neutron Scattering Investigations on Polymeric Aqueous Solutions." *Journal of Molecular Structure* 523 (1–3): 47–59.

[90] Faraone, A., Magazù, S., Maisano, G., Ponterio, R. and Villari, V. 1999. "Experimental Evidence of Slow Dynamics in Semidilute Polymer Solutions." *Macromolecules* 32 (4): 1128–1133.

[91] Faraone, A., Magazù, S., Maisano, G., Migliardo, P., Tettamanti, E. and Villari, V. 1999. "The Puzzle of Poly(Ethylene Oxide) Aggregation in Water: Experimental Findings." *The Journal of Chemical Physics* 110 (3): 1801–1806.

[92] Branca, C., Faraone, A., Magazù, S., Maisano, G., Migliardo, P., Villari, V. 2000. "Polyethylene Oxide: A Review of Experimental Findings by Spectroscopic Techniques." *Journal of Molecular Liquids* 87 (1): 21–68.

[93] Branca, C., Faraone, A., Maisano, G., Magazù, S., Migliardo, P., Triolo, A., Triolo, R. and Villari, V. 1999. "Can the Isotopic H<->D Substitution Affect the Conformational Properties of Polymeric Aqueous Solutions? The Poly(ethylene Oxide)-Water Case." *Journal of Physics: Condensed Matter*. 11: 6079–6098.

[94] Branca, C., Magazù, S., Maisano, G., Migliardo, P., Migliardo, F. and Romeo, G. 2002. "Hydration Parameters of Aqueous Solutions of Poly(Ethylene Glycol)s by Viscosity Data." *Physica Scripta* 66 (2): 175-179.

[95] Branca, C., Magazù, S., Maisano, G., Migliardo, F., Migliardo, P. and Romeo, G. 2003. "Study of Conformational Properties of Poly (Ethylene Oxide) by SANS and PCS Techniques." *Physica Scripta* 67: 551–554.

[96] Branca, C., Faraone, A., Magazù, S., Maisano, G., Migliardo, P., Triolo, A., Triolo, R. and Villari, V. 2000. "Anomalous Conformational Properties of PEO in H_2O and D_2O by SANS, PCS and Raman Scattering." *Journal of Applied Crystallography* 33 (3): 709–713.

[97] Magazù, S., Maisano, G. 2001. "New Experimental Results in Physics of Liquids." *Journal of Molecular Liquids* 93 (1–3): 7–27.

[98] Branca, C., Magazù, S., Maisano, G., Auditore, L., Barnà, R. C., De Pasquale, D., Emanuele, U., Trifirò, A., Trimarchi, M. 2006. "Synthesis of PolyEthylene Oxide Hydrogels by Electron Radiation." *Journal of Applied Polymer Science* 102: 820–824.

[99] Branca, C., Magazù, S., Maisano, G., Migliardo, P. and Tettamanti, E. 1999. "Criticism to Light-Heavy Water Substitution in Structural Studies of Macromolecular Aqueous Solutions." *Physica B: Condensed Matter* 270 (3–4): 350–359.

[100] Branca, C., Faraone, A., Lokotosh, T., Magazù, S., Maisano, G., Malomuzh, N. P., Migliardo, P. and Villari, V. 2001. "Diffusive Dynamics: Self vs. Collective Behaviour." In *Journal of Molecular Liquids*, 93:139–149.

[101] Faraone, A., Branca, C., Magazù, S., Maisano, G., Middendorf, H. D., Migliardo, P. and Villari, V. 2000. "QENS and PCS Study of Aqueous BSA-PEO `crowded' Solutions." *Physica B: Condensed Matter* 276–278: 524–525.

[102] Triolo, R., V. Arrighi, A. Triolo, P. Migliardo, S. Magazù, J. B. McClain, D. Betts, J. M. Desimone, and H. D. Middendorf. 2000. "QENS from Polymer Aggregates in Supercritical CO2." *Physica B: Condensed Matter* 276–278: 386–387.

[103] Branca, C., Faraone, A., Magazù, S., Maisano, G., Migliardo, P., Villari, V. 1999. "Swelling Processes in Aqueous Polymer Solutions by PCS and Raman Scattering." In *Journal of Molecular Structure*, 482–483:503–507.

[104] Magazù, S., Villari, V., Faraone, A., Maisano, G. and Janssen, S. 2002. "Effect of the Monomer Structure on the Dynamics of Semidilute Polyalkylmethacrylate Solutions: A Quasielastic Light and Neutron Scattering Investigation." *Journal of Chemical Physics* 116 (1): 427–435.

[105] Faraone, A., Magazù, S., Maisano, G., Villari, V. and Maschio, G. 1999. "Possibilities and Limits of Photon Correlation Spectroscopy in Determining Polymer Molecular Weight Distributions." *Macromolecular Chemistry and Physics* 200 (5): 1134–1142.

[106] Branca, C., Magazù, S., Maisano, G., Migliardo, F., Migliardo, P., Romeo, G., Vertessy, B. 2001. "Conformational Studies of Poly(Ethylene Oxide) in Crystalline, Molten, and Solution Phase." *Molecular Crystals and Liquid Crystals Science and Technology Section A: Molecular Crystals and Liquid Crystals* 372: 17–23.

[107] Magazù, S., Migliardo, F., Barreca, D., Bellocco, E. and Laganà, G. 2008. "Neutron Scattering Study on the Interaction between Polyethylene Glycol and Lysozyme." *Physica B: Condensed Matter* 403 (13–16): 2408–2412.

[108] Villari, V., Faraone, A., Magazù, S., Maisano, G., Ponterio, R. 2000. "Dynamical Properties of Highly Entangled Polyalkylmethacrylate Solutions: A Comparative Study." *Journal De Physique. IV: JP* 10 (7): 321–24.

[109] Branca, C., Faraone, A., Magazù, S., Maisano, G., Migliardo, P., Triolo, A., Triolo, R. and Villari, V. 2000. "Effects of Isotopic Substitution on the Conformational Properties of Polymeric Aqueous Solutions." *Physica B: Condensed Matter* 276–278: 332–333.

[110] Faraone, A., Branca, C., Magazù, S., Maisano, G., Migliardo, P., Villari, V. 2000. "Slow Dynamics Features in Aqueous Solutions of High Molecular Weight Poly (Ethylene Oxide)." *AIP Conference Proceedings, 513*, 118–121.

[111] Magazù, S., Branca, C., Faraone, A., Maisano, G., Migliardo, P., Villari, V. 2000. "On the Aggregation of Poly (Ethylene Oxide) in Water." *AIP Conference Proceedings, 513*, 146–149.

[112] Triolo, R., Arrighi, V., Triolo, A., Migliardo, P., Magazù, S., McClain, J. B., Betts, D., DeSimone, J. M. and Middendorf, H. D. 2000. "QENS from Polymeric Micelles in Supercritical CO_2." In *AIP Conference Proceedings 513*, 234.

[113] Faraone, A., Magazù, S., Maisano, G., Migliardo, P., Tniolo, A., Triolo, R., Vlllari, V. 1999. "PCS and SANS Studies on PEO-H_2O Systems." *Nuovo Cimento Della Societa Italiana Di Fisica D - Condensed Matter, Atomic, Molecular and Chemical Physics, Biophysics* 20: 2531–2540.

[114] Magazù, S., Maisano, G., Migliardo, R., Tettamanti, E. 1999. "Diffusive Dynamics of Polymeric Aqueous Solutions by NMR and DLS." *Nuovo Cimento Della Societa Italiana Di Fisica D - Condensed Matter, Atomic, Molecular and Chemical Physics, Biophysics* 20: 2521–2530.

[115] Aliotta, F., Fontanella, M. E., Magazù, S., Wanderlingh, U. 1991. "Hypersonic Properties in Macromolecular Aqueous Solutions." *Progress in Colloid and Polymer Science*. 84: 483–486.

[116] Branca, C., Magazù, S., Maisano, G., Migliardo, P. and Villari, V. 1998. "Conformational Distribution of Poly(ethylene Oxide) in Molten Phase and in Aqueous Solution by Quasi-Elastic and Inelastic Light Scattering." *Journal of Physics: Condensed Matter* 10 (45): 10141-10157.

[117] Migliardo, F., Magazù, S. and Caccamo, M. T. 2013. "Infrared, Raman and INS Studies of Poly-Ethylene Oxide Oligomers." *Journal of Molecular Structure* 1048: 261–266.

[118] Caccamo, M. T. and Magazù, S. 2016. "Tagging the Oligomer-to-Polymer Crossover on EG and PEGs by Infrared and Raman Spectroscopies and by Wavelet Cross-Correlation Spectral Analysis." *Vibrational Spectroscopy* 85: 222–227.

[119] Caccamo, M. T., Magazù, S. 2017. "Ethylene Glycol - Polyethylene Glycol (EG-PEG) Mixtures: Infrared Spectra Wavelet Cross-Correlation Analysis." *Applied Spectroscopy* 71 (3): 401–409.

[120] Caccamo, M. T., and S. Magazù. 2017. "Multiscaling Wavelet Analysis of Infrared and Raman Data on Polyethylene Glycol 1000 Aqueous Solutions." *Spectroscopy Letters*. 50:130-136.

[121] Caccamo, M. T. and Magazù, S. 2017. "Thermal Restraint on PEG-EG Mixtures by FTIR Investigations and Wavelet Cross-Correlation Analysis." *Polymer Testing* 62: 311–318.

[122] Apicella, A., Cappello, B., Del Nobile, M. A., La Rotonda, M. I., Mensitieri, G. and Nicolais, L. 1993. "Poly(Ethylene Oxide) (PEO) and Different Molecular Weight PEO Blends Monolithic Devices for Drug Release." *Biomaterials* 14 (2): 83–90.

[123] Branca, C., Magazù, S., Maisano, G., Migliardo, F., Migliardo, P. and Romeo, G. 2002a. "Hydration Study of PEG/water Mixtures by Quasi Elastic Light Scattering, Acoustic and Rheological Measurements." *Journal of Physical Chemistry B* 106 (39): 10272–76.

[124] Chen, Ji, Scott, K., Spear, Jonathan G., Huddleston and Robin D. Rogers. 2005. "Polyethylene Glycol and Solutions of Polyethylene Glycol as Green Reaction Media." *Green Chemistry* 7 (2): 64.

[125] Gonzalez-Tello, P., Camacho, F. and Blazquez, G. 1994. "Density and Viscosity of Concentrated Aqueous Solutions of Polyethylene Glycol." *Journal of Chemical & Engineering Data* 39 (3): 611–14.

[126] Acharya, S. A.; Acharya, V. N.; Kanika, N. D.; Tsai, A. G. M. Intaglietta, B. Manjula, N. 2007. "Non-Hypertensive TetraPEGylated Canine Haemoglobin: Correlation Between PEGylation, O_2 Affinity and Tissue Oxygenation." *Biochemical Journal* 405 (3): 503–11.

[127] Hu, T., Manjula, B. N.; Li, D. X.; Brenowitz, M.; Acharya, S. A. 2007. "Influence of Intramolecular Cross-Links on the Molecular, Structural and Functional Properties of PEGylated Haemoglobin." *Biochemical Journal* 402: 143–151.

[128] Arumugam, V., Akalya, A., Rajasekaran, J. F., Balakrishnan, B. 2000. "Ultrasonic Studies on PEG in Benzene." *Journal of Polymer Materials* 17: 371–76.

[129] Smith, G. D., Bedrov, D. and Borodin, O. 2000. "Conformations and Chain Dimensions of Poly (Ethylene Oxide) in Aqueous Solution: A Molecular Dynamics Simulation Study." *Journal of the American Chemical Society* 122: 9548–9549.

[130] Rostovtseva, Tatiana K., Ekaterina M. Nestorovich, and Sergey M. Bezrukov. 2002. "Partitioning of Differently Sized Poly(ethylene Glycol)s into OmpF Porin." *Biophysical Journal* 82 (1 Pt 1): 160–69.

[131] Venkatramanan, K. 2011. "A Study on the Molecular Interaction of PEG 1000 and Its Blend in Toluene Using Ultrasonic Technique." *International Review of Chemical Engineering* 3: 308–11.

[132] Cerveny, S., Alegría, A. and Colmenero, J. 2008. "Universal Features of Water Dynamics in Solutions of Hydrophilic Polymers, Biopolymers, and Small Glass-Forming Materials." *Physical Review E - Statistical, Nonlinear, and Soft Matter Physics* 77 (3).

[133] Jonsson, B., Lindman, B. and Holmberg, K. 1998. "Surfactants and Polymers in Aqueous Solutions." *IEEE Electrical Insulation Magazine* 14 (5): 42–43.

[134] Flory, P. J. 1953. "Principles of Polymer Chemistry." *Cornell University Press, Ithaca, New York*, 399.

[135] Li, W., Kim, Y., Lia, J., Lee, M. 2014. "Dynamic Self-Assembly of Coordination Polymers in Aqueous Solution." *Soft Matter* 10: 5231–42.

[136] Cappello, B., Del Nobile, M. A., La Rotonda, M. I., Mensitieri, G., Miro, A. and Nicolais, L. 1994. "Water Soluble Drug Delivery Systems Based on a Non-Biological Bioadhesive Polymeric System." *Farmaco (Societa Chimica Italiana : 1989)* 49 (12): 809–18.

[137] Braun, A., Stenger, Patrick C., Heidi, Warriner E., Zasadzinski, Joseph A., Karen, Lu W. and Taeusch, William H. 2007. "A Freeze-Fracture Transmission Electron Microscopy and Small Angle X-Ray Diffraction Study of the Effects of Albumin, Serum, and Polymers on Clinical Lung Surfactant Microstructure." *Biophysical Journal* 93 (1): 123–39.

[138] Zimmerberg, J. and Parsegian, V. A. 1986. "Polymer Inaccessible Volume Changes during Opening and Closing of a Voltage-Dependent Ionic Channel." *Nature* 323 (6083): 36–39.

[139] Magazù, S., Migliardo, F., Malomuzh, Nicolay P. and Blazhnov, Ivan V. 2007. "Theoretical and Experimental Models on Viscosity: I. Glycerol." *Journal of Physical Chemistry B* 111 (32): 9563–9570.

[140] Chelli, R., Procacci, P., Cardini, G. and Califano, S. 1999. "Glycerol Condensed Phases {P}art {II}. {A} Molecular Dynamics Study of the Conformational Structure and Hydrogen Bonding." *Phys. Chem. Chem. Phys.* 1 (5): 879–85.

[141] Zondervan, R., Kulzer, F., Berkhout, Gregorius C. G. and Orrit, M. 2007. "Local Viscosity of Supercooled Glycerol near Tg Probed by Rotational Diffusion of Ensembles and Single Dye Molecules." *Proc. Natl. Acad. Sci. U. S. A.* 104 (31): 12628–33.

[142] Bradbury, S. L. and Jakoby, W. B. 1972. "Glycerol as an Enzyme-Stabilizing Agent: Effects on Aldehyde Dehydrogenase." *Proceedings of the National Academy of Sciences of the United States of America* 69 (9): 2373–76.

[143] Grandori, R., Matecko, I., Mayr, P. and Muller, N. 2001. "Probing Protein Stabilization by Glycerol Using Electrospray Mass Spectrometry." *J Mass Spectrom* 36 (8): 918–22.

[144] Towey, J. J., Soper, A. K. and Dougan, L. 2011a. "Preference for Isolated Water Molecules in a Concentrated Glycerol-Water Mixture." *Journal of Physical Chemistry B* 115 (24): 7799–7807.

[145] Towey, J. J., Soper, A. K. and Dougan, L. 2011b. "The Structure of Glycerol in the Liquid State: A Neutron Diffraction Study." *Physical Chemistry Chemical Physics : PCCP* 13 (20): 9397–9406.

[146] Bonaccorsi, L., Lombardo, D., Longo, A., Proverbio, E. and Triolo, A. 2009. "Dendrimer Template Directed Self-Assembly during Zeolite Formation." *Macromolecules* 42: 1239–1243.

[147] Calandra, P., Caschera, D., Liveri, V. T., Lombardo, D. 2015. "How Self-Assembly of Amphiphilic Molecules Can Generate Complexity in the Nanoscale." *Colloids and Surfaces A: Physicochemical and Engineering Aspects* 484: 164–83.

[148] Lombardo, D. 2014. "Modeling Dendrimers Charge Interaction in Solution: Relevance in Biosystems." *Biochemistry Research International* 2014.

[149] Kiselev, M. A., Lombardo, D., Lesieur, P., Kisselev, A. M., Borbely, S., Simonova, T. N., Barsukov, L. I. 2008. "Membrane Self Assembly in Mixed DMPC/NaC Systems by SANS." *Chemical Physics* 345: 173–80.

[150] Kiselev, M. A., Janich, M., Hildebrand, A., Strunz, P., Neubert, R. H. H., Lombardo D. 2013. "Structural Transition in Aqueous Lipid/bile Salt [DPPC/NaDC] Supramolecular Aggregates: SANS and DLS Study." *Chemical Physics* 424: 93–99.

[151] Magazù, S., Migliardo, F., Caccamo, M. T. 2013. "Upgrading of Resolution Elastic Neutron Scattering (RENS)." *Advances in Materials Science and Engineering.* 2013: 695405.

[152] Magazù, S., Maisano, G., Migliardo, F., Galli, G., Benedetto, A., Morineau, D., Affouard, F., Descamps M. 2008. "Characterization of Molecular Motions in Biomolecular Systems by Elastic Incoherent Neutron Scattering." *Journal of Chemical Physics* 129: 155103-1- 155103-7.

[153] Magazù, S., Migliardo, F., Benedetto, A. 2011. "Elastic Incoherent Neutron Scattering Operating by Varying Instrumental Energy Resolution: Principle, Simulations, and Experiments of the Resolution Elastic Neutron Scattering (RENS)." *Review of Scientific Instruments* 82 (10): 105115-1 - 105115-11.

[154] Magazù, S., Maisano, G., Migliardo, F., Benedetto A. 2008. "Elastic Incoherent Neutron Scattering on Systems of Biophysical Interest: Mean Square Displacement Evaluation from Self-Distribution Function." *Journal of Physical Chemistry B* 112: 8936–8942.

[155] Magazù, S., Maisano, G., Migliardo, F., and Benedetto, A. 2009. "Biomolecular Motion Characterization by a Self-Distribution-Function Procedure in Elastic Incoherent Neutron Scattering." *Physical Review E* 79: 041915.

[156] Brenn, G., Wiedemann, T., Reinsink, D., Kastner, O., Yarin, A. L. 2001. "Modeling and Experimental Investigation of the Morphology of Spray Dryed Particles." *Chemical Engineering Technologies* 24.

[157] Kiselev, M. A., Lombardo, D. 2017. "Structural Characterization in Mixed Lipid Membrane Systems by Neutron and X-Ray Scattering." *Biochimica et Biophysica Acta - General Subjects* 1861 (1): 3700–3717.

[158] Brenn, G., Reinsink, D., Tropea C., Yarin, A. L. 1997. "Investigation of Droplet Drying Characteristics Using an Acoustic-Aerodynamic Levitator." *7th International Conference on Liquid Atomization and Spray Systems (ICLASS) Seoul (Korea).*

[159] Yarin, A. L., Pfaffenlehner, M., Tropea C. 1998. "On the Acoustic Levitation of Droplets." *Journal of Fluid Mechanics* 356: 65–91.

[160] Yarin, A. L., Weiss, D. A., Brenn, G., Reinsink, D. 2002. "Acoustically Levitated Drops: Drop Oscillation and Break-up Driven by Ultrasound Modulation." *International Journal of Multiphase Flow* 28: 887–910.

[161] Groenewold, C., Möser, C., Groenewold, H., Tsotsas, E. 2002. "Determination of Single-Particle Drying Kinetics in an Acoustic Levitator." *Chemical Engineering Journal* 86: 217–22.

[162] Kawahara, N., Yarin, A. L., Brenn, G., Kastner, O., Durst, F. 2000. "Effect of Acoustic Streaming on the Mass Transfer from a Sublimating Sphere." *Physics of Fluids* 12.

[163] Caccamo, M. T. and Magazù, S. 2017b. "Variable Mass Pendulum Behaviour Processed by Wavelet Analysis." *European Journal of Physics* 38 (1): 15804.

[164] Caccamo, M. T., Calabró, E., Cannuli, A. and Magazù, S. 2016. "Wavelet Study of Meteorological Data Collected by Arduino-Weather Station: Impact on Solar Energy Collection Technology." In *MATEC Web of Conferences*. 55: 02004.

[165] Marchese, N., Cannuli, A., Caccamo, M. T. and Pace, C. 2017. "New Generation Non-Stationary Portable Neutron Generators for Biophysical Applications of Neutron Activation Analysis." *Biochimica et Biophysica Acta - General Subjects* 1861: 3661-3670.

[166] Cannuli, A., Caccamo, M. T., Marchese, N., Tomarchio, E. A., Pace, C., Magazù, S. 2018. "Indoor Fast Neutron Generator for Biophysical and Electronic Applications." In press on *Journal of Physics: Conference Series*.

[167] Magazù, S., Migliardo, F. and Caccamo, M. T. 2012. "Innovative Wavelet Protocols in Analyzing Elastic Incoherent Neutron Scattering." *Journal of Physical Chemistry B* 116 (31): 9417–9423.

[168] Grinsted, A., Moore, J. C. and Jevrejeva, S. 2004. "Application of the Cross Wavelet Transform and Wavelet Coherence to Geophysical Time Series." *Nonlinear Processes in Geophysics* 11 (5/6): 561–66.

[169] Li, H. H., Nozaki, T. 1997. "Wavelet Analysis for the Plane Turbulent Jet (Analysis of Large Eddy Structure)." *International Journal Series B Fluids and Thermal Engineering* 40: 58–66.

[170] Daubechies, I. 1990. "The Wavelet Transform, Time-Frequency Localization and Signal Analysis." *IEEE Transactions on Information Theory* 36: 961–1005.

[171] Chen, X. J., Wu, D., He, Y., Liu Y., Liu, S. 2009. "Detecting the Quality of Glycerol Monolaurate: A Method for Using Fourier Transform Infrared Spectroscopy with Wavelet Transform and Modifued Uninformative Variable Elimination." *Analytica Chimica Acta* 638: 16–22.

[172] Caccamo, M. T., Cannuli, A. and Magazù, S. 2018. "Wavelet Analysis of near-Resonant Series RLC Circuit with Time-Dependent Forcing Frequency." *European Journal of Physics* 39: 045702.

PORTABLE NEUTRON SOURCE

[1] J. Chadwick, Possible existence of a neutron, Nature 129 (1932) 312.

[2] W. N. Cottingham, D. A. Greenwood, An Introduction to Nuclear Physics, Second ED., Cambridge University Press, Cambridge, 2001, pp. 19-32.

[3] B.K. Das, A. Shyam, Development of compact size penning ion source for compact neutron generator, Rev. Sci. Instrum. 79 (2008) 123305.

[4] J. Csikai, CRC Handbook of Fast Neutron Generators, CRC Press, Boca Raton, 1987.

[5] W. Liu, M. Li, K. Gao, D. Gu, Discharge Characteristics of a Penning Ion Source for Compact Neutron Generator, Nucl. Instrum. Methods Phys. Res. A 768 (2014) 120–123.

[6] International Atomic Energy Agency, Neutron generators for analytical purposes, International Atomic Energy Agency, Vienna, 2012.

[7] B.A. Ludewigt, R.P. Wells, J. Reijonen, High-Yield D–T Neutron Generator, Nucl. Instrum. Methods Phys. Res. B 261 (2007) 830–834.

[8] J. Reijonen, Compact Neutron Generators for Medical, Home Land Security, and Planetary Exploration, in: Particle Accelerator Conference, 2005. PAC 2005. Proceedings of the, IEEE, 2005, pp. 49–53.

[9] L. Liang, R. Rinaldi, H. Schober, Neutron Applications in Earth, Energy and Environmental Sciences, Springer, New York, 2009.

[10] A. Hershcovitch, T. Roser, Compact, Energy Efficient Neutron Source: Enabling Technology for Various Applications, BNL report CA/AP/364, unpublished, 2009.

[11] S. E. Oswald, M. Menon, A. Carminati, P. Vontobel, E. Lehmann, R. Schulin, Quantitative Imaging of Infiltration, Root Growth, and Root Water Uptake via Neutron Radiography, Vad. Zone J., 7 (2007) 1035-1047.

[12] Y.J. Park, B.C. Song, H.-J. Im, J.-Y. Kim, Performance Characteristics of a Prompt Gamma-Ray Activation Analysis (PGAA) System Equipped with a New Compact D–D Neutron Generator, Nucl. Instrum. Methods Phys. Res. A 606 (2009) 243–247.

[13] J. R. De Voe, P. D. La Fleur, Modern Trends in Activation Analysis, Proceedings of the 1968 International Conference held at the National Bureau of Standards, Gaithersburg, Maryland, October 7-11, 1968.

[14] W. D. James, 14 MeV Fast Neutron Activation Analysis in the Year 2000, J. Radioanal. Nucl. Chem. 243 (2000) 119.

[15] J. Ghassoun, D. Mostacci, A Compact Neutron Beam Generator System Designed for Prompt Gamma Nuclear Activation Analysis, Appl. Radiat. Isot. 69 (2011) 1138–1142.

[16] F. Gabel, D. Bicout, U. Lehner, M. Tehei, M. Weik, G. Zaccai, Protein Dynamics Studied by Neutron Scattering, Quart. Rev. Biophys. 35 (2000) 327-367.

[17] S. Magazù, F. Migliardo, A. J. Ramirez-Cuesta, Inelastic Neutron Scattering Study on Bioprotectant Systems, J. Roy. Soc. Interf. 2 (2005) 527-532.

[18] G. Zaccai, How Soft Is a Protein? A Protein Dynamics Force Constant Measured by Neutron Scattering, Science 288 (2000) 1604-1607.

[19] C. Branca, S. Magazù, G. Maisano, S. M. Bennington, B. Fak, Vibrational Studies on Disaccharide/H2O Systems by Inelastic Neutron Scattering, Raman, and IR Spectroscopy, J. Phys. Chem. B 107 (2003) 1444-1451.

[20] G. Zaccai, The Effect of Water on Protein Dynamics, Philos. Trans. R. Soc. Lond. B Biol. Sci., 359 (2004) 1269-1275.

[21] S. Magazù, F. Migliardo, M. T. F. Telling, Structural and Dynamical Properties of Water in Sugar Mixtures. Food Chem. 106 (2008) 1460-1466.

[22] L.M. Stimson, M.R. Wilson, Molecular Dynamics Simulations of Side Chain Liquid Crystal Polymer Molecules in Isotropic and Liquid-Crystalline Melts, J. Chem. Phys. 123 (2005).

[23] S. Magazù, IQENS - Dynamic Light Scattering Complementarity on Hydrogenous Systems, Physica B 226 (1996) 92-106.

[24] S. O. Diallo, Q. Zhang, H. O'Neill, E. Mamontov, High-Pressure Dynamics of Hydrated Protein in Bioprotective Trehalose Environment, Phys. Rev. E 90 (2014).

[25] M. P. Jannelli, S. Magazù, P. Migliardo, F. Aliotta, E. Tettamanti, Transport Properties of Liquid Alcohols Investigated by IQENS, NMR and DLS Studies, J Phys-Condens. Mat. 8 (1996) 8157-8171.

[26] A. D'Aprano, R. Giordano, M. P. Jannelli, S. Magazù, G. Maisano, B. Sesta, QELS and SANS Studies of Octyl-Beta-Glucoside Micellar Solutions, J. Mol. Struct. 383 (1996) 177-182.

[27] D. J. Bicout, G. Zaccai, Protein Flexibility from the Dynamical Transition: A Force Constant Analysis, Biophys. J. 80 (2001) 1115-1123.

[28] S. Magazù, F. Migliardo, M. T. Caccamo, Upgrading of Resolution Elastic Neutron Scattering (RENS), Adv. Mat. Sci. Eng. 2013 (2013) 1-7.

[29] H. Frauenfelder, Ask not What Physics Can Do for Biology-Ask What Biology Can Do for Physics. Phys. Biol. 11 (2014).

[30] S. E. Pagnotta, M. A. Ricci, F. Bruni, S. McLain, S. Magazù, Water Structure Around Trehalose, Chem. Phys. 345 (2008) 159-163.

[31] H. Frauenfelder, P. W. Fenimore, R. D. Young, A Wave-Mechanical Model of Incoherent QuasiElastic Scattering in Complex Systems, PNAS USA 111 (2014) 12764-12768.

[32] C. Branca, S. Magazù, G. Maisano, P. Migliardo, V. Villari, Conformational Distribution of Poly(Ethylene Oxide) in Molten Phase and in Aqueous Solution by Quasi-Elastic and Inelastic Light Scattering, J. Phys. Cond. Matter. 10 (1998) 10141-10157.

[33] X.Q. Chu, M. Gajapathy, K.L. Weiss, E. Mamontov, J.D. Ng, L. Coates, Dynamic Behavior of Oligomeric Inorganic Pyrophosphatase Explored by Quasielastic Neutron Scattering, J. Phys. Chem. B, 116 (2012) 9917-9921.

[34] N. Osaka, M. Shibayama, T. Kikuchi, O. Yamamuro, Quasi-Elastic Neutron Scattering Study on Water and Polymer Dynamics in Thermo/Pressure Sensitive Polymer Solutions, J. Phys. Chem. B, 113 (2009) 12870-12876.

[35] S. Magazù, F. Migliardo, M. T. F. Telling, Study of the Dynamical Properties of Water in Disaccharide Solutions, Eur. Biophys. J. Biophy. 36 (2007) 163-171.

[36] F. Cousin, Small Angle Neutron Scattering, Neutr. and Mater. for En., 104 (2015).

[37] S. Zaritskiy,B. Osmera, F. Cvachovec, M. Marik, S. Posta,V. Rypar, et al. Neutron and Gamma Spectrometry in the Research Reactor LR-0. Ieee Trans. Nucl. Sc. 62 (2015) 1212-1217.

[38] S. Magazù, F. Migliardo, A. Benedetto, C. Mondelli, M. A. Gonzalez, Thermal Behaviour of Hydrated Lysozyme in the Presence of Sucrose and Trehalose by EINS, J. Non-Cryst. Solids. 357 (2011) 664-670.

[39] G. Zaccai, The Environmental Force Constant Approach to Protein Dynamics Measured In-Situ by Neutron Scattering, Biophys. J. 78 (2000) 394a-394a.

[40] I. Hoffmann, Neutrons for the study of dynamics in soft matter systems, Colloid. Polym. Sci., 292 (2014) 2053-2069.

[41] S. Magazù, NMR, Static and Dynamic Light and Neutron Scattering Investigations on Polymeric Aqueous Solutions, J. Mol. Struct. 523 (2000) 47-59.

[42] G. Zaccai, M. Tehei, I.Scherbakova, I. Serdyuk, C. Gerez, C. Pfister, Incoherent Elastic Neutron Scattering as a Function of Temperature: A Fast Way to Characterise In-Situ Biological Dynamics in Complex Solutions, J. De Physique Iv. 10 (2000) 283-287.

[43] C. Branca, A. Faraone, S. Magazù, G. Maisano, P. Migliardo, V. Villari, PolyEthylene Oxide: a Review of Experimental Findings by Spectroscopic Techniques, J. Mol. Liquids, 87 (2000) 21-68.

[44] S. Mantha, A. Yethiraj, Dynamics of water confined in lyotropic liquid crystals: Molecular dynamics simulations of the dynamic structure factor, J. Chem. Phys. 144 (2016).

[45] F. Boue, F. Cousin, J. Gummel, J. Oberdisse, G. Carrot, A. El Harrak, Small angle scattering from soft matter - application to complex mixed systems, Cr. Phys. 8 (2007) 821-844.

[46] A. Buffler, F.D. Brooks, M.S. Allie, K. Bharuth-Ram, M.R. Nchodu, Material Classification by Fast Neutron Scattering Analysis. Nucl. Instrum. Meth. B 173 (2001) 483–502.

[47] S. Magazù, F. Migliardo, A. Benedetto, Mean Square Displacements from Elastic Incoherent Neutron Scattering Evaluated by Spectrometers Working with Different Energy Resolution on Dry and Hydrated (H2O and D2O) Lysozyme, J. Phys. Chem. B 114 (2010) 9268-9274.

[48] R. Soheilifard, D.E. Makarov, G.J. Rodin, Rigorous coarse-graining for the dynamics of linear systems with applications to relaxation dynamics in proteins, J. Chem. Phys. 135 (2011).

[49] C. Branca, S. Magazù, G. Maisano, P. Migliardo, Alpha, Alpha-Trehalose-Water Solutions. 3. Vibrational Dynamics Sudies by Inelastic Light Scattering, J. of Phys. Chem. B 103 (1999) 1347-1353.

[50] J. Pieper, G. Renger, Protein dynamics investigated by neutron scattering, Photosynth Res, 102 (2009) 281-293.

[51] Y. Kawabata, M. Hino, M. Kitaguchi, H. Hayashida, S. Tasaki, T. Ebisawa, D. Yamazaki, R. Maruyama, H. Seto, M. Nagao, T. Kanaya, Neutron resonance spin echo and MIEZE spectrometer development project in Japan, Physica B, 385-86 (2006) 1122-1124.

[52] A. Szytula, Neutron scattering for materials science, Solid State Phenomen, 112 (2006) 39-59.

[53] C. Branca, S. Magazù, G. Maisano, F. Migliardo, Vibrational and Relaxational Contributions in Disaccharide/H2O Glass Formers, Phys. Rev. B 64 (2001) 224204-1- 224204-8.

[54] M. Bee, Application of elastic scattering to disordered systems, J. Phys. Iv. 111 (2003) 259-296.

[55] K. Mitamura, N.L. Yamada, H. Sagehashi, N. Torikai, H. Arita, M. Terada, M. Kobayashi, S. Sato, H. Seto, S. Goko, M. Furusaka, T. Oda, M. Hino, H. Jinnai, A. Takahara, Novel neutron reflectometer SOFIA at J-PARC/MLF for in-situ soft-interface characterization, Polym. J. 45 (2013) 100-108.

[56] T. Kanaya, N. Takahashi, K. Nishida, H. Seto, M. Nagao, Y. Takeba, Dynamic and static fluctuations in polymer gels studied by neutron spin-echo, Physica B, 385 (2006) 676-681.

[57] R. Wagner, W. Bräutigam, D. Filges, H. Ullmaier, The Project “European Spallation Neutron Source (ESS)”: Status of R&D Programme, Phys. B: Cond. Matter 276–278, (2000) 38-44.

[58] L.K. Mansur, J.R. Haines, Status of the Spallation Neutron Source with Focus on Target Materials, J. Nucl. Mater. 356 (2006) 1-15.

[59] F. Mezei, New Perspectives from New Generations of Neutron Sources, Cr .Phys. 8 (2007) 909-920.

[60] D.N. Argyriou, H.N. Bordallo, Decisions on the European Spallation Source, Nat. Mater. 8 (2009) 440-440.

[61] S. Peggs, The European Spallation Source, Proceedings of IPAC2011, San Sebastián, Spain 2011, 3789-3793.

[62] E. Mamontov, K. W. Herwig, A Time-Of-Flight Backscattering Spectrometer at the Spallation Neutron Source, BASIS, Rev. Sci. Instr. 82 (2011) 080509-1-080509-10.

[63] M. Lindroos, S. Bousson, R. Calaga, H. Danared, G. Devanz, R. Duperrier, J. Eguia, M. Eshraqi, S. Gammino, H. Hahn, A. Jansson, C. Oyon, S. Pape-Moller, S. Peggs, A. Ponton, K. Rathsman, R. Ruber, T. Satogata, G. Trahern, The European Spallation Source, Nucl. Instrum. Meth. B. 269 (2011) 3258-3260.

[64] D. McGinnis, M. Lindroos, The European Spallation Source, 2013 IEEE 14th International Vacuum Electronics Conference (Ivec), (2013).

[65] R. Hall-Wilton, C. Theroine, Status of the European Spallation Source ESS AB, the Instrument Selection Process, and a Fundamental Physics Beamline at the ESS, Phys. Procedia 51 (2014) 8–12.

[66] J. A. N. Malik, Plans for European Spallation Source on Schedule, Mrs. Bull. 39 (2014) 764-764.

[67] J. R. Haines, T. J. McManamy, T. A. Gabriel, R. E. Battle, K. K. Chipley, J. A. Crabtree, L. L. Jacobs, D. C. Lousteau, M. J. Rennich, B. W. Riemer, Spallation Neutron Source Target Station Design, Development, and Commissioning, Nucl. Instr. Meth. Phys. Res. Sec. A 764 (2014) 94-11.

[68] C. Zendler, D. Martin Rodriguez, P.M. Bentley, Generic guide concepts for the European Spallation Source, Nucl. Instr. Meth. Phys. Res. A 803 (2015) 89–99.

[69] J. Yeck, European Spallation Source is on Track, Nature, 519 (2015) 291-291.

[70] A. Hilger, N. Kardjilov, I. Manke, C. Zendler, K. Lieutenant, K. Habicht, J. Banhart, M. Strobl, Neutron Guide Optimisation for a Time-Of-Flight Neutron Imaging Instrument at the European Spallation Source, Opt. Express, 23 (2015) 301-311.

[71] D. L. Chichester, M. Lemchak, J. D. Simpson, The API 120: A Portable Neutron Generator for the Associated Particle Technique, Nucl. Instr. Meth. Phys. Res. B 241 (2005) 753-758.

[72] J. C. Cooper, D. S. Koltick, J. T. Mihalczo, J. S. Neal, Evaluation of ZnO (Ga) Coatings as Alpha Particle Transducers within a Neutron Generator, Nucl. Instr. Meth. Phys. Res. A 505 (2003) 498-501.

[73] B. K. Das, A. Shyam, Development of Compact Size Penning Ion Source for Compact Neutron Generator, Rev. Sci. Instrum., 2008 Dec, 79, 123305-1-123305-4.

[74] S.S. Nargolwalla, E.P. Przybylowicz, Activation Analysis with Neutron Generators, John Wiley and Sons, New York, (1973).

[75] J. Reijonen, F. Gicquel, S. K. Hahto, M. King, T. P. Lou, K. N. Leung, D-D Neutron Generator Development at LBNL, Appl. Radiat. Isotopes 63, 8th International Conference on Applications of Nuclear Techniques, 2005, pp. 757-763.

[76] F. Gicquel, Engineering Drawings of a Compact Neutron Generator, Lawrence Berkeley National Laboratory, 2003.

[77] J. Reijonen et al., First PGAA and NAA Experimental Results from a Compact High Intensity D-D Neutron Generator, Nucl. Instr. Meth. Phys. Res. Sec. A 522 (2004) 598-602.

[78] D. L. Chichester, J. D. Simpson, M. Lemchak, Advanced Compact Accelerator Neutron Generator Technology for Active Neutron Interrogation Field Work, J. Radio Anal. Nucl. Chem. 271 (2007) 629-637.

[79] Y. Wu, J. P. Hurley, Q. Ji, J. Kwan, K.N. Leung, Development of a RF-Driven Neutron Generator for Associated Particle Imaging, IEEE Trans. Nucl. Sci. 56 (2009) 1306-1311.

[80] J. Reijonen, K. N. Leung, G. Jones, RF Ion Source Development for Neutron Generation and for Material Modification, Rev. Sci. Instr. 73 (2002) 934.

[81] Y. Wu, J. P. Hurley, Q. Ji, J. Kwan, K. N. Leung, Characteristics of a RF-Driven Ion Source for a Neutron Generator Used for Associated Particle Imaging, AIP Conf. Proc., 1099, 2009, pp. 614.

[82] Y. Wu, J. P. Hurley, Q. Ji, J. Kwan, K. N. Leung, Rev. Sci. Instrum., Sealed Operation of a RF Driven Ion Source for a Compact Neutron Generator to be Used for Associated Particle Imaging, Proceedings of the International Conference on Ion Sources (ICIS 09), 2010.

[83] F. Gicquel, Engineering Drawings of a Compact Neutron Generator for Associated Particle Imaging, Lawrence Berkeley National Laboratory, 2005.

[84] X. Lu, J. Wang, Y. Zhang, J. Li, L. Xia, et al., Design of a High-Current Low-Energy Beam Transport Line for an Intense D-T/D-D Neutron Generator, Nucl. Instr. Meth. Phys. Res. A, 811 (2016) 76-81.

[85] A. Skoulakis, G. C. Androulakis, E. L. Clark, S. M. Hassan, P. Lee, J. Chatzakis, M. Bakarezos, V. Dimitriou, C. Petridis, N. A. Papadogiannis, M. Tatarakis, A Portable Pulsed Neutron Generator, Applic. Nucl. Tech. 27 (2014) 1460127-1 -1460127-8.

[86] K. Nishimura, Y. Miake, M. Kato, Y. Rintsu, Development of Portable Pulsed Neutron Generators Utilizing a D-T or D-D Fusion Reaction, Fus. Sc. Tech. 39 (2001) 1174-1181.

[87] A. Caruso, S. Y. Gus'kov, V. B. Rozanov, C. Strangio, Direct Ignition of DT and DD Fuels by Laser-Produced Plasma Plow. Eclim 2000: 26th European Conference on Laser Interaction with Matter, 2001, 4424.

[88] E. S. Grishnyaev, S. V. Polosatkin, Modeling of Deuterium Ionization and Extraction From an Ion Source Driven by Heated Cathode, IEEE Trans. Plasma Sc. 43 (2015) 3856-3867.

[89] Y. Z. Liu, P. Byrne, H. Y. Wang, D. Koltick, W. Zheng, L. D. H. Nie, A Compact DD Neutron Generator-Based NAA System to Quantify Manganese (Mn) In Bone In Vivo, Physiol. Meas. 35 (2014) 1899-1911.

[90] F. Mostafaei, S. P. Blake, Y. Z. Liu, D. A. Sowers, L. H. Nie, Compact DD Generator-Based Neutron Activation Analysis (NAA) System to Determine Fluorine in Human Bone In Vivo: a Feasibility Study, Physiol. Meas. 36 (2015).

[91] A. A Naqvi, A Monte Carlo comparison of PGNAA System Performance Using Cf-252 Neutrons, 2.8-MeV Neutrons and 14-MeV Neutrons, Nucl. Instr. Meth. Phys. Res. A 511 (2003) 400-407.

[92] E. H. Seabury, B. W. Blackburn, D. L. Chichester, C. J. Wharton, A. J. Caffrey, Comparison of D-D, D-T and Cf-252 Neutron Excitation of Light and Medium Mass Nuclei for Field PGNAA Applications, Nucl. Instr. Meth. Phys. Res. B 261 (2007) 839-844.

[93] P. Srinivasan, S. Priya, T. Patel, R. K. Gopalakrishnan, D. N. Sharma, Assessment of Radiation Shield Integrity of DD/DT Fusion Neutron Generator Facilities by Monte Carlo and Experimental Methods, Nucl. Instr. Meth. Phys. Res. B 342 (2015) 125-132.

[94] T. J. Langford, C. D. Bass, E. J. Beise, H. Breuer, D. K. Erwin, C. R. Heimbach, J. S. Nico, Fast Neutron Detection with a segmented spectrometer, Nucl. Instr. Meth. Phys. Res. A 771 (2015) 78-87.

[95] J. Agresti, I. Osticioli, M.C. Guidotti, N. Kardjilov, S. Siano, Non-Invasive Archaeometallurgical Approach to the Investigations of Bronze Figurines Using Neutron, Laser, and X-ray Techniques, Microchem. J. 124 (2016) 765-774.

[96] Z. D. Whetstone, K. J. Kearfott, A Method for Using Neutron Elastic Scatter to Create a Variable Energy Neutron Beam from a Nearly Monoenergetic Neutron Source, Radiat. Phys. Chem. 112 (2015) 22-28.

[97] Y. P. Bogolubov, Y. G. Polkanov, T. O. Khasaev, B. G. Titov, V. D. Alexandrov, L. A. Korytko, System for Identification of Toxic Chemicals in Hermetically Sealed Containers on the Basis of a Neutron Gamma-Method with Application of the VNIIA-Developed Portable Neutron Generator, Penetr. Rad. Syst. and Appl. II, 4142 (2000) 314-320.

[98] D. Chernikova, V. L. Romodanov, A. G. Belevitin, V. V. Afanas'ev et al., Experimental and Numerical Investigations of Radiation Characteristics of Russian Portable/Compact Pulsed Neutron Generators: ING-031 ING-07, ING-06 and ING-10-20-120, Nucl. Instrum. Meth. A. 746 (2014) 74-86.

[99] D. L. Chichester, J. T. Johnson, E. H. Seabury, Measurement Of The Neutron Spectrum Of A D-D Electronic Neutron Generator, Application of Accelerators in Research and Industry: Twenty-First International Conference, 1336 (2011) 519-523.

[100] D. L. Chichester, M. Lemchak, J. D. Simpson, The API 120: A Portable Neutron Generator for the Associated Particle Technique, Nucl. Instr. Meth. B. 241 (2005) 753-758.

[101] J. T. Cremer, D. L. Williams, C. K. Gary, M. A. Piestrup, D. R. Faber, M. J. Fuller, J. H. Vainionpaa, M. Apodaca, R. H. Pantell, J. Feinstein, Large Area Imaging of Hydrogenous Materials Using Fast Neutrons from a D-D Fusion Generator, Nucl. Instr. Meth. A. 675 (2012) 51-55.

[102] J. L. Ellsworth, S. Falabella, J. Sanchez, V. Tang, H. Wang, Compact Deuterium-Tritium Neutron Generator Using a Novel Field Ionization Source, J. Appl. Phys. 116 (2014).

[103] E. V. Gromov, V. M. Gulko, A. V. Izmaliov, A. S. Khimchenko et al., Progress in Neutron Logging in Russia Describing a New Portable Neutron Generator, Appl. Radiat. Isotopes. 46 (1995) 639-640.

[104] V. I. Mikerov, I. A. Zhitnik, J. N. Barmakov, A. I. Isakov et al., Investigation of Prospects of Fast Neutron Radiography on the Basis of Portable Neutron Generators, Penetr. Rad. Syst. Appl. II, 4142 (2000) 74-80.

[105] A. A. Naqvi, F. A. Al-Matouq, F. Z. Khiari, Khateeb-ur-Rehman, M. A. Gondal, A. A. Isab, Optimization of a Prompt Gamma Setup for Analysis of Environmental Samples, J. Radioanal. Nucl. Ch. 296 (2013) 215-221.

[106] A. A. Naqvi, Z. Kalakada, M. S. Al-Anezi, F. Al-Matouq, M. Maslehuddin, O.S.B. Al-Amoudi, Performance Evaluation of a Portable Neutron Generator for Prompt Gamma-Ray Applications, Arab. J. Sci. Eng. 39 (2014) 531-539.

[107] K. Nishimura, Y. Miake, M. Kato, Y. Rintsu, Development of Portable Pulsed Neutron Generators Utilizing a D-T or D-D Fusion Reaction, Fusion Technol. 39 (2001) 1174-1181.

[108] V. L. Romodanov, V. K. Sakharov, D. N. Chernikova, V. I. Ryzhkov, T. O. Khasaev, A. A. Sladkov, Properties of Radiation from Portable Pulsed Neutron Generators, Atom. Energy 111 (2011) 42-47.

[109] R. J. Shypailo, K. J. Ellis, Prompt-Gamma Neutron Activation Analysis System Design: Effects of D-T Versus D-D Neutron Generator Source Selection, J. Radioanal. Nucl. Ch. 276 (2008) 71-77.

[110] J. Reijonen, et al., D-D Neutron Generator Development at LBNL, Appl. Radiat. Isot. 63 (2005) 757–763.

[111] J. Reijonen, Compact Neutron Generators for Medical, Homeland Security and Planetary Exploration, Nucl. Instrum. Methods Phys. Res. B 261 (2007) 272.

[112] B. A. Ludewigt, R. P. Wells, J. Reijonen, High-Yield D-T Neutron Generators Tar, Nucl. Instrum. Methods Phys. Res. B 261 (2007) 830.

[113] J. Reijonen, et al., Compact Neutron Generator Development at LBNL (Proc. American Nucl. Soc. San Diego, Lawrence Berkeley National Laboratory, Berkely (2003).

[114] J. Reijonen, K.N. Leung, G. Jones, RF Ion Source Development for Neutron Generation and for Material Modification, Rev Sci. Instr. 73 (2002) 934.

[115] G.H. Miley, R. Stubbers, Y. Yang, J. Webber, Y. Shaban, Advances in IEC Technology for a Portable Neutron/Proton Source, 14th Pacific Basin Nuclear Conf., 2004.

[116] P. A. Tulle, Recent Works with Sealed Tube Neutron Generators, Use of Accelerator Based Neutron Sources, IAEA-TECDOC-1153, IAEA, Vienna, 2000, pp. 59–63.

[117] R. W. Hamm, Multipurpose Neutron Generators Based on the Radiofrequency Quadrupole Linear Accelerator, Penetr. Rad. Syst. Appl. II, (Proc. of SPIE, 2000), 4142 (2000) 39–47.

[118] T. Sztaricskai, Problems Related to the Optimal Use of Accelerator Based Neutron Generators, Use of Accelerator Based Neutron Sources, IAEA-TECDOC- 1153, IAEA, Vienna 2000, pp. 53–58.

[119] S. A. Jonah, Utilization of a sealed-tube neutron generator for training and research, Use of Accelerator Based Neutron Sources, IAEA-TECDOC-1153, IAEA, Vienna, 2000, pp. 45–51.

[120] Z. F Song, J. B. Chen, Z. J. Liu, X. Y. Zhan, Q. Tang, The Calibration of the D-D Neutron Indium Activation Diagnostic, Plasma Sc. Tech. 17 (2015) 337-339.

[121] M. Stefanik, P. Bem, M. Gotz, K. Katovsky, M. Majerle, J. Novak, E. Simeckova, Neutron Spectrum Determination of the p(35 MeV)-Be Source Reaction by the Dosimetry Foils Method, Nucl. Data Sheets 119 (2014) 422-424.

[122] Q. Shan, S. N. Chu, W. B. Jia, Monte Carlo Simulation of Moderator and Reflector in Coal Analyzer Based on a D-T Neutron Generator. Appl. Rad. Isot. 105 (2015) 204-208.

[123] G. Hevesy, Adventures in Radioisotope Research, Vol. 1, Pergamon Press, New York, 1962, pp. 47–62.

[124] L. P. Bedard, Neutron Activation Analysis, Atomic Absorption and X-ray Fluorescence Spectrometry Review for 2004-2005, Geostand, Geoanal. Res. 30 (2006) 183-186.

[125] W. D. Ehmann, 14-MeV Neutron Activation Analysis: Methodology, Applications, and Potential, J. Radioanal. Nucl. Chem. 167 (1993) 67.

[126] American Society for Testing and Materials, Standard Test Method for Oxygen Content Using a 14-MeV Neutron Activation and Direct-Counting Technique, E385-90, Philadelphia (1991).

[127] W. D. James, 14 MeV Fast Neutron Activation Analysis in the Year 2000, J. Radioanal. Nucl. Chem. 243 (2000) 119.

[128] M. A. Hannan, A. F. Oluwole, L. O. Kehinde, A. B. Borisade, Determination of Oxygen, Nitrogen, and Silicon in Nigerian Fossil Fuels by 14 MeV Neutron Activation Analysis, J. Radioanal. Nucl. Chem. 256 (2003) 61.

[129] S. A. Jonah, I. O. Okunade, B. W. Jimba, I. M. Umar, Application of a Low-Yield Neutron Generator for Rapid Evaluation of Alumino-Silicate Ores from Nigeria by FNAA, Nucl. Instrum. Methods Phys. Res.A 463 (2001) 321.

[130] W. D. James, R. Zeisler, Uptake of Oxygen in a Coal Standard Reference Material® Determined by Fast (14-MeV) Neutron Activation Analysis, J. Radioanal. Nucl. Chem. 248 (2001) 233.

[131] S. S. Nargolwalla, E. P. Przybylowicz, Activation Analysis with Neutron Generators, John Wiley and Sons, New York, (1973).

[132] J. Reijonen, et al., First PGAA and NAA Experimental Results from a Compact High Intensity D-D Neutron Generator, Nucl. Instrum. Methods Phys. Res. A 522 (2004) 598–602.

[133] C.S. Lim, Recent Developments in Neutron-Induced Gamma Activation for On-Line Multi-Elemental Analysis in Industry, J. Radioanal. Nucl. Chem. 262 (2004) 525–532.

[134] International Atomic Energy Agency, Use of Research Reactors for Neutron Activation Analysis, IAEA-TECDOC-1215, IAEA, Vienna, 2001.

[135] G. P. Westphal, F. Grass, H. Lemmel, J. Sterba, A Low-Cost System for Rapid Automatic Neutron Activation Analysis at Small Research Reactors, J. Radioanal. Nucl. Chem. 272 (2007) 267–271.

[136] J. R. De Voe, P. D. La Fleur, Modern Trends In Activation Analysis, Proceedings of the 1968 International Conference held at the National Bureau of Standards, Gaithersburg, Maryland, October 7-11, 1968.

[137] G. P. Westphal et al., Automatic Activation Analysis, J. Radioanal. Nucl. Chem. 271 (2007) 145–150.

[138] W. D. James, 14 MeV Fast Neutron Activation Analysis in the Year 2000, J. Radioanal. Nucl. Chem. 243 (2000) 119.

[139] W. S. Jr. Lyon (Ed.), Guide to Activation Analysis, Van Nostrand, New York (1964).

[140] F. Girardi, G. Guzzi, J. Pauly, Data Handbook for Sensitivity Calculations in Neutron Activation Analysis, Euratom-1898e, Euratom, Ispra, Italy (1965).

[141] R. Hancock, Neutron Activation Analysis, Encyclopedia of Scientific Dating Methods Part of the series Encyclopedia of Earth Sciences Series 2015, pp. 607-608.

[142] S. Sekimoto, N. Shirai, M. Ebihara, Application of Neutron Activation Analysis to Micro Gram Scale of Solid Samples, J. Radioanal. Nucl. Chem. 307 (2016) 1757-1764.

[143] R. Z. Selden, T. K. Perttula, D. L. Carlson, INAA and the Provenance of Shell-Tempered Sherds in the Ancestral Caddo Region, J. Archaeol. Sc. 47 (2014) 113-120.

[144] Q. Shan, Q. Li, C. Cheng, W. B. Jia, D. Q. Hei, Y. S. Ling, Simulation Study on the Moderator in PGNAA-Based Online Coal Measurement System, Environ. Tech. Res. Util. II, 675-677 (2014) 1316-1320.

[145] N. Shirai, Y. Hidaka, A. Yamaguchi, S. Sekimoto, M. Ebihara, H. Kojima, Neutron Activation Analysis of Iron Meteorites, J. Radioanal. Nucl. Chem. 303 (2015) 1375-1380

[146] N. Siddique, M. Jawad, S. Waheed, Instrumental Neutron Activation Analysis for the Study of Size-Fractionated Airborne Particulate Matter Samples, Radiochim. Acta, 101 (2013) 273-277.

[147] K. K. Swain, N. Ajith, R. Acharya, R. Verma, A. V. R. Reddy, Large Sample Neutron Activation Analysis of Dross for Gold and Silver, J. Radioanal. Nucl. Chem. 294 (2012) 319-322.

[148] A. Szymczycha-Madeja, M. Welna, P. Pohl, Elemental Analysis of Teas and Their Infusions by Spectrometric Methods. Trac-Trends Analyt. Chem. 35 (2012) 165-181.

[149] J. H. Vainionpaa, A. X. Chen, M. A. Piestrup, C.K. Gary, G. Jones, R. H. Pantell, Development of High Flux Thermal Neutron Generator for Neutron Activation Analysis, Nucl. Instr. Meth. Phys. Res. B 350 (2015) 88-93.

[150] S. Waheed, I. Fatima, Instrumental Neutron Activation Analysis of Emblica Officinalis, Terminalia Belerica and Terminalia Chebula for Trace Element Efficacy and Safety, Appl. Rad. Isot. 77 (2013) 139-144.

[151] M. Zehringer, J. Mazacek,R. Dolf,G. Testa, J. Jourdan, Neutron Activation Analysis - Another Approach to Uranium and Thorium Analysis in Environmental Samples. Chimia, 67 (2013) 828-828.

[152] R. Zeisler, B. E. Tomlin, K. E. Murphy, J. Kucera, Neutron Activation Analysis with Pre- and Post- Irradiation Chemical Separation for the Value Assignments of Al, V, and Ni in the New Bovine Liver SRM 1577C, J. Radioanal. Nucl. Chem. 282 (2009) 69-74.

[153] Y. Katoh, T. Sato, Y. Yamamoto, Use of Instrumental Neutron Activation Analysis to Determine Concentrations of Multiple Trace Elements in Human Organs, Arch. Environ. Health (2003) 655-661.

[154] M. Yukawa, M. Suzuki-Yasumoto, K. Amano, M. Terai, Distribution of Trace Elements in the Human Body Determined by Neutron Activation Analysis, Arch. Environ. Health 35 (1980) 36–44.

[155] A. Danielsen, E. Steinnes, A Study of Some Selected Trace Elements in Normal and Cancerous Tissue by Neutron Activation Analysis, J. Nucl. Med. 11 (1970) 260–264.

[156] C. J. Yi, S. Nilsuwankosit, Development of Fast Neutron Radiography System Based on Portable Neutron Generator, International Nuclear Science, Technology and Engineering Conference 2015 (Inustec2015), 1704 (2016).

[157] P. Andersson, E. Andersson-Sunden, H. Sjostrand, S. Jacobsson-Svard, Neutron Tomography of Axially Symmetric Objects Using 14 MeV Neutrons from a Portable Neutron Generator, Rev. Sci. Instr. 85 (2014).

[158] P. Andersson, J. Valldor-Blucher, E. A. Sunden, H. Sjostrand, S. Jacobsson-Svard, Design and Initial 1D Radiography Tests of the FANTOM Mobile Fast-Neutron Radiography and Tomography System, Nucl. Instr. Meth. A 756 (2014) 82-93.

[159] A. J. Kapadia, A. C. Sharma, G. D. Tourassi, J. E. Bender, C. R. Howell, A. S. Crowell, M. R. Kiser, B. P. Harrawood, R. S. Pedroni, C. E. Jr. Floyd, Neutron Stimulated Emission Computed Tomography for Diagnosis of Breast Cancer, IEEE Trans. Nucl. Sc. 55 (2008) 501-509.

[160] C. E. Floyd, J. E. Bender, A. C. Sharma, A. J. Kapadia, J. Q. Xia, B. P. Harrawood, G. D. Tourassi, J.Y. Lo, A.S. Crowell, C.R. Howell, Introduction to Neutron Stimulated Emission Computed Tomography, Phys. Med. Biol. 51 (2006) 3375–3390.

[161] D. J. Rhee, G. A. Agasthya, A. J. Kapadia, Neutron Stimulated Emission Computed Tomography for Brain Cancer Imaging, 2013 IEEE Nuclear Science Symposium And Medical Imaging Conference.

[162] C. Floyd, E. Jr Carey, J. E. Bender, A. C. Sharma, A. J. Kapadia, Introduction to neutron stimulated emission computed tomography, Phys. Med. Biol. 51 (2006) 3375-3390.

[163] R. Adamsa, L. Borta, R. Zborayb, H. M. Prassera, Development and characterization of a D-D fast neutron generator for imaging applications, Appl. Rad. Isot. 96 (2015) 114-121.

[164] F. H. Kim, D. Penumadu, N. Kardjilov, I. Manke, High-Resolution X-ray and Neutron Computed Tomography of Partially Saturated Granular Materials Subjected to Projectile Penetration. Inter. J. Imp. Eng. 89 (2016) 72-82.

[165] C. Ritzoulis, M. Strobl, C. Panayiotou, G. Choinka, C. Tsioptsias, C. Vasiliadou, et al., Ultra-Small Angle Neutron Scattering and X-ray Tomography Studies of Caseinate-Hydroxyapatite Microporous Materials, Mat. Chem. Phys. 123 (2010) 77-82.

[166] L. G. Tumlinson, H. Y. Liu, W. K. Silk, J. W. Hopmans, Thermal Neutron Computed Tomography of Soil Water and Plant Roots, Soil Sc. Soc. Am. J. 72 (2008) 1234-1242.

[167] U. Garbe, T. Randall, C. Hughes, The New Neutron Radiography/Tomography/Imaging Station DINGO at OPAL, Nucl. Instr. Meth. Phys. Res. A 651 (2011) 42-46.

[168] A. J. Gilbert, M. R. Deinert, Neutron Tomography of Axisymmetric Flow Fields in Porous Media, Nucl. Instr. Meth. Phys. Res. B 301 (2013) 23-28.

[169] F. Hameed, S. Karimzadeh, M. Zawisky, Neutron imaging of radioactive sources, Penetr. Rad. Syst. Appl. IX, 7080 (2008)

[170] E. Hammarlund, B. Schillinger,E. Calzada, Neutron Tomography for Understanding the Evolution of Life, Neut. Radiog. (2008) 448-451.

[171] H. K. Jenssen, B. C. Oberlander, J. D. Beenhouwer, J. Sijbers, M. Verwerft, Neutron Radiography and Tomography Applied to Fuel Degradation During Ramp Tests and Loss of Coolant Accident Tests in a Research Reactor, Prog. Nucl. En. 72 (2014) 55-62.

[172] T. Kamiyama, D. Tsukui, H. Sato,Y. Kiyanagi, Accelerator-Based Neutron Tomography Cooperating with X-ray Radiography Nucl. Instr. Meth. Phys. Res. A 651 (2011) 28-31.

[173] B.A. Ludewigt, Neutron Generators for Spent Fuel Assay, Lawrence Berkeley National Laboratory (2011).

[174] S.K. Sharma, S. Jakhar, R. Shukla, A. Shyam, C.V.S. Rao, Explosive Detection System Using Pulsed 14MeV Neutron Source, Fus. Engin. Des. 85 (2010) 1562–1564.

[175] T.R. Twomey, A.J. Caffrey, D.L. Chichester, Identification of Chemical Warfare Agents and Explosives by Neutron Generator-Driven PGNAA, (2007).

[176] S. Van Liew, X-ray and neutron interrogation of air cargo for mobile applications, Nucl. Instr. Meth. Phys. Res. A 784 (2015) 417–422.

[177] E.P. Cippo, A. Borella, G. Gorini, W. Kockelmann, M. Moxon, H. Postma, N.J. Rhodes, P. Schillebeeckx, E.M. Schoonenveld, M. Tardocchi, K. Dusz, Z. Hajnal, K. Biro, S. Porcinai, C. Andreani, G. Festa, Imaging of cultural heritage objects using neutron resonances, J. Anal. Atom. Spectr. 26 (2011) 992.

[178] G. Festa, E.P. Cippo, D. Di Martino, R. Cattaneo, R. Senesi, C. Andreani, E. Schooneveld, W. Kockelmann, N. Rhodes, A. Scherillo, P. Kudejova, K. Biro, K. Duzs, Z. Hajnal, G. Gorini, Neutron Resonance Transmission Imaging for 3D Elemental Mapping at the ISIS Spallation Neutron Source, J. Anal. At. Spectrom. 30 (2015) 745–750.

[179] A. Miceli, G. Festa, G. Gorini, R. Senesi, C. Andreani, Pulsed Neutron Gamma-Ray Logging in Archaeological Site Survey, Meas. Sci. Tech. 24 (2013) 125903.

[180] O. Shulyakova, P. Avtonomov, V. Kornienko, New Developments of Neutron Activation Analysis Applications, Procedia – Soc. Behav. Sci. 195 (2015) 2717–2725.

[181] C. Grünzweig, D. Mannes, A. Kaestner, F. Schmid, P. Vontobel, J. Hovind, S. Hartmann, S. Peetermans, E. Lehmann, Progress in Industrial Applications Using Modern Neutron Imaging Techniques, Physics Procedia 43 (2013) 231–242.

[182] V. Kornienko, P. Avtonomov, Application of Neutron Activation Analysis for Heavy Oil Production Control, Procedia – Soc. Behav. Sci. 195 (2015) 2451–2456.

[183] F. Zhou, X. Xiao, K. Fang, C. Lan, X. Kong, Activation Cross Sections for (n, p) Reactions on Nickel Isotopes Induced by Neutrons Around 14MeV, Nucl. Instr. Meth. Phys. Res. B 269 (2011) 642–643.

[184] Y. Song, F. Zhou, M. Tian, Y. Li, S. Yuan, C. Lan, Measurements of the Cross Section for the ^{182}W(n,p)^{182}(m+g)Ta and ^{184}(n,p)184Ta Reactions in the 14MeV Energy Range Using the Activation Technique, Appl. Rad. Isot. 98 (2015) 29–33.

[185] M.S. Herrera, G.A. Moreno, A.J. Kreiner, New Method to Evaluate the ^{7}Li(p,n)^{7}Be Reaction Near Threshold, Nucl. Instr. Meth. Phys. Res. B 349 (2015) 64–71.

[186] W.S. Charlton, D. Boyle, S. Chirayath, D.G. Ford, C.A. Gariazzo, C. Marianno, K. Ragusa, A. Solodov, Educating the Next Generation of Nuclear Safeguards and Security Experts at TAMU, in: Proceedings of GLOBAL, 2011, pp. 11–16.

[187] R. Berndt, K. Abbas, V. Berthou, C.D.A. Carrapico, G. Eklund, V. Forcina, V. Mayorov, P. Mortreau, M. Mosconi, B. Pedersen, others, Evolution of the Nuclear Safeguards Performance Laboratory PERLA of the Ispra Site of the Institute for Transuranium Elements, (2015).

[188] A. Parsons, J. Bodnarik, L. Evans, S. Floyd, L. Lim, T. McClanahan, M. Namkung, S. Nowicki, J. Schweitzer, R. Starr, J. Trombka, Active Neutron and Gamma-Ray Instrumentation for In Situ Planetary Science Applications, Nucl. Instr. Meth. Phys. Res. A 652 (2011) 674–679.

[189] H.-R. Wenk, Application of Neutron Scattering in Earth Sciences, JOM. 64 (2012) 127–137.

[190] H.-R. Wenk, others, Neutron scattering in earth sciences, Mineralogical Society of America, 2006.

[191] B. Reddell, P. O'Neill, C. Bailey, K. Nguyen, Single Event Effects Testing For Low Earth Orbit Missions with Neutrons, (2015).

[192] D. Nikolić, A. Vasić-Milovanović, Comparative Study of Gamma and Neutron Irradiation Effects on the Silicon Solar Cells Parameters, FME Transactions 44 (2016) 99–105.

[193] M. Rebai, C. Cazzaniga, G. Croci, M. Tardocchi, E.P. Cippo, P. Calvani, M. Girolami, D.M. Trucchi, G. Grosso, G. Gorini, Pixelated Single-crystal Diamond Detector for Fast Neutron Measurements, J. Instr. 10 (2015) C03016–C03016.

[194] G. Consentino, M. Laudani, G. Privitera, A. Parlato, N. Marchese, E. Tomarchio, C. Pace, C. Giordano, M. Mazzeo, J.H. Ambato, Dangerous Effects Induced on Power MOSFETs by Terrestrial Neutrons, (2013).

[195] G. Consentino, M. Laudani, G. Privitera, C. Pace, C. Giordano, J. Hernandez, M. Mazzeo, Effects on Power Transistors of Terrestrial Cosmic Rays: Study, Experimental Results and Analysis, Applied Power Electronics Conference and Exposition (APEC), 2014, pp. 2582–2587.

[196] Y. Liu, D. Koltick, P. Byrne, H. Wang, W. Zheng, L.H. Nie, Development of a Transportable Neutron Activation Analysis System to Quantify Manganese In Bone In Vivo: Feasibility and Methodology, Physiological Measurement 34 (2013) 1593–1609.

[197] F. Mostafaei, S.P. Blake, Y. Liu, D.A. Sowers, L.H. Nie, Compact DD Generator-Based Neutron Activation Analysis (NAA) System to Determine Fluorine in Human Bone In Vivo: a Feasibility Study, Physiological Measurement 36 (2015) 2057–2067.

[198] S.N.A. Tahir, D.R. Chettle, Identification of Oxygen-19 During In Vivo Neutron Activation Analysis of Water Phantoms, Physiological Measurement 36 (2015) N127–N134.

[199] A. Bell, G.A. McRae, R. Wassenaar, R.G. Wells, D. Faber, nSPECT: A Radioisotope-Free Approach to Nuclear Medicine Imaging, IEEE Transactions on Nuclear Science 62 (2015) 791–798.

[200] Y. Iguchi, H. Michiue, M. Kitamatsu, Y. Hayashi, F. Takenaka, T. Nishiki, H. Matsui, Tumor-Specific Delivery of BSH-3R for Boron Neutron Capture Therapy and Positron Emission Tomography Imaging in a Mouse Brain Tumor Model, Biomaterials 56 (2015) 10–17.

[201] S. Magazù, F. Migliardo, M.T. Caccamo, Innovative Wavelet Protocols in Analyzing Elastic Incoherent Neutron Scattering, J. Phys. Chem. B 116 (2012) 9417-9423.

[202] F. Migliardo, M.T. Caccamo, S. Magazù, Thermal Analysis on Bioprotectant Disaccharides by Elastic Incoherent Neutron Scattering, Food Biophys. 9 (2014) 99-104.

[203] S. Magazù, F. Migliardo, B. G. Vertessy, M. T. Caccamo, Investigations of homologous disaccharides by elastic incoherent neutron scattering and wavelet multiresolution analysis Chem. Phys. 424 (2013) 56-61.

[204] F. Migliardo, M.T. Caccamo, S. Magazù, Elastic incoherent neutron scatterings wavevector and thermal analysis on glass-forming homologous disaccharides, J. Non-Cryst. Solids 378 (2013) 144-151.

[205] F. Migliardo, S. Magazù, M. T. Caccamo, Infrared, Raman and INS studies of poly-ethylene oxide oligomers, J. Mol. Struct. 1048 (2013) 261-266.